Politecnico di Torino

Master Degree in Energy and Nuclear Engineering 2024/2025

Heat Pumps as Flexible Resources for a Resilient Electrical Grid

Author Pietro Merandino

Supervisor PoliTo Gianfranco Chicco

Supervisor UPC Joan Marc Rodrìguez Bernuz

Date of presentation 16 October 2025

Contents

1	Abstract				
2	Introduction	6			
3	Transformation of the power system	9			
4	Power System Stability with Low-Inertia Generation: Evolution and Emerging Approaches 4.1 Demand Response	12 17 19 20 21 22 24 24			
5	Heat Pump model 5.1 Liquid refrigerator R-410A 5.2 Compressor State of Art 5.3 Fans state of art 5.4 Condenser and Evaporator 5.5 Liquid Receiver 5.6 Thermostatic Expansion Valve 5.7 House model 5.7.1 Legiferation on HVAC system	26 29 31 34 37 40 42 44 47			
6	Characterization of the Heat Pump6.1PID Controller6.2Steady State	50 52 54			
7	 Results of the First Test 7.0.1 Comparative analysis in the case where T_{ext} = 30°C, in which the fan operating frequency was varied — once set to 60 Hz, once to 50 Hz and once to 40 Hz 7.1 First Test — the desired indoor temperature is fixed (in this case, T_{set point} = 22 °C)—the behavior of the modeled heat pump parameters is observed as the angular velocity of the compressor decreases. The study is performed for five different outdoor temperatures 7.2 First Test second part - results concerning the characterization of the air conditioning system, keeping the outdoor temperature constant (set at T_{ext} = 30°C) while varying the indoor set-point temperature of the house 	58616366			
8	Results of the Second Test	69			
9	Results on the support provided9.1 European Scenario9.2 Italian Scenario	72 75 81			
10	Grid Flexibility and Energy Efficiency: An Integrated Assessment of Heat Pump Performance	84			
11	Conclusion	89			

List of Figures

1	Increase in renewable energy production [5]	6
2	Loss of production during Spain's blackout [7]	7
3	Inertia-Demand 2009-2019 [11]	8
4	Comparison of the main results in TYNDP 2022 and TYNDP 2024	11
5	Intervention modes prescribed by ENTSO-E for the sequential activation of con-	
	trols/regulations [30]	12
6	Grid frequency dynamics following a generation loss, with different system in-	
	ertia values	15
7	Inertia duration curve of the Continental Europe Synchronous Area	
8	DR programs around the world [45]	18
9	SoC area of possible operation	23
10	Energy storage technology [43]	25
11	Simulink Heat Pump model	
12	Simulink Heat Pump model implemented	
13	External environment subsystem on Simulink	
14	House subsystem on Simulink	
15		30
16	Pressure-temperature graph for R-410A refrigerant	31
17	Simulink Compressor [87]	
	Simulink Compressor characteristics [87]	
18	Simulink Fan block [89]	34
19	Simulink House Fan characteristics	
20	Simulink External Fan characteristics	
21	System-Level Condenser Evaporator (2P-MA) Simulink's block	
22	System-Level Condenser Evaporator (2P-MA) Simulink's block	
23	System-Level Condenser Evaporator (2P-MA) Simulink's block	39
24	Receiver Accumulator (2P) Simulink's block	40
25	Receiver Accumulator (2P) Simulink's block specifications	41
26	Thermostatic Expansion Valve (2P) block	
27	Thermostatic Expansion Valve (2P) block specifications	43
28	House Model	44
29	House parameters	
30	House thermal network subsystem [77]	
31	PID Controller on Simulink	52
32	PID Controller working principle	53
33	PID Controller working principle on the Temperature of the house	53
34	Ideal Angular Velocity block connected to the Compressor	54
35	Compressor and Fans powers	55
36	Compressor and Fans frequency	55
37	Mass flow rate of R-410A	56
38	Heats exchanged in the system	56
39	Energy balance of a Heat Pump	57
40	Normalized Input for the Compressor angular velocity to obtain the $+0.5^{\circ}\text{C}$	58
41	Temperature increase due to minimum Compressor power	58
42	Input for the First test	59
43	Fans frequencies for each External temperature	59
44	(p-h) state diagram for T_{ext} =35°C	60
45	Text=30°C Power comparison between fans frequencies	61
46	Text=30°C EER comparison between fans frequencies	62
47	Fans Frequency/ Compressor Power	63
48	Fans Frequency/ Compressor Power	

49	$Q_{evaporator}$ / Compressor Power	64
50	mass flow rate R-410A depending on the Compressor power	64
51	Compressor Power / EER_M	65
52	First test: results on the maximum ΔP for each external temperature	66
53	Fans Frequency/ Compressor Power	66
54	$Q_{evaporator}$ / Compressor Power	67
55	Compressor Power / EER_M	67
56	First test second part: results on maximum ΔP	68
57	Fans frequencies for each External temperature	69
58	Text=32°C temperature and heat exchange behaviour stopping the system	70
59	Thermal inertia of the house in [s] and the resulting power capacity that can be	
	gained	71
60	Local primary frequency control algorithm flowchart	72
61	European maxima and minima demand curve [27]	75
62	Heat pump units in Europe [27]	76
63	First Test: Frequency support to the grid due to ΔP_{HP}	77
64	Difference in max and min case for T_{ext} =35°C and T_{ext} =25°C	78
65	Inertia results of the second test	79
66	Inertia results of the second test	79
67	Inertia results of the second test	79
68	European maxima and minima demand curve [27]	81
69	Results of the First Test for the Italian area	82
7 0	Results of the Second Test for the Italian area	83
7 1	First Test: Heat Pump performance vs frequency response in Europe	85
72	First Test: Heat Pump performance vs frequency response in Italy	86
7 3	First Test (second part): Europe	87
7 4	First Test (second part): Italy	88
	- · · · · · · · · · · · · · · · · · · ·	

1 Abstract

The increasing need to introduce more and more energy from renewable energy sources into the energy mix has brought with it numerous challenges to be solved within today's electricity grid.

A prominent challenge is that these new technologies, such as wind and solar photovoltaic power generation, connect to the grid mainly through power electronic converters. This has led to a growing concern about grid stability, particularly regarding the decrease in system inertia and the increase in the rate of change of frequency (RoCoF) following contingencies. As a result, there is an urgent need to find ways to maintain stability in compliance with the regulations in force in various countries.

The problems can be addressed through demand response programs, which are designed to adapt the demand side in order to balance and synchronize the power system. These methods decouple renewable energy generation from demand, enabling the demand side to support the grid when needed.

Going to the extremes of the previous idea, one can introduce grid-forming loads, i.e. loads connected with special converters to the electricity grid and able to fully manage and support the grid services for frequency adaptation and voltage control.

This paradoxical change of vision could produce an electricity grid in which renewable energies could proliferate, always operating at nominal points and at maximum power, and in which grid control would fall entirely on the demand side.

The loads that could be used for this purpose are numerous, but the common factors are that they must be able to have a flexible demand, and so a certain type of inertia, without affecting the end user too much. In this thesis, we go on to analyse the behaviour of a heat pump, at a domestic level, used for cooling the air in a house and how it is able to support the network for providing grid services. To do this, various models are used and implemented in Matlab/Simulink, and case study applications are also presented based on test results.





2 Introduction

At a global level, there is an increasing commitment to reducing CO_2 emissions, as demonstrated, for instance, by the various targets pursued by the European Union through the European Climate Act, which aims for the economy and society to become climate-neutral by 2050 [1]. This has provided the impetus over the last decades to modify the technologies employed across numerous sectors—most notably, the electricity generation sector, which, as reported by EDGAR (Emissions Database for Global Atmospheric Research), has experienced the largest percentage growth in emissions since 1990 (+96% in emissions) [2].

From a scenario in which electricity was primarily generated from fossil fuels, today the global energy mix has progressively integrated new sources, particularly renewables, alongside more traditional ones [3]. Despite the persistence of fossil fuel lock-in and the ongoing construction of new fossil-based plants, electricity generation from renewable sources has been expanding at a remarkable pace. In 2024, global electricity production increased by more than 1200 TWh, over 80% of which was met by clean energy [4]. The leading drivers of this green transformation are wind power, solar energy (primarily photovoltaics), and hydropower [5].

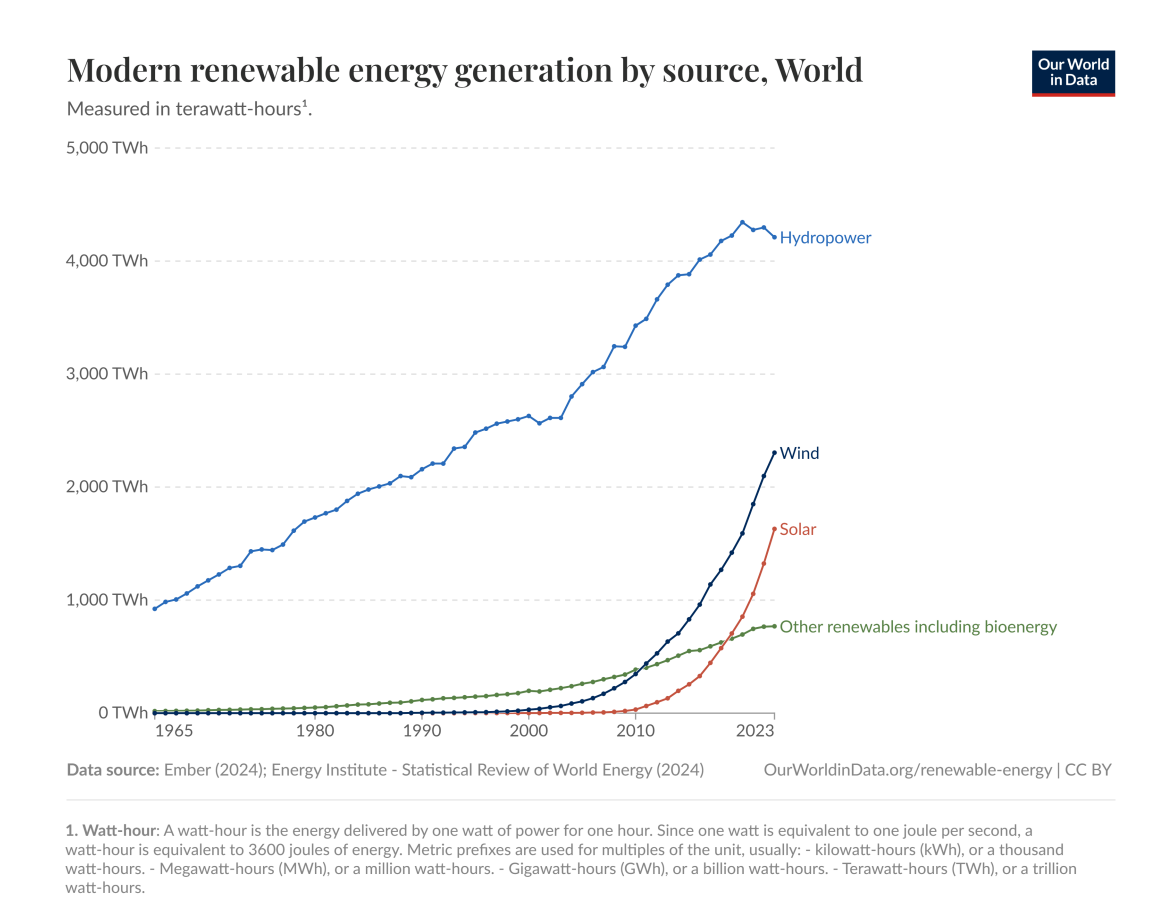


Figure 1: Increase in renewable energy production [5]

The most significant challenges that wind and solar energy ("jointly accounting for 96.6% of all net renewable additions in 2024" [4]) introduce into the power infrastructure are related to their variable (non-dispatchable) generation capacity, the fact that they lead to a low-inertia power system, and, moreover, their lack of inherent capability to store energy or provide support to the grid when needed. This results in an increasing demand for regulation capacities to maintain the system balanced between generation and consumption [6].





To understand the enormous impact of these green energies on the stability of the electricity system, one can consider the events of April 28, 2025, at approximately 12:30 PM (Madrid time), when the entire Spain experienced a widespread blackout that also affected parts of neighboring France and Portugal. The triggering causes are multiple and still not fully understood. The first noticeable sign was certainly an important deviation in grid frequency (nominally 50 Hz in Europe). What is particularly interesting, however, is how the Spanish TSO (Transmission System Operator, REE – Red Eléctrica de España) managed renewable generation, with particular attention to photovoltaic production.

It is important to note that photovoltaic generation is managed in such a way that, during a large grid imbalance, it is disconnected almost immediately (within a few milliseconds [ms]). This led, in the Spanish grid—at that time supplied approximately 53.34% by solar energy (15 GW, practically at its peak capacity) [7]—to a sudden and substantial energy shortfall.

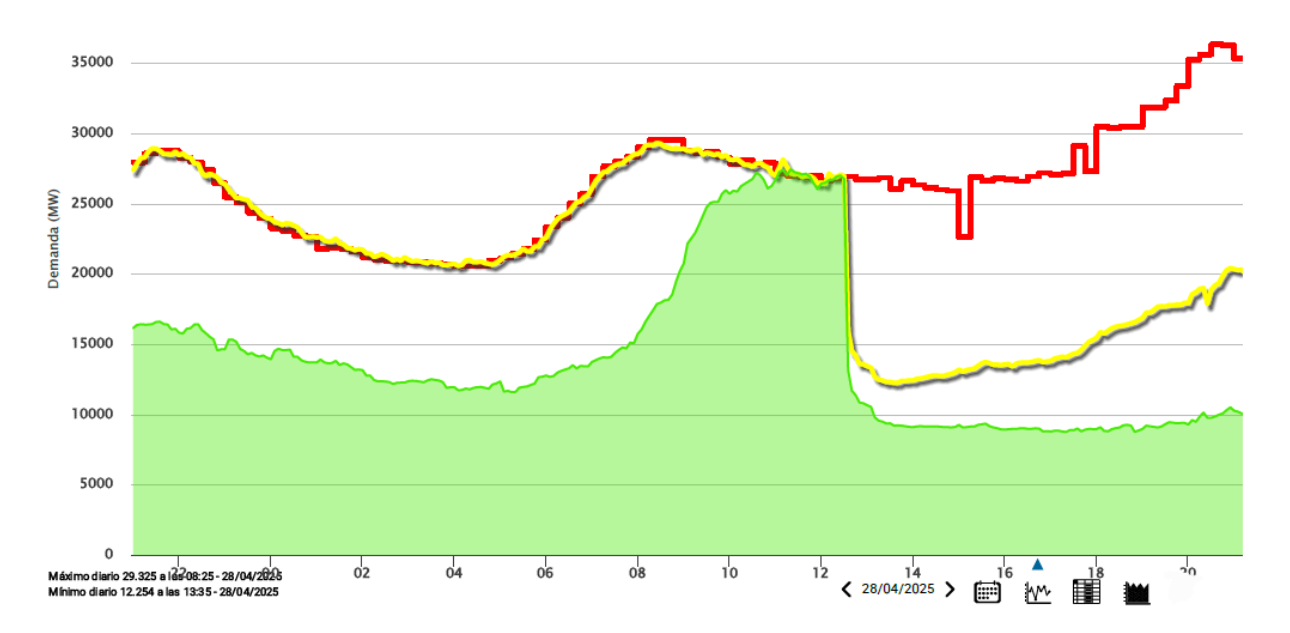


Figure 2: Loss of production during Spain's blackout [7]

In Figure 2, it is clearly observable how the total generation (yellow line) experienced a sharp drop at 12:30 PM, failing to meet the demand (red line). In particular, the green area representing renewable generation undergoes a sudden collapse precisely during those minutes at the national level.

Although various experts, including REE—which is headed by Beatriz Corredor—agree that the full blackout cannot be solely attributed to this contingency [8], there is consensus that there is an increasing shortage of production plants utilizing traditional generating units [9], such as thermal units and gas turbines [10]. These units are the pillars of a fundamental ingredient for power system stability, namely System Inertia, which is a measure of the energy stored in a system. Over the years, with the increasing share of inverter-based resources (IBRs), this inertia has been decreasing rapidly.





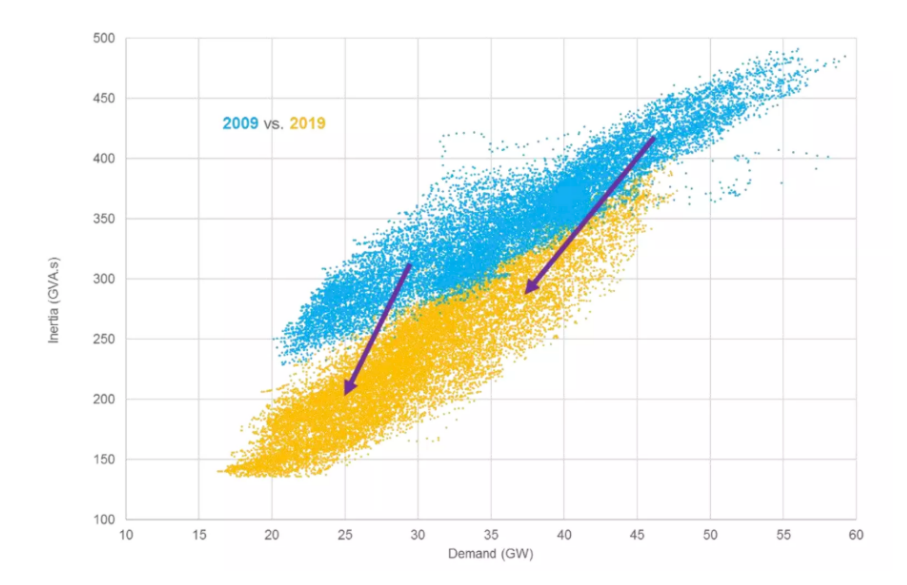


Figure 3: Inertia-Demand 2009-2019 [11]

The curve presented, although specific to the United Kingdom, is highly representative of global trends. It primarily shows how the share of system inertia has decreased uniformly over the years, as well as how it depends on the level of demand from loads. When demand is high—typically during winter peaks—renewable energy is often unable to meet the demand (as is the case for solar), making the use of traditional production plants necessary. Conversely, during the summer period, when demand is lower and the share of renewables in the energy mix is much higher, there is a significant reduction in system inertia.

The Spanish blackout incident was certainly the result of multiple contributing factors; however, the fact that, at that time, approximately half of the demand was supplied by renewable energy—which is unable to provide inertial support to the grid, especially in the summer—undoubtedly played a role in the catastrophic event.

This experience should not generate distrust towards renewable energy; rather, it should drive innovation in the methodologies and approaches used in the field of regulation reserves. Among the potential solutions to mitigate frequency and voltage fluctuations in the grid, Demand Response (DR) programs are playing an increasingly important role. These are "an alternative approach to traditional generating units to provide regulation services for the power system by adjusting the power consumption of loads" [12].

Various types of electrical loads have been tested for these DR programs over the years [13], and it has been observed that inverter air conditioners (IACs) possess multiple characteristics suitable for grid-balancing regulation [14]. What makes these machines even more compelling—which, by their nature, use the same cycle as heat pumps (HP) to produce heat or cold—is that "the electrification of the heat and DH networks is indicated in the European Union's (EU) strategic long-term vision as the main energy transition pathways" [15]. Furthermore, according to the International Energy Agency (IEA), approximately 25% of Europe's final energy consumption is used by the industrial and residential sectors [15], with a very large portion of that dedicated solely to heating and cooling. This means we have a technology that, for obvious reasons, will become one of the most common and widely used in the near future.

Therefore, it is both necessary and of vital importance to study how these machines can also be made active toward ancillary challenges, such as providing grid support.





3 Transformation of the power system

Modern power systems are facing the growing challenge of integrating an ever-increasing amount of renewable energy capacity into their energy mix, which is often granted dispatching priority, alongside the surge in electric mobility and the widespread trend of full digitalization across all sectors [16]. Among renewable energies, as previously mentioned, the primary sources are photovoltaic solar and wind power. The main challenges introduced by these renewables result from their variable (non-dispatchable) energy production, their electrical interfacing with the grid through power electronics—which decouples generation from the grid—, their lack of intrinsic physical inertia (hence referred to as Inertia-Free Generators, IFGs), and the fact that they are currently exempt from providing frequency regulation services [17].

It should be noted that not all renewable energy sources exhibit these drawbacks. Exceptions include constant-speed hydropower plants, biomass/biogas facilities, and first-generation wind turbines that employ variable-slip asynchronous generators, although these are now largely obsolete. This shift has necessitated a complete rethinking of power system design, operation, and protection [18].

A key difference compared to the control and management of traditional power systems lies in the loss of conventional power plants (thermal and hydro), which were able to adjust the injected power simply due to the abundant availability of their primary resources (fuel or gas tanks, or water reservoirs). Moreover, these plants were interfaced through synchronous or asynchronous generators, which were essential for managing voltage and frequency regulation, providing a voltage-source behavior, and supplying system inertia [16]. By introducing these new forms of renewable generation, what is significantly lost is system inertia, primary reserve, and flexibility, all of which must be allocated to other units. Specifically, the reintroduction of HVDC (High Voltage Direct Current) transmission systems in place of AC cables for long distances has also introduced an inertial decoupling between geographically interconnected areas, resulting in an overall reduction of system-wide inertia [19].

Some definitions of previously introduced concepts are provided here to clarify their logical and semantic meanings:

System Inertia: "Inertia in power systems refers to the energy stored in large rotating generators and some industrial motors, which gives them the tendency to continue rotating. This stored energy can be particularly valuable when a large power plant fails, as it can temporarily make up for the power lost from the failed generator. This temporary response—which is typically available for a few seconds—allows the mechanical systems that control most power plants time to detect and respond to the failure" [16].

This property is particularly associated with primary frequency response (traditionally derived from slow-responding mechanical systems), which can also be enhanced by various electronic-based renewable resources, capable of responding many times faster than traditional ones. Furthermore, increasing their share in the energy mix reduces the total amount of inertia required [16].

Flexibility: "the extent to which a power system can modify electricity production or consumption in response to variability, expected or otherwise" [20] or "the modification of generation injection and/or consumption patterns in reaction to an external signal (price signal or activation) in order to provide a service within the energy system" [21].





Reliability: "Operational reliability is the ability of the power system to balance supply and demand in real time by managing variability, ramping constraints, and flexible loads—including immediately following an "event" like a large power plant or transmission line failure" [22].

To maintain these three specifications in modern power systems, it is therefore necessary to reconsider how to operate electric system control using new technologies and methodologies, such as energy storages, demand management programs (like DR), and, in the case of renewable energies, ensuring a certain degree of reserve, curtailing the output power (with the associated loss of generation) [23].

Obviously, solar PV and wind have limited operational flexibility (due to their complete dependence on non-programmable natural factors) and no physical inertia, compared to other more conventional technologies which allow storing the primary resource. However, this should not exempt them from being included in various electric system regulation schemes, from fast primary frequency support [24] to slow secondary frequency control [25], or finally from grid-forming provision [26] [23].

When discussing Europe, it is possible to mention an interesting study, carried out every two years by ENTSO-E and updated on 1 January 2025, aims to identify a common European strategy for achieving all common objectives in the field of electricity infrastructure. To be precise, the study covers all 36 European countries that are members of ENTSO-E, as well as the United Kingdom, Moldova, Georgia, Malta and Med-TSO countries bordering the Mediterranean Sea (Morocco, Algeria, Tunisia, Libya, Egypt, Palestine, Israel and Turkey).

In particular, the report produces a ten-Year Network Development Plan (TYNDP) which "is a biennial European electricity infrastructure development plan. It aims to provide a European-wide vision of the future power system, focusing on how cross-border power transmission and storage can facilitate the energy transition in a cost-effective, secure, and environmentally sound manner" and also "the TYNDP aligns with the European Green Deal and the EU's ambitious climate targets, including carbon neutrality by 2050 and a 55% reduction in greenhouse gas emissions by 2030" [27]. Next, the figure 4 highlights the differences in forecasts between the TYNDP study carried out in 2022 and that of 2024, with a further sub-categorization depending on the time horizon for which the forecast is set. Specifically, the two time horizons, which are independent of each other, are 2030 and 2040, and the discrepancy between the solutions found depends precisely on the targets that the European Union has set itself for these deadlines. Specifically, it is important to note that the study area was not treated as a single entity but rather "the study was performed on the National Trends scenario, which reflects National Energy and Climate Plans and other long-term national strategies" [27].





	In 2030, for the entire area studied		In 2040, for the entire area studied	
	TYNDP 2022	TYNDP 2024	TYNDP 2022	TYNDP 2024
Identified needs (additional to 2025 in TYNDP 2022, additional to 2030 in TYNDP 2024)	64 GW	88 GW	88 GW of cross-border capacity increases 41 GW of storage	108 GW 0 GW of storage
Total transmis- sion capacity (identified needs + starting grid)	184 GW	249 GW	208 GW	269 GW
Increase in socio-economic welfare	5 bn €/year	8 bn €/year	9 bn €/year	13 bn €/year
Avoided curtailment	32 TWh/year	52 TWh/year	110 TWh/year	175 TWh/year
Avoided CO ₂ emissions	38 Mton CO₂/year	31 Mton CO₂/year	44 Mton CO ₂ /year	30 Mton CO₂/yea

Figure 4: Comparison of the main results in TYNDP 2022 and TYNDP 2024

Ultimately, [27] aims to emphasise how the increase in the share of RES is obviously linked to the modernisation and expansion of the European electricity interconnection and how this is necessary from a socio-economic perspective. It also shows how a failure to improve the efficiency of these transmission systems will clearly lead to a forced cut in RES production at peak times (which vary in value and time period in the area studied) and more besides. It is estimated that by applying the TYNDP 2024 with a forecast to 2040, it will be possible to avoid cutting 114 TWh in 2040 in the EU. This result is obviously a warning for the development of RES, as no investor will be interested in seeing their profits cut simply because there is no market to sell to.





4 Power System Stability with Low-Inertia Generation: Evolution and Emerging Approaches

When talking about stability in a power system, numerous considerations must be taken into account. Here, a more specific discussion will be presented on frequency imbalances and current and future regulation methods.

Frequency variations in a system are produced by two phenomena:

- if generation exceeds demand, then the frequency will rise
- if demand exceeds generation, then the frequency will fall

"The size of a frequency deviation is proportional to the size of the mismatch between generation and demand; bigger mismatches lead to bigger and faster deviations. Transient frequency deviations outside of steady state frequency limits only occur if a sufficiently large generation or large demand loss happens over very short timescales" [28].

The methods to address these network imbalances obviously vary from country to country and depend on historical, technical, and economic factors. To highlight some of them, one can mention the structure of the electric grid and the type of interconnection, the mix of national energy resources, the market model, the various regulatory and legislative frameworks in use, and many others.

Regarding European countries, they use a coordinated scheme called ENTSO-E (European Network of Transmission System Operators for Electricity) but then have specific regulations depending on their national TSOs and DSOs.

ENTSO-E specifically prescribes in [29] the frequency regulation procedures following a generation/load imbalance in the grid. Figure 5 shows how the ancillary frequency regulation services are activated sequentially according to the time elapsed since the contingency.

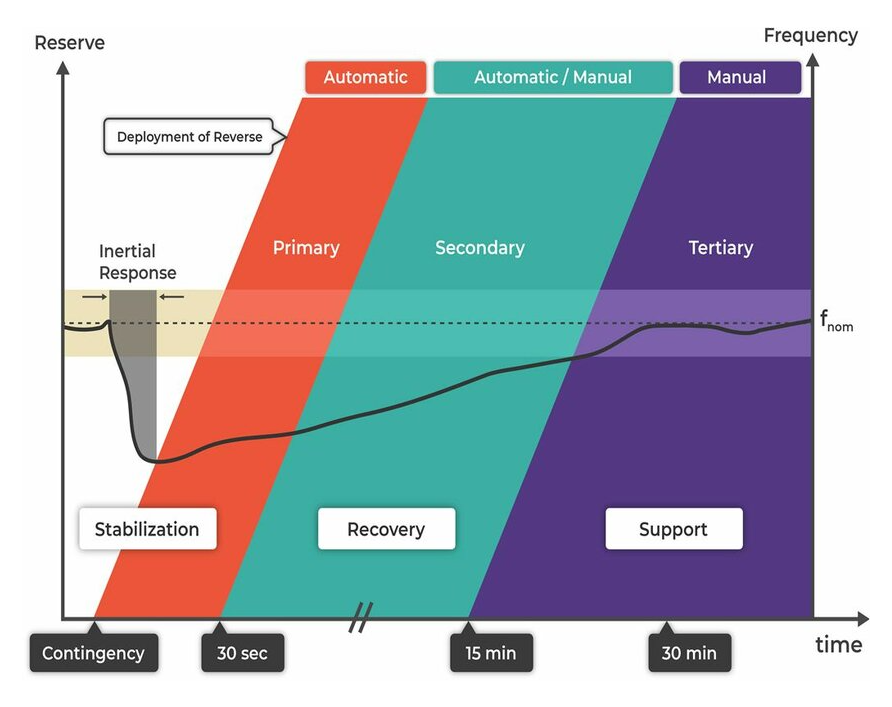


Figure 5: Intervention modes prescribed by ENTSO-E for the sequential activation of controls/regulations [30]





Figure 5 shows the three primary methods for grid frequency restoration.

- **Primary control** (**Frequency Containment Reserve, FCR**): This is an automated and decentralized response provided by all interconnected countries. In the event of a frequency deviation, generating units adjust their output within a few seconds in order to stabilize the system frequency.
- Secondary control (Automatic Frequency Restoration Reserve, aFRR): This is coordinated at the national level (in Italy by Terna) and aims to restore scheduled cross-border power exchanges and bring the system frequency back towards its nominal value within several minutes.
- Tertiary control (Manual Frequency Restoration Reserve, mFRR or Replacement Reserve): This involves manual activation by system operators to replace previously deployed reserves and to re-establish adequate balancing capacity in the system. [31]

By integrating these specific regulations with the historical context of increasing the share of renewable energy, concerns mainly arise for the first two responses: the inertial and the primary response. The inertial response is entirely dependent on the amount of rotating masses directly connected to the grid and is the first to react, responding within the first few moments (500–1000 ms [32]) following the disturbance, capable of limiting the amplitude and rate of frequency oscillation. The primary response, on the other hand, is related to the amount of energy reserves present in the various plants connected to the grid.

Regarding secondary and tertiary regulation, these still depend in their response on more traditional and conventional methods and, moreover, have the advantage of being able to activate "gradually," allowing for a very broad overview of possible interventions.

Going more in detail on system inertia, this is defined by the ability of the rotating masses connected to the system to store or release kinetic energy following frequency imbalances. The kinetic energy stored in a rotating mass of a synchronous generator [MW·s] is defined by the following formula:

$$E_{cin} = \frac{1}{2}J(2\pi f)^2 \tag{1}$$

where $J [kg*m^2]$ is the moment of inertia and f [Hz] is the frequency.

The inertia constant H [MW*s/MVA] or [s] can thus be calculated by dividing the kinetic energy by the rated apparent power of the machine S_n [MVA].

$$H = \frac{E_{cin}}{S_n} = \frac{J(2\pi f)^2}{2S_n}$$
 (2)

Table 1 shows some typical values for rotating machines commonly present in the grid [33].

Type of Machine	Inertia Constant H [s]
Thermal power generators	3–9
Hydropower generators	2–4
Synchronous condensers	1–1.25
Diesel generators	1–3
Synchronous motors	2
Loads, induction motors	0.5–3

Table 1: Typical values of inertia constant *H* for different rotating machines.





Once the inertia constant of a machine is obtained, the *Swing Equation* can be introduced, which describes the disturbed motion of a rotating machine following an imbalance between the mechanical power applied to the shaft P_m [MW] and the electrical power delivered by the generator P_e [MW] [34].

$$\frac{dE_{\text{cin}}}{dt} = J(2\pi)^2 f \frac{df}{dt} = \frac{2HS_n}{f} \frac{df}{dt} = (P_m - P_e)$$
(3)

From this formula, it can be seen that the derivative of the frequency df/dt $[Hz^2]$, known as RoCoF (Rate of Change of Frequency), is inversely proportional to the total system inertia constant $H_{tot} = \sum_{i=1}^{n} H_i$ [s]. Obviously, this total inertia is given by the sum of all the inertias of the machines connected to the system, weighted by their respective rated power S_i [MVA] [35].

$$\frac{df}{dt} = (P_g - P_l) \frac{f_n}{2H_{tot}S_{tot}} = (P_g - P_l) \frac{f_n}{2\sum_{i=1}^n H_i S_i}$$
(4)

In this case, the power disturbance is expressed as a function of the generated power (P_g) [MW] and the load power (P_l) [MW].

It is therefore easy to observe that, as the total inertia H_{tot} decreases, the RoCoF increases, leading to greater frequency oscillations during the transient following a contingency.

"Measuring the inertia level of an electrical power system and the most important indicator of its state of health from the point of view of frequency stability, the RoCoF ... means to determine the "maximum stress" that it can sustain and survive. This implies that under these conditions all the control loops, active power control and protection systems, including defence systems are able to trigger and react in accordance with their system governance settings" [36]. An illustrative example of the described behavior is shown below, where, as the network inertia decreases due to an increase of the share of PV in the energy mix, the aforementioned issues can be observed.





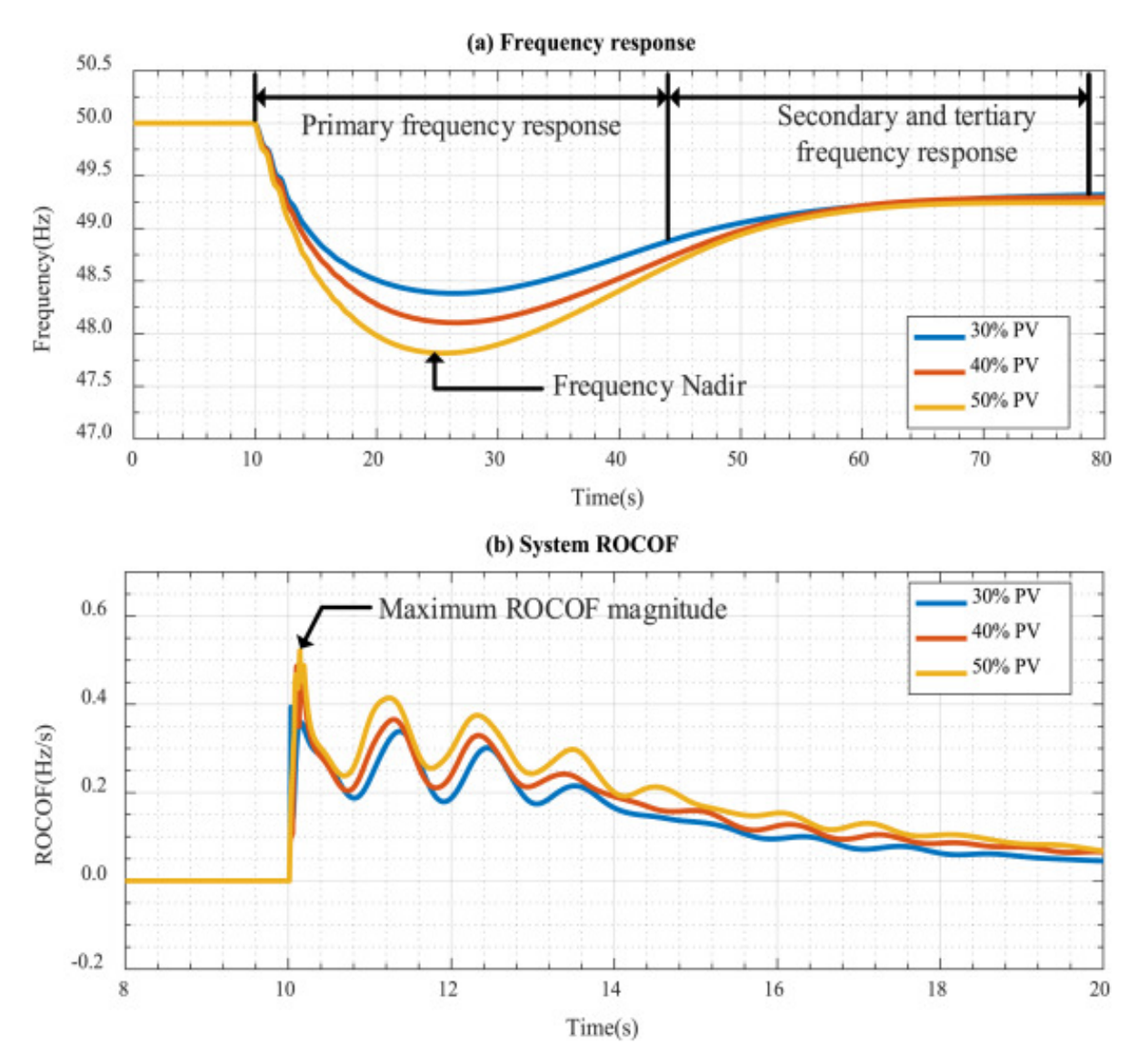


Figure 6: Grid frequency dynamics following a generation loss, with different system inertia values

Supporting this issue of decreasing inertia, as already introduced, it is important to recall that several operating conditions of power networks have already been observed worldwide (Germany, South Australia, Sicily, United Kingdom [33]) in which the contribution of IFGs exceeded 50% of the national energy mix (periods with high solar irradiation and wind availability combined with low demand). Moreover, as a consequence of the stochastic nature of renewable primary sources, it is worth noting that system inertia not only decreases but also becomes time-varying [37].

Referring back to the report drawn up by ENTSO-E, which states that in order to achieve decarbonisation targets through an increase in RES, a vast improvement in European transmission and distribution networks is required, it is important to note that there is also a chapter on electrical inertia. The report states that, considering all the aspects already introduced in this paragraph, "for this synchronous area, ENTSO-E identified an increased challenge to keep frequency stability in all those situations and ensure the effectiveness of emergency measures in extreme cases, e.g. out-of-range events such as system splits of the CE SA" [27].





Figure 7 shows the forecasts for the National Trends scenarios of TYNDP 2022 and TYNDP 2024 for the two different target years (2030 and 2040).

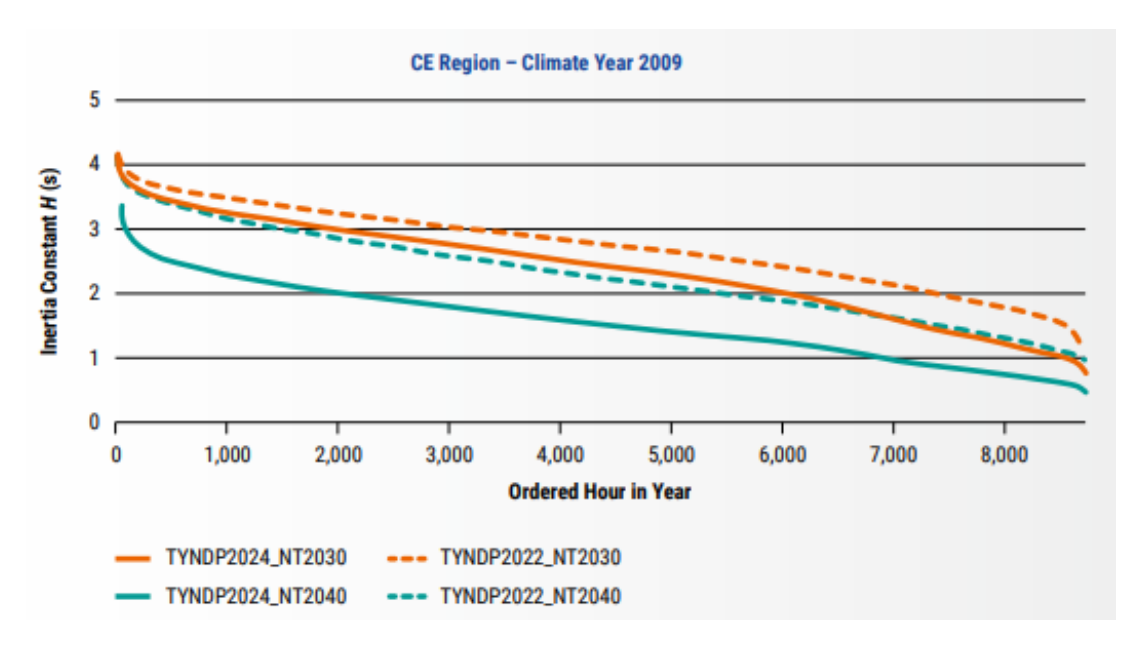


Figure 7: Inertia duration curve of the Continental Europe Synchronous Area

The first observation to make is that the study carried out in 2024, which is therefore more up to date, immediately shows how the estimates made in 2022 to achieve the 2030 and 2040 targets underestimated the impact on reducing inertia. The second feature worth highlighting is how the 2024 forecast for 2040 reduces the inertia curve significantly compared to the same study with a time horizon limited to 2030. This disparity highlights the problem of having to find technical and economic solutions quickly.

The report [27] give also some solutions and states: "Beyond the optimisation of enhanced remedial and preventive measures of the system defence plan, the following solutions will be necessary in terms of network assets or by relevant capabilities and availabilities of system users' installations: Synchronous Condensers; Energy storage with Grid Forming Capability; STATCOMs with Grid Forming Capability and storage; Power Park Modules with Grid Forming Capability and storage."

To conclude this chapter, it is interesting to introduce also the ENTSO-E specifications regarding large frequency imbalances at the European level. These regulations prescribe a load reduction of 10–20% when the frequency drops below 49 Hz, and a further reduction of 10–15% if the frequency disturbance reaches 48.4–48.7 Hz [38]. What is interesting is that this practice directly involves the loads. To date, this protection measure is implemented only as a last resort to prevent extensive damage or total blackouts, and it is developed in two ways:

- **Automatic:** where an immediate intervention is performed by protection systems, such as frequency relays.
- Manual: which is planned and decided by network operators according to the type of problem.

The point is that using loads solely as a last resort is becoming an outdated practice, and today their properties are intended to be utilized in an active and dynamic way, as demonstrated by all the studies going on throughout the Demand Response practices.





4.1 Demand Response

As seen, the constant increase in the share of renewable energy within the energy mix has led to a growing demand for grid regulation capacity to maintain the basic balance between generation and consumption [6]. Concurrently, with the rapid growth and integration of communication systems (ICT), smart and automated sensors, and specialized processors capable of increasing interconnection among all actors in the grid, new control and management methods have been developed [39]. One of these, developed and tested by the U.S. Federal Energy Management Agency (USA) as early as 1975 and called the "Load Management" Program, introduced a new concept in control later defined as Demand Side Management (DSM). The purpose of this is to achieve a variable but controlled evolution of electrical demand over time by modifying and adjusting the power consumed by loads. This idea thus introduces numerous advantages into the electric landscape, such as the possibility of increasing power system stability [40], reducing total system operating costs while ensuring end-user comfort [41], increasing the share of renewable energy, and promoting customer participation within market mechanisms [39]. Some of the operations intended to be achieved through DSM [42] are, for example:

- Peak shaving (or clipping)
- Valley filling
- Load shifting
- Strategic load reduction (conservation)
- Strategic load growth
- Flexible load shape

The capacity and amount of load power available from a DSM perspective vary and generally increase over time, obviously depending on the normal evolution and growth of global electrical load (+4.3% in 2024 [4]), the continuous innovation and integration of intelligent communication systems, as previously mentioned, and last but not least, the degree of customer participation. Specifically, there are various possibilities to manage loads and consumers depending on the actors actively participating in the grid, such as the Transmission System Operator (TSO), the Distribution System Operator (DSO), load aggregators (LA) of various sizes, prosumers, or simple consumers with small-scale loads.

In parallel with the various studies introduced on DSM, an increasingly economic approach has been integrated to increase and incentivize the number of consumers—and therefore the amount of controllable load—participating in these programs. Numerous examples exist of time-dependent tariffs, such as the Time-Of-Use (TOU) rate based on dividing the year into periods with different tariffs used to shift consumption toward low-load hours, the Real-Time Pricing (RTP), which is a more precise evolution of the former, and finally the Spot Pricing (SP), where the tariff is defined a few moments before its application [43].

As previously introduced, the actors involved in the electric grid are varied, and consequently, the type of load management that can be implemented may differ depending on the degree of customer participation. An example already mentioned is the case of Load Shedding (LS), in which the System Operator cuts off power to various loads in emergency situations, giving priority only to some; in this case, there is no free or voluntary participation by the customer. In the case of Interruptible Load Management (ILM), on the other hand, the System Operator and customers agree on which loads can be reduced in exchange for specific compensation. Other examples include Real-Time Pricing (RTP), where the cost of electricity varies and is





communicated in advance by the producer/distributor to the consumer, leaving them free to decide whether to take advantage of it; Direct Load Control (DLC), which aims to modify the load pattern based on the network's ability to accept supply changes relative to standards [43]. A final example, where the previously mentioned economic incentives are particularly used and studied, is in the case of Demand Response (DR) programs. DR refers to "changes in electric usage by end-use customers from their normal consumption patterns in response to changes in the price of electricity over time, or to incentive payments designed to induce lower electricity use at times of high wholesale market prices or when system reliability is jeopardized" [39]. The concept of DR varies greatly depending on where it is implemented, whether in a Smart Grid or a larger interconnected system, on the type of incentives, classical or market-based, and on the characteristics of the loads (controllable, deferrable, curtailable, or critical ones [44]). To provide a careful geographical overview, today DR programs are mainly concentrated in Europe, North America, and East Asia [45], as shown in Figure 8.

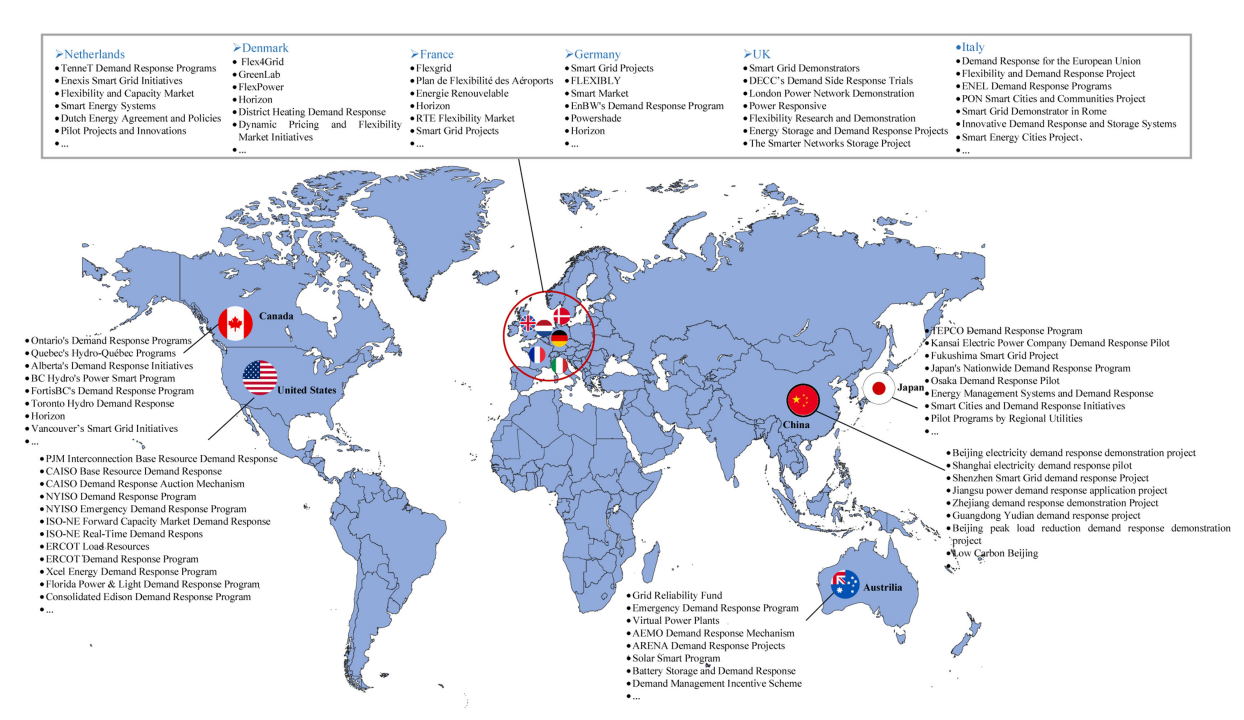


Figure 8: DR programs around the world [45]

It should be emphasized that, although all these regions aim to achieve a general energy efficiency improvement in the system while also promoting the increase of the renewable share, the operational mechanisms used to achieve these goals are obviously different, shaped by technologies, industrialization, state and political targets, and territorial geographies.

In Europe, the introduction of DR programs primarily aims to promote the share of renewable energy in view of the much-discussed and acclaimed energy independence [46] associated with Climate Neutrality [1]. In North America, on the other hand, DR projects are more focused on reducing electricity consumption peaks during certain periods of grid overload. The last example is China, where years of industrialization and intensive urbanization promoted by the state itself [47] to become a global superpower have polluted and made various metropolises in the country nearly uninhabitable. Here, DR projects aim at reducing pollution, as evidenced by the "Low Carbon Beijing" project [48].

As mentioned, the objectives of implementing DR projects are varied, as are the technologies deployed to promote them. Depending on the type of customer targeted—industrial scale [49],





[50], commercial [51], [50], public organization [51], or residential/household [50]—the capabilities and control possibilities will differ.

The systems and technologies used to implement DR projects are diverse, but what they have in common is the enormous amount of data generated and the absolute necessity to analyze it in order to obtain the best economic and energy strategies. The technologies employed include Smart Meters, capable of obtaining bidirectional, real-time measurements of consumption; the Internet of Things (IoT), which generally creates an intelligent network able to "recognize" and connect all devices for distributed and automated load control (notably, studies have been conducted on the use of Blockchain to securely and accurately transfer the collected data [52]); various algorithms and Artificial Intelligence (AI) to optimize the response of interconnected devices; and cloud-based aggregation platforms to aggregate and manage hundreds of devices capable of DR procedures, which can be at the residential level, as in the case of Home Energy Management Systems (HEMS) [53], or commercial/industrial Building Energy Management Systems (BEMS) [54].

One of the most important barriers to the widespread adoption of these DR programs is the protection of participants' private information. Indeed, participants cannot, and often do not want to, fully share their personal data regarding consumption and consequent economic decisions, which reduces the effectiveness of DR and what could be the optimal choice by the various actors involved [48].

4.2 Demand side response

DR programs, as mentioned in the previous paragraph, act as intermediaries between producers or retailers and consumers to shape the load curve in order to maintain grid stability, achieve energy savings, and also economic savings.

In this paragraph, the focus will be solely on analyzing the structural support that certain loads can provide within an interconnected intelligent electrical grid (Smart Grid SG or Super Smart Grid SSG). By SSG, we mean a grid capable of transferring electricity from centralized and decentralized generation resources located across a wide geographical area, required to manage demand and generation response [55].

As already mentioned, one of the main problems is the reduction of flexibility and inertia of the entire power system, due to the high penetration of renewable energy generation, and how to maintain the entire system balanced and in synchrony in the new scenario that is developing [16], [18].

To address this complex issue, various studies over the past several decades have been promoting the rather revolutionary idea of placing the responsibility for compensating the aforementioned shortcomings on the demand side (understood as electrical load). This approach is generally called Demand Side Response (DSR) and is defined as the changing of end-users' demand patterns in response to an external signal [56], and the methods proposed to implement it are indexed under the term Load Resource Management (LRM).

When modeling the loads used for this DSR technology, it is important to identify appliances that have a certain degree of freedom and independence from the consumer, such as thermal loads (Thermostatically Controlled Loads (TCLs)), which can be interrupted or managed in power, for a limited period, without causing significant discomfort to the user. These loads must have the ability to provide support to the voltage and frequency of the entire grid; indeed,





there are various studies on the applications of loads in Fast Frequency Control (FFC) [14], [57], [58], [23] and Voltage Support (VS) [58], [23].

Looking also at the latest advancements in these technologies, the literature discusses the concept of grid-forming load, which can be considered as a fully flexible demand capable of supporting grid stability and additionally ensuring that the "load is actually contributing to form the grid and to provide synchronization power to the overall system. In this sense, the new concept allows running a system powered only by renewables operating at maximum power (or operator defined set-point) in grid-following mode, while the overall system control is ubicated in the demand side. This is an important change of paradigm as it considers that all the flexibility, synchronism and stability provision is on the demand side. This concept can applied either to isolated systems or also to future power systems, where millions of loads steer the power system while the renewables are operating at full power" [23].

In order for these loads to be effectively integrated into this new vision, they must be equipped with specific characteristics. Leaving aside the concept of "forming the grid," which today is somewhat paradoxical as a load contributing in the same manner as a synchronous generator, it is still possible to talk about grid support. Specifically, these loads should be able to emulate traditional mechanical inertia (virtual inertia [35]), thus reducing RoCoF, have the capability to distribute active and reactive power among multiple resources (power sharing), dynamically support the grid against disturbances (faults or load/generation variations), operate in islanded mode, and be compatible with DR programs.

4.3 Panoramic on possible loads application

The idea of using electrical loads and residential appliances, even small-scale ones, to provide voltage-frequency support to the grid is therefore becoming increasingly adopted since the concept of smart loads was introduced. These loads must be able to go beyond the simple concept of optimizing their consumption and ensuring end-user satisfaction; indeed, they must use their **flexibility** to also provide frequency and reactive power reserves [58]. The characteristics that these loads must possess are numerous, as described in the previous paragraph, and generally also depend on the context in which they are used. Many studies of this type exist within Microgrids [59], [60] or Smart Grids. Obviously, the concept of flexibility also depends on the size of the load, that is, whether it is individual or part of a load aggregation. In the case of individual appliances, some possible definitions of flexibility are introduced:

- 1. Acceptable Delay Time (ADT): maximum period of time to postpone the operation of an appliance without sacrificing the consumers' comfort [61].
- 2. Appliance Flexibility Index (AFI): is a measure of the adjustable range of time of the appliances [62].
- 3. Maximum Interruption Time (MIT): maximum period of time for which the operation of an appliance can be interrupted once it has started, without compromising its functionality or user comfort.
- 4. Demand Flexibility Range (DFR): maximum adjustable power reduction (or increase) of an appliance without compromising its service

These definitions require a high level of knowledge and forecasting of the consumer's preferences (obtained through questionnaires or surveys), of their possible load demand curve, and





also of the production curve, in order to match them and support the grid in the long term.

Regarding the methodologies mentioned previously, they can be categorized into two types based on the time period in which the load flexibility is used to support the grid. Specifically, if it is done immediately and in the short term, it is referred to as support for increasing the Reliability, Safety, and Productivity of the grids (Power-based); otherwise, if the support occurs over a longer time horizon, it is referred to as network development in terms of its Profitability (Energy-based).

One of the first studies conducted with the idea of enabling loads to be used as frequency controlled reserves (DFCR) was carried out on an island in the Baltic Sea, Bornholm, which is connected to the Nordic transmission grid by a 60 kV under-sea cable. Approximately 70 DFCR appliances with programmable thermostats and controlled hardware were used. It was observed that "the tests show that a population of refrigerators was able to deliver frequency reserves approximately equal to their average power consumption. Electric space heaters in the autumn season were able to provide frequency reserves of a magnitude 2.7 times their average power consumption" [63]. The result obtained was therefore a success and immediately highlighted the still untapped potential of loads if used correctly.

The same study, although conducted in 2013, makes a very important remark regarding the difficulty, still valid today 17 years later, of implementing these techniques: "Today, many loads are equipped with microprocessors running firmware for controlling local processes. These loads could be programmed to actively monitor the state of the power system as a whole and schedule their own power use to help balance consumption with production. Despite the declining cost of communications devices, providing a real-time digital communications interface from a system operator to small loads represents a significant cost barrier to widespread deployment" In the same way, it provides a very practical solution, already introduced previously: "However, there is already a parameter which is universally available to indicate the instantaneous balance of electric energy production and consumption, namely the system frequency.

The relation between power generated, $P_M(t)$, power consumed, $P_L(t)$, and deviations in system frequency, $\Delta f(t)$, is given by the swing equation:

$$\Delta P_{\rm M}(t) - \Delta P_{\rm L}(t) = 2H \frac{d\Delta f(t)}{dt} + D\Delta f(t)$$
 (5)

where H is the inertia constant, and D is the load damping coefficient.

Loads may measure the system frequency and by adjusting their power consumption up or down as the system frequency rises or falls, they are able to provide reserves for frequency regulation. This concept is known as demand as a frequency controlled reserve (DFCR)" [63].

It follows that it would be sufficient to develop microprocessors that are intelligent, fast, and dynamic enough to capture these frequency movements and apply them to flexible loads in order to immediately support the grid.

4.3.1 Heat Pump

"Air conditioning (AC) has become the fastest-growing energy end-use in buildings worldwide, and its adoption is expected to increase further due to various socioeconomic factors and climate change" [64]. That said, it is evident that Heat Pumps will be a crucial resource for achieving the European Carbon Neutrality goals by 2050.

According to Eurostat data, 50% of all consumed energy is used for cooling and heating, and unfortunately more than 70% of this still comes from fossil sources (mostly Natural Gas). At





the residential level alone, it is estimated that 80% of final consumption is used for space and water heating [65], and of this, 50% is solely dedicated to providing indoor thermal comfort through heating, ventilation, and air conditioning (HVAC) systems [66].

Another interesting fact is that cooling, especially in humid environments, requires energy-intensive consumption, even in the most energy-efficient buildings, ranging from 90–180 kWh/m² per year, unlike heating, whose values are around 15 kWh/m² [67].

From this, the obvious conclusion follows that Heat Pumps will be a fundamental technology for the future due to their ability to electrify this sector and thereby take advantage of the growth of renewable energy. An IEA report from 2022 predicted that by 2030, the latter could reduce European gas demand by at least 21 billion cubic meters [68].

The load appliances that provide thermal energy services (those using a thermostat, TCL) are well suited to follow and adapt to grid fluctuations due to generation, as their inherent heat capacity (like that of a house or building) acts as an energy storage device, allowing for a temporary reduction or shifting of power demand without significantly compromising end-user comfort [63].

One of the applications studied for these Heat Pumps is Fast Frequency Response (FFR) services, used to balance the grid within a few seconds (1–2 seconds) [14]. In fact, at the residential level, these are equipped with a compressor that can be quickly modulated in its rotational speed, thanks to the fact that they are compact in size and therefore have a lower rotational mass to overcome. Obviously, the consequences are immediate at the application level; modifying the speed, from an FFR perspective, means changing the power required and therefore obtaining a different heat exchange than the norm (the result of internal heat pump logic), which leads to a degradation of the set-point temperature and sub-optimal energy consumption. Still in the context of FFR, it should be noted that the service is a matter of seconds, which leads to current energy consumption that is not so different from the norm, in addition to the fact that this technology is also used because it has considerable thermal inertia, thus almost cancelling out the negative effect on temperature.

4.3.2 Electric vehicles

Electric vehicles (EV) are considered as one of the three main technologies that will contribute to the energy transition [69]. The number of electric vehicles is rapidly increasing, just in 2023 there are more than 40 million of EVs (+12 millions sales in one year) [43].

The Standard IEC 61851 defines an Electric Vehicle as: "any vehicle propelled by an electric motor drawing current from a rechargeable storage battery of from other portable storage devices (rechargeable, using energy from a source off the vehicle such as a residential or public electric service), which is manufactured primarily for use on public streets, roads or highways".

By combining their rapid expansion with the fact that they have also been identified as potential candidates for grid's frequency regulation, these EVs become a key technology for our future.

It's estimated that these vehicles remain parked for more than 90% of their lifespan [70]. Given this data, it's clear that EVs can serve as a flexible load. The end-user isn't concerned with the specific method or logic used to charge their car when it's parked for several hours; they simply need to find it ready when they need it. The only exception to this flexibility occurs when the consumer requires a fast-charge [23].





All of this introduces significant opportunities and challenges for EVs, giving rise to concepts such as smart charging, Grid-to-Vehicle (G2V) and its impact on the distribution network, Vehicle-to-Grid (V2G), or more generally, Vehicle-to-X.

The concept of an EV's charge is expressed by the battery's State of Charge (SoC), which is:

$$SoC(t) = \frac{Q(t)}{Q_{\text{nom}}} \times 100\%, \tag{6}$$

where Q(t) is the remaining charge (Ah) at time t and $Q_{\rm nom}$ is the nominal capacity (Ah). What introduces flexibility into the concept of charging is that we can choose how to recharge the battery in order to reach the *final range allowed* at a specified time (h). Figure 9 shows all the area where it's possible to operate to achieve the predefined point, remembering that increasing the SoC means charging the battery, but "going down" and so discharging means applying a V2G idea to give operational flexibility to the grid and so support in some way the system. In the same figure it's also possible to observe the two extreme charging strategies, which define the boundaries for more general Grid-to-Vehicle (G2V) charging. On one hand, there is the Minimum Time (MT) strategy, characterized by the immediate charging of the car's battery. On the other hand, there is the Most Delayed (MD) strategy, with charging delayed as much as possible depending on the constraints on the final value.

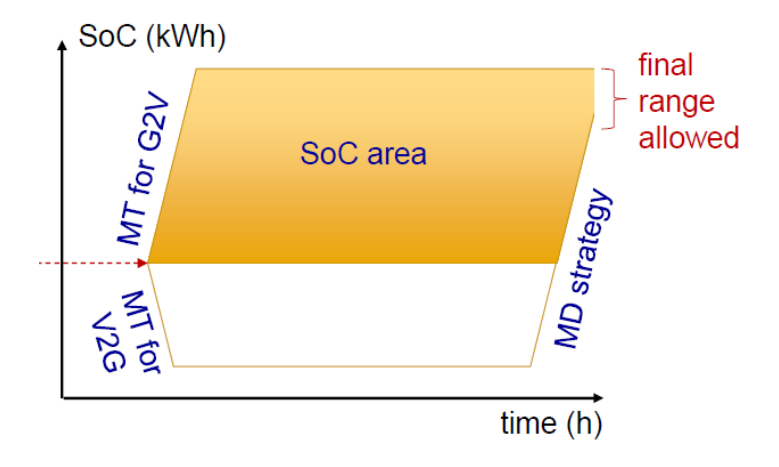


Figure 9: SoC area of possible operation

The opportunities and scenarios that arise are, of course, dynamic and highly dependent on the existing infrastructure. There are some positive examples, such as in California, where the growth of the EV fleet has been politically and technically associated with the rise of Variable Renewable Generation (VRE), allowing them to actively participate in local flexibility [43].

CEN-CENELEC (the European standardisation body) define the smart charging as follows: "... when the charging cycle can be altered by external events, allowing for adaptive charging habits, providing the EV with the ability to integrate into the whole power system in a grid and user-friendly way".

Supporting the ability of EVs to increase grid stability, the paper [71] states that Plug-in Electric Vehicles (PEVs) can be used as "battery storage devices for grid support via the Vehicle-to-Grid (V2G) concept" to "reduce frequency deviation, resulting in microgrid stability." Furthermore, the paper [72] even declares that EVs "have been identified as the major frequency regulation agents (on the demand side) due to their inherent ability to provide instantaneous frequency support."





4.3.3 Electrolyzers

Recently, hydrogen electrolyzers (that use the hydrogen electrolysis that is an electrochemical process that uses electrical energy to split water (H_2O) into its constituent elements, hydrogen (H_2) and oxygen (O_2)) due to their ability to operate as flexible loads, have been increasingly integrated into systems capable of participating in Demand Response programs. It has been found out that this technology has the capacity to provide many ancillary services to modern electricity grids. Their unique feature of producing hydrogen by consuming electricity, and subsequently using the same hydrogen to regenerate electricity, when coupled with physical hydrogen storage, enable these systems to fulfill a dual function: producing hydrogen for endusers while offering grid balancing services, thereby ensuring greater economic feasibility. For instance, they can absorb electricity during periods of surplus or, when paired with fuel cells, generate electricity during peak demand, contributing to overall grid stability [73]. Another fundamental characteristic is that they are able to adjust their power consumption

Another fundamental characteristic is that they are able to adjust their power consumption within fractions of a second, which makes them suitable for implementation in frequency response technologies, as mentioned in [74], in FFR as proposed in [75] and in many other ancillary services, including voltage control, congestion management, and black start [73].

4.3.4 Others

In addition to the most well-known flexible loads mentioned above, numerous other domestic and industrial loads can be considered, where it is possible to control energy demand and use it for various grid services [23].

However, it is important to mention one last category of fundamental importance: Energy Storage Systems.

The CEI 0-16 Italian standard [76], which refers to the European standards, specifically the EU Regulation 2016/1388 (DCC - Demand Connection Code), considers a system as an energy storage system if it is defined by the following three parameters:

- A set of devices and control systems
- Used to absorb or deliver electricity
- Operating in continuous mode in parallel with the distribution network, or suitable to alter the energy exchanges with the network (input from or injection into), even though determined by voluntary disconnections/reconnections of part of the system or the whole system

As for the other technology the main objective of storage is to enhance system flexibility by improving power quality (voltage regulation and mitigation of network disturbances), supporting network management (frequency control, oscillation damping, system reinforcement, and stability enhancement), and enabling efficient energy management (storing energy for later use, facilitating market participation, increasing efficiency in multi-energy systems, and optimizing the use of existing resources)[43].

To give a general idea of the types of flexibility that can be provided (in terms of response time and energy capacity) depending on the storage technology used, the diagram of Figure 10 is shown.





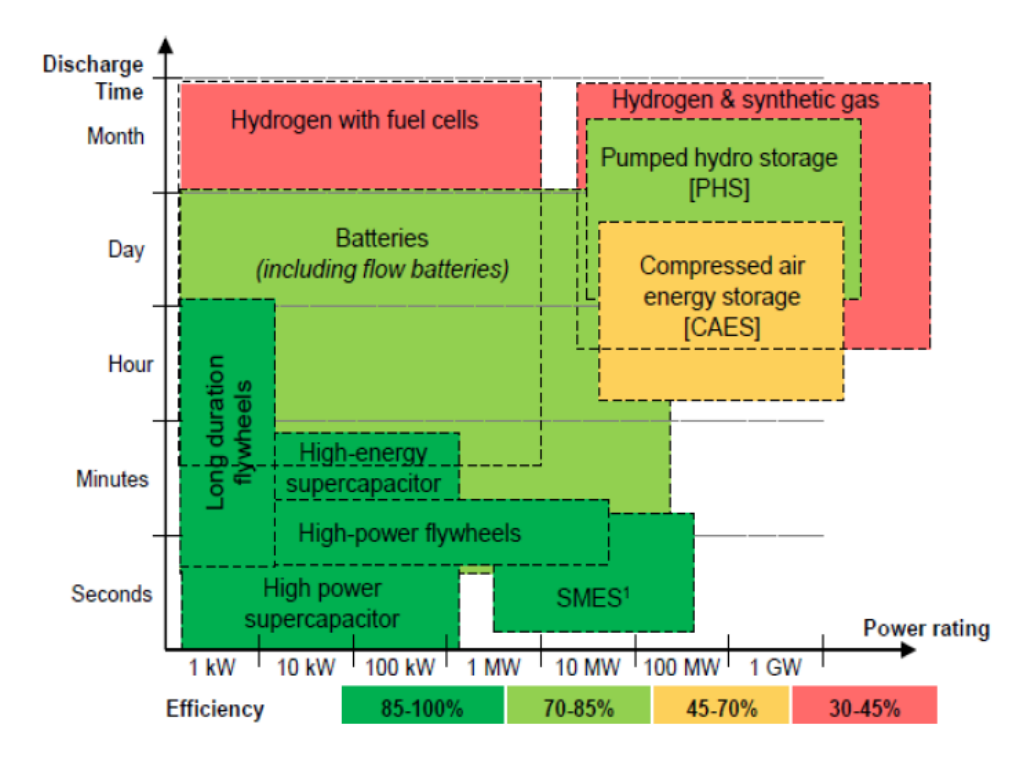


Figure 10: Energy storage technology [43]

Therefore, mainly for this technology, thanks to its wide range of characteristics, it's possible to say that energy storage can help address challenges associated with high renewable penetration by smoothing variable generation, minimizing RES curtailment, reducing reserve requirements during RES-dominated periods, stabilizing electricity prices in systems with significant wind power [30], and limiting the need for new infrastructure as demand grows [43].

The final consideration regarding these technologies is that they are generally very expensive (although prices have been decreasing over the years due to technical development) and, by their nature, they are additional elements to be integrated into the electrical system rather than already physically present, as is the case for the loads presented in the previous sections. Therefore, it is essential to ensure that their appropriate sizing and operational strategy are carefully defined.





5 Heat Pump model

The heat pump studied in this thesis is modeled based on an existing model available in the Simulink libraries, called *Refrigerant Cycle* (*Air Conditioning*) [77], which can be generated in MATLAB using the following line of code:

openExample('simscapefluids/RefrigerationCycleAirConditioningExample')

Model

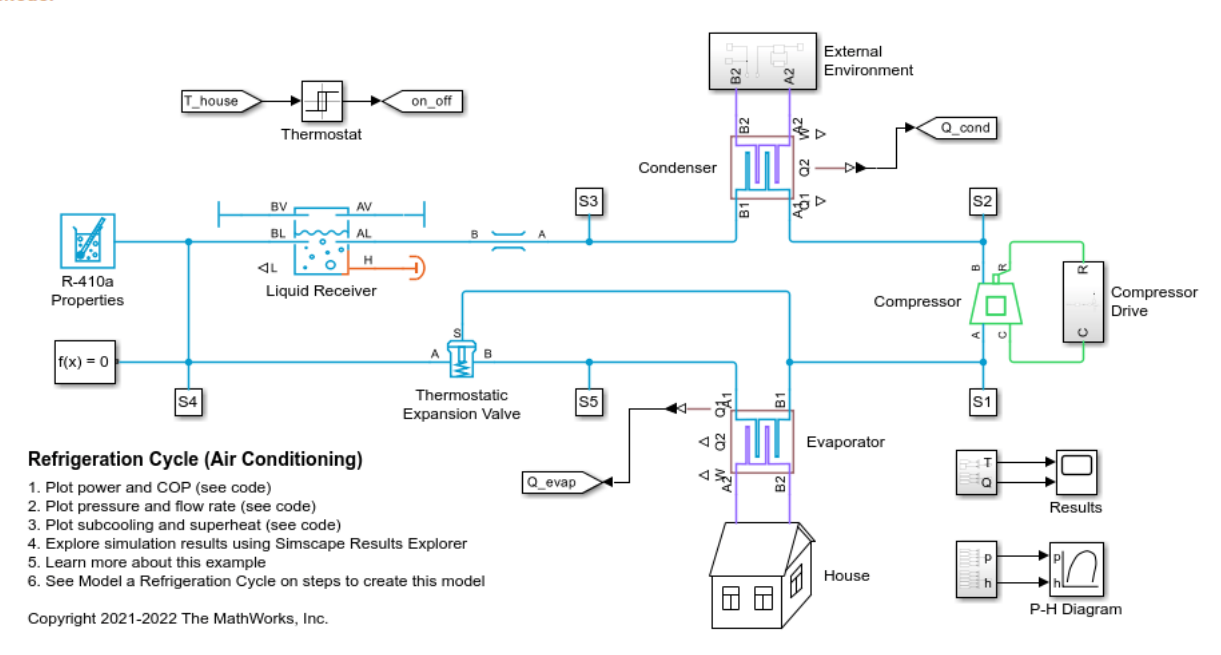


Figure 11: Simulink Heat Pump model

In [77], the system is defined as follows: "The refrigerant in this system is R-410a. The evaporator absorbs heat from the air in the house and turns the refrigerant into a superheated vapor. The compressor then pressurizes and drives the refrigerant through the condenser, where the heat absorbed by the refrigerant and the compression work is rejected to the external environment. This causes the refrigerant to condense into a subcooled liquid which is then stored in the liquid receiver. The valve controls the amount of refrigerant that flows from the liquid receiver to the evaporator to maintain the desired amount of superheat. The valve also causes a drop in pressure which cools the refrigerant and allows it to absorb heat in the evaporator.

The cooling load in this model is the house, represented as a volume of air in the moist air domain. A thermal network models heat transfer between the hot external environment and the air in the house via the walls, roof, and windows. Additionally, occupants and appliances generate heat inside the house. A fan circulates air between the house and the evaporator for cooling. The system is controlled by a thermostat which turns the system on and off to maintain a temperature of 22 °C".

The differences between the model implemented in this thesis and the standard Simulink model are several and will be described in detail in the following sections. However, what remains unchanged is the theoretical foundation of the refrigeration cycle.

In order to provide a further explanation of what is meant by the theoretical cycle of a refrigeration machine, in addition to the very practical yet correct description given by MATLAB, it can be stated that a refrigeration machine is a heat engine, namely "a set of devices that collectively realize a cyclic process, during which the machine exchanges heat (with at least two sources)





and work with the external environment" [78].

In this case, thermal power $\dot{Q}_{\rm C}$ and $\dot{Q}_{\rm E}$ are exchanged with two thermal reservoirs at temperatures $T_{\rm C}$ (external environment) and $T_{\rm E}$ (internal house), respectively, with $T_{\rm C} > T_{\rm E}$.

More precisely, a refrigeration machine is a purely dissipative device that employs mechanical energy (supplied to the Compressor) in order to achieve, as its useful effect, the cooling of the low-temperature reservoir at $T_{\rm E}$. Consequently, the useful output of the system is the thermal power removed from this source ($\dot{Q}_{\rm E}$).

The thermodynamic cycle performed by these machines is fundamentally based on the reversible Carnot cycle, but is then modified by introducing practical considerations such as design choices, plant engineering constraints, efficiency improvements, and the inherent irreversibilities that occur in real processes.

The refrigeration cycle illustrated above consists of the following transformations:

- $1 \rightarrow 2$: Isoentropic compression
- 2 \rightarrow 3: Heat rejection $\dot{Q}_{\rm C}$ at constant temperature in the condenser
- 3 \rightarrow 5: Joule–Thomson expansion through the throttling valve
- 5 \rightarrow 1: Heat absorption $\dot{Q}_{\rm E}$ at constant temperature in the evaporator

Given the theoretical explanation of how the cycle works and the actors involved, both in the basic model proposed by Simulink and in the one implemented in this thesis, it is important to highlight the main difference between the two models: the type of control applied to the compressor. The Simulink model adopts an ON-OFF control strategy, which activates or deactivates the compressor and the fans when the temperature falls below 21 °C or rises above 23 °C, respectively. By contrast, this thesis proposes the use of a dynamic and continuous control strategy, which represents the most advanced solution currently available on the market thanks to its superior energy and economic performance.

Subsequently, the model under examination in this study is presented, showing also the subsystem of the External Environment and of the House Subsystem.

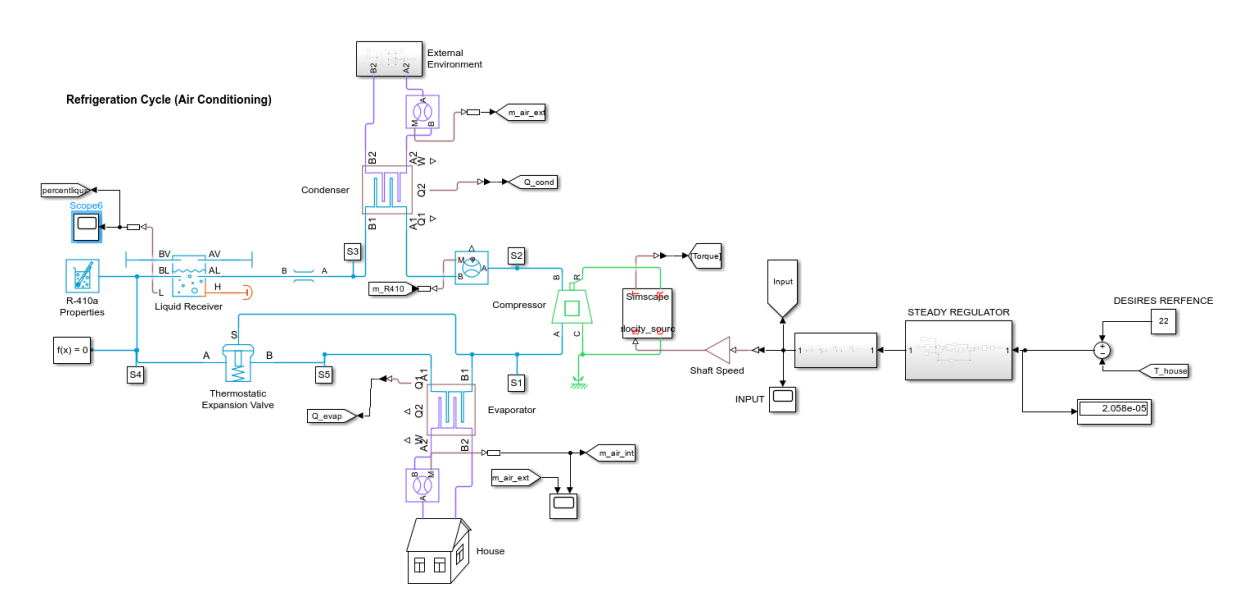


Figure 12: Simulink Heat Pump model implemented





External Environment Subsystem

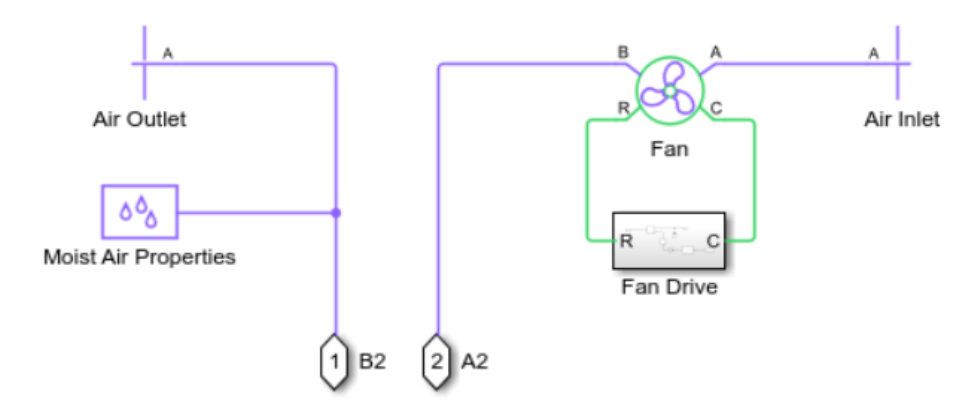


Figure 13: External environment subsystem on Simulink

House Subsystem

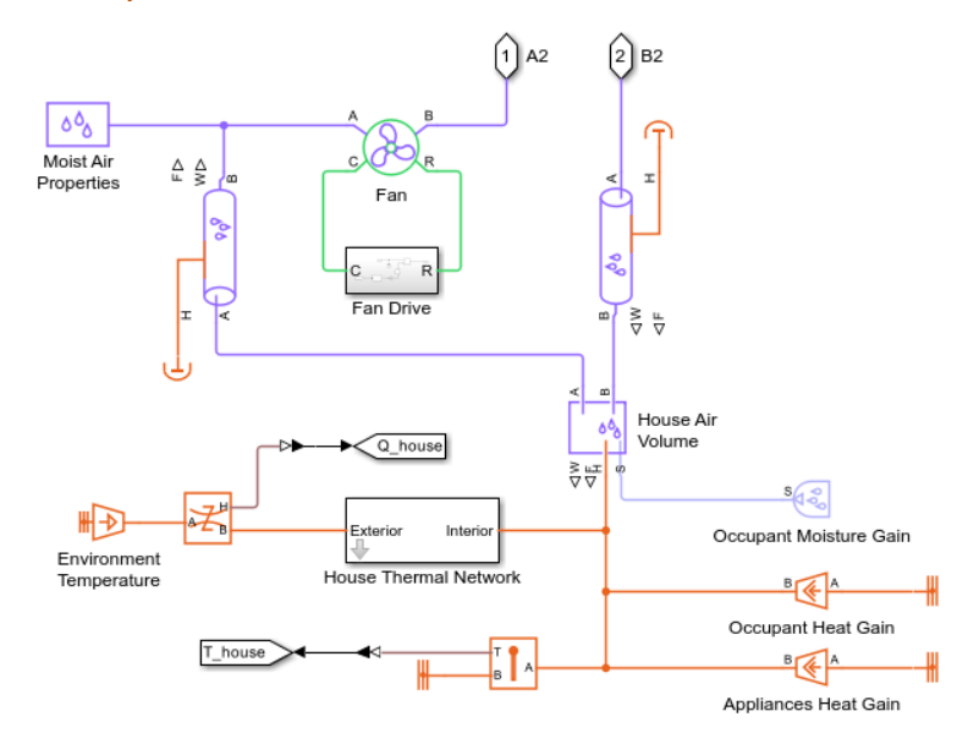


Figure 14: House subsystem on Simulink





5.1 Liquid refrigerator R-410A

The use of R-410A refrigerant gas is mainly dictated by a preset Simulink programme that develops the characteristics of this gas on all devices included in the thermodynamic cycle.

To provide some general context for the development of these gases for this type of technology, historically various chemical families have been used and gradually phased out due to their significant contribution to specific environmental issues. The best gases were those known as chlorofluorocarbons, which contained chlorine, carbon and fluorine (CFCs). The main problem is that when there were leaks or decommissioning of plants, these halogenated fluids, when transported to high altitudes due to convective motions, decomposed due to solar radiation, releasing chlorine which, when in contact with ozone (O_3) , acts as a catalyst and reduces it. All this led to what was a huge problem about 50 years ago, namely the destruction of the stratospheric ozone layer. To address this problem, the Montreal Protocol (1987) [79] was created, which completely banned the use of F-gases containing chlorine and bromine. To monitor the contribution of a substance to the depletion of the ozone layer, the ODP (Ozone Depletion Potential) index was introduced, which uses trichlorofluoromethane (CFC-11) as a benchmark. Nowadays, substances with very low or even zero ODP are generally used in refrigeration cycle applications.

The next problem that arose was that of the anthropogenic greenhouse effect [80], i.e. all those additional emissions of various pollutants due to human activities that increase global warming. To take into account the contribution of a substance, or in this case a gas, to the greenhouse effect, the GWP (Global Warming Potential) was introduced, which takes the contribution of CO_2 as its base case (GWP $CO_2 = 1$) [81].

$$GWP_{total} = \sum_{x} (GWP_x \cdot q_x)$$
 (7)

where x represents each molecule present in the substance multiplied by the percentage weight q it occupies in the substance [81].

Each GWP must be analysed (and integrated) over a specific time interval called the Integral Time Horizon (ITH), which is generally 20, 100 or 500 years. This is because the GWP is extremely dependent on the average life of the substance in the atmosphere, i.e. if it decomposes and neutralises quickly, the GWP will certainly be lower. Substances with good GWPs are, for example, HydroFluoroOlefins (HFOs), which have a very low average life and can also be used for open compressor applications.

These are the two environmental parameters that must be taken into account when choosing a refrigerant, but in addition to these, the energy efficiency of these fluids must also be considered in order to keep consumption low, as well as their intrinsic safety, such as their toxicity to humans and the ease with which they can ignite.

That said, R-410A is a near-azeotropic HFC refrigerant gas blend composed of 50% R-32 (difluoromethane) and 50% R-125 (pentafluoroethane) developed mainly to replace R-22 in new air conditioning equipment (it is not suitable for retrofitting existing equipment working with R-22) . R-410A is currently the leading refrigerant used in residential and commercial air conditioning. It has an ODP of 0 but a GWP of 2088, which is extremely high [82].

The following table summarises the descriptive values of the gas obtained from the NIST property database REFPROP 9.1 [83].





Table 2: Saturated R-410A Tables – Engineers Edge [84]

Property	R-410A
Composition	R-32 (0.5) / R-125 (0.5)
GWP AR4	2088
Temperature glide [K]	0.1
Boiling point at 1 atm (°C)	-51.4
Critical temperature (°C)	71.3
Liquid density at 25 °C (kg/m³)	1058.6
Vapor density (kg/m³)	64.8
ASHRAE class	A1

Pressure-temperature graph for R-410A

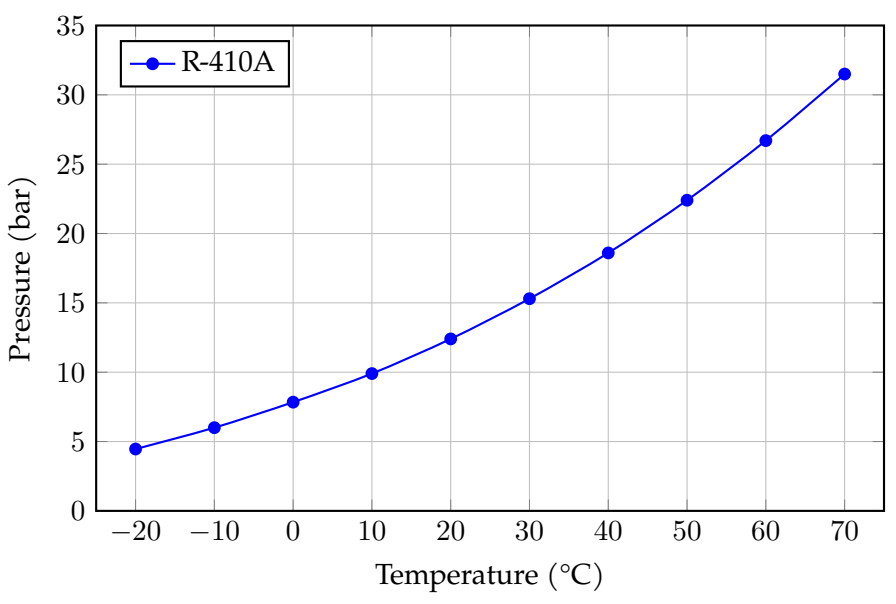


Figure 15: Pressure-temperature graph for R-410A refrigerant

The replacement options of R-410A in residential and commercial air conditioning are R-454B (A2L, GWP of 466), R32 (A2L, GWP of 675), and R-466A (A1, GWP of 733) [82].





5.2 Compressor State of Art

In heat pumps, the choice of the appropriate compressor is a challenge for manufacturers, depending on the unit's size, the required thermal power range, the refrigerant used, and the desired control mode (ON/OFF or continuous). Currently, reciprocating, rotary screw, and scroll compressors are the main types used [85].

Numerous studies have already extensively demonstrated that using variable-speed drive technology in air conditioning systems is a significant improvement over the ON/OFF control method, which leads to wasteful energy consumption [86]. These compressors can modulate the speed of their induction motor based on the cooling or heating demand by using electronic inverters. These inverters regulate the frequency and voltage supplied to the motor, thereby altering its rotational speed.

A simplified operational working schematic is presented [31]:

- The inverter starts the compressor at a *high speed* to cool the environment quickly
- As the temperature approaches the desired value, the system gradually reduces the speed of the compressor
- The compressor continues to operate at a *low power* level, maintaining a constant temperature and avoiding abrupt starts and stop

Anyway, the selection of the most suitable compressor is not the objective of this thesis. As previously mentioned, the study conducted in this thesis was carried out in the Simulink environment, where the block chosen idealizes a *Positive-Displacement Compressor* (2P) that combined with an analytical approach, was deliberately chosen to broaden the range of usable compressors, allowing the modeling of most of them through their fundamental constituent equations.

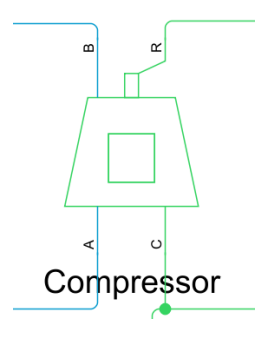


Figure 16: Simulink Compressor [87]

Figure 16 shows the block utilized in Simulink which "represents a positive-displacement compressor, such as a reciprocating piston, rotary screw, rotary vane, or scroll, in a two-phase fluid network" [87]. It's possible to precisely characterize this block by setting its nominal mass flow rate, nominal shaft speed, efficiency type, and other parameters as shown in Figure 17. By doing so, it's possible to model the compressors actually used in these applications. The most important specifications are the Displacement specification, Efficiency specification, and Thermodynamic model, which in turn dictate the specific equations that MATLAB uses to obtain the model's results.





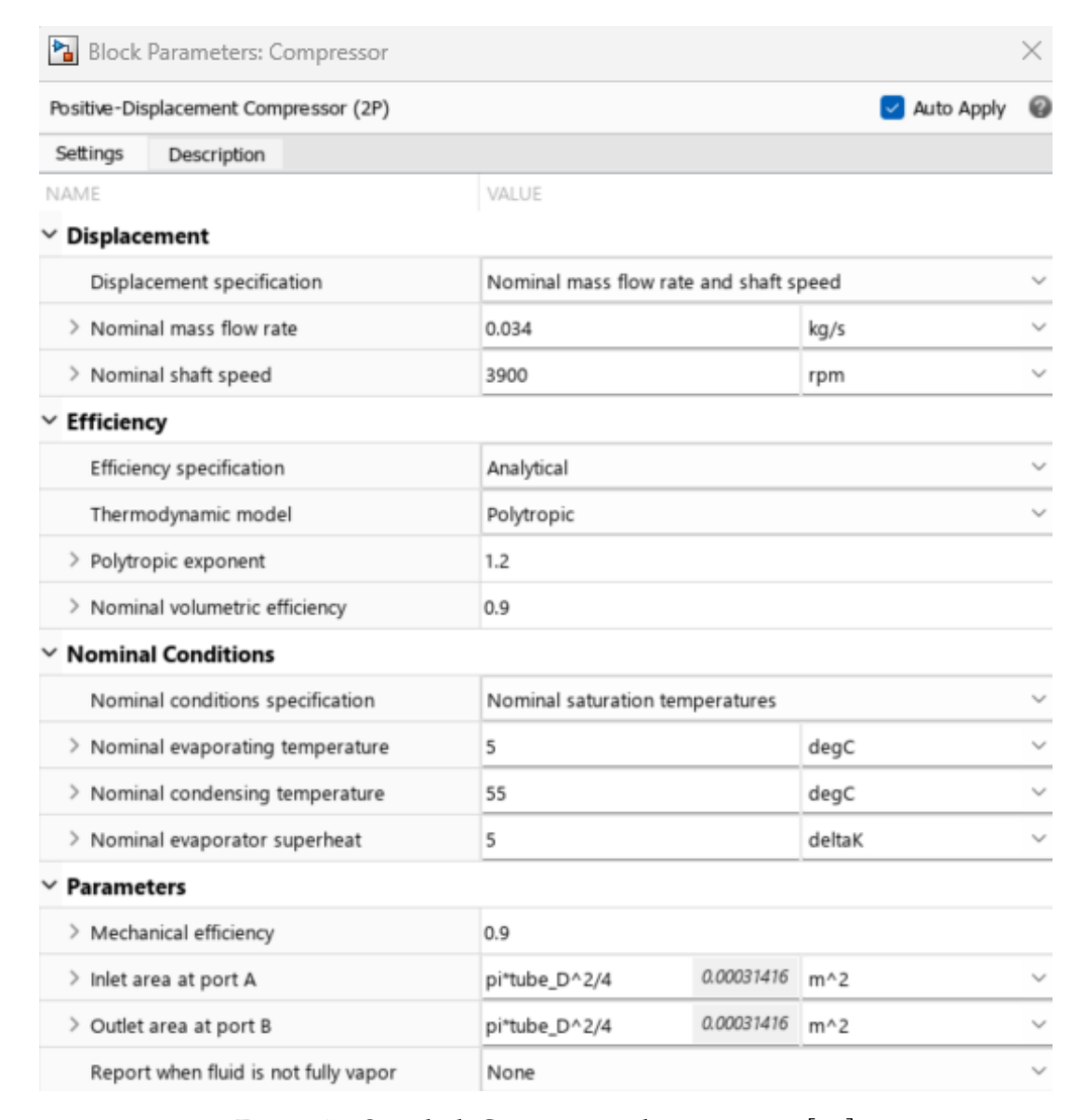


Figure 17: Simulink Compressor characteristics [87]

Based on these selected specifications, MATLAB uses the following formulas to calculate all the relevant variables and model the compressor's behavior within the system [87].

The **mass flow rate** \dot{m} is calculated as:

$$\dot{m} = \eta_V \,\omega \, \frac{V_{\rm disp}}{v_s} \tag{8}$$

where:

- \dot{m} is the mass flow rate;
- η_V is the volumetric efficiency;
- ω is the angular velocity of port R relative to port C;
- \bullet $V_{\rm disp}$ is the displacement volume;
- v_s is the specific volume at the inlet.





The *specific volume* v_s is calculated based on the *Nominal conditions specification* parameter and the specified nominal inlet conditions.

When the **Displacement specification** is set to *Nominal mass flow rate and shaft speed*, the displacement volume V_{disp} is calculated as:

$$V_{\text{disp}} = \frac{\dot{m}_{\text{nominal}} \cdot v_{s,\text{nominal}}}{\omega_{\text{nominal}} \cdot \eta_{V,\text{nominal}}} \tag{9}$$

where:

- \dot{m}_{nominal} is the nominal mass flow rate;
- $v_{s,\text{nominal}}$ is the specific volume at nominal conditions;
- ω_{nominal} is the nominal shaft speed;
- $\eta_{V,\text{nominal}}$ is the nominal volumetric efficiency (when the efficiency specification is *Analytical*).

Analytical Volumetric Efficiency

When you set Efficiency specification to Analytical, the block calculates the volumetric efficiency by using analytical values. When the Thermodynamic model parameter is Polytropic, the volumetric efficiency is

$$\eta_V = 1 + C - C \left(\frac{p_{\text{out}}}{p_{\text{in}}}\right)^{\frac{1}{n}},\tag{10}$$

where $p_{\rm in}$ and $p_{\rm out}$ are the inlet and outlet pressures, respectively, and n is the value of the Polytropic exponent parameter. The block calculates the clearance volume fraction, C, as

$$C = \frac{1 - \eta_{V,\text{nominal}}}{p_{\text{ratio}}^{\frac{1}{n}} - 1},\tag{11}$$

where $\eta_{V,\text{nominal}}$ is the value of the Nominal volumetric efficiency parameter and p_{ratio} is the value of the Nominal pressure ratio parameter.

Continuity Equations

The block conserves mass such that

$$\dot{m}_A + \dot{m}_B = 0,\tag{12}$$

where \dot{m}_A and \dot{m}_B are the mass flow rates at ports A and B, respectively. The block conserves energy such that

$$\phi_A + \phi_B + \dot{m}_A \Delta h_t = 0, \tag{13}$$

where Δh_t is the change in specific total enthalpy and $\dot{m}_A \Delta h_t$ is the fluid power, which is equal to the mechanical power, torque $\times \omega$.

When the Thermodynamic model parameter is Polytropic, the fluid power is

$$\dot{W}_c = \omega \frac{n}{n-1} \eta_V p_{\rm in} V_{\rm disp} \left[\left(\frac{p_{\rm in}}{p_{\rm out}} \right)^{\frac{n-1}{n}} - 1 \right], \tag{14}$$

where the block uses the polytropic relationship $pv^n = \text{constant to relate } p_{\text{in}}$, p_{out} , v_{in} , and v_{out} [87].





5.3 Fans state of art

Fans are another fundamental piece of equipment in a heat pump that consumes electrical energy. In this study, two were used: one to exchange air and heat with the external environment and another placed inside the house to circulate the air cooled by the heat pump.

In commercially available units, other fans can also be found for auxiliary purposes, such as cooling the refrigerant fluid in the condenser when the thermal load increases. Generally, two types of fans are found in domestic air conditioners: Axial Fans and Centrifugal Fans [31]. The mechanical characteristics of these are, of course, numerous and varied. For an axial fan, for instance, the propeller diameter, number of blades, and blade pitch (angle of attack) on the air flow rate all play a fundamental role in calculating the static pressure rise or the static efficiency [88].

The proposed study does not aim to conduct a performance analysis of the various technologies on the market. Instead, it is limited to using the setup provided by Simulink when employing the Fan (MA) block [89], which is shown below.

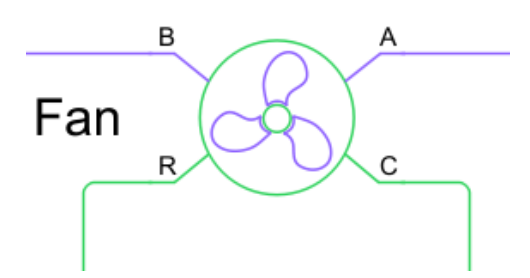


Figure 18: Simulink Fan block [89]

Even in this case, there are various characteristics that can be set for the Fan block, and those introduced for the purpose of this study are shown below, Figure 19 and Figure 20. In this case, the mathematical model that will replace the component is chosen by indicating the Fan parametrization and the Shaft power specification.

All the equations of the mathematical model, which are based on the specifications just shown, are listed below the two figures.

A clarification must be made about the Nominal Volumetric flow rate and consequently the Maximum Volumetric flow rate at zero pressure. They are not the same for the two fans. Specifically, the fan located inside the house has a Nominal Volumetric flow rate of $0.5~\text{m}^3/\text{s}$ and a Maximum Volumetric flow rate at zero pressure of $0.55~\text{m}^3/\text{s}$. The corresponding values for the fan placed outside the house are $0.6~\text{m}^3/\text{s}$ and $0.66~\text{m}^3/\text{s}$, respectively.

The reason behind this choice lies in a systematic analysis performed in combination with the Nominal mass flow of the compressor, aimed at respecting all the limitations imposed by a real-world model (these will be expressed in subsequent paragraphs)





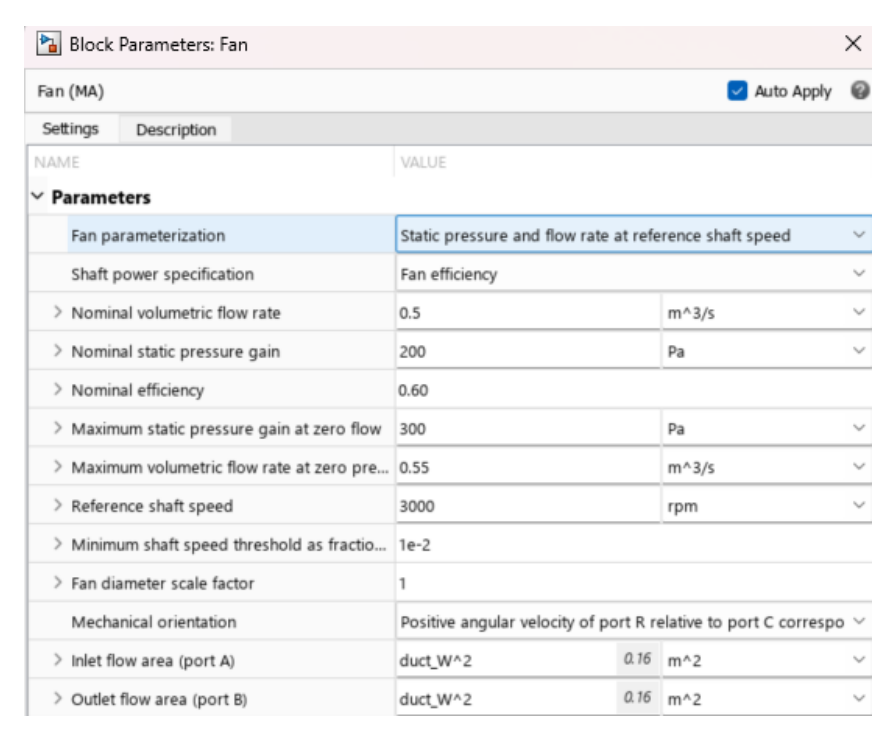


Figure 19: Simulink House Fan characteristics

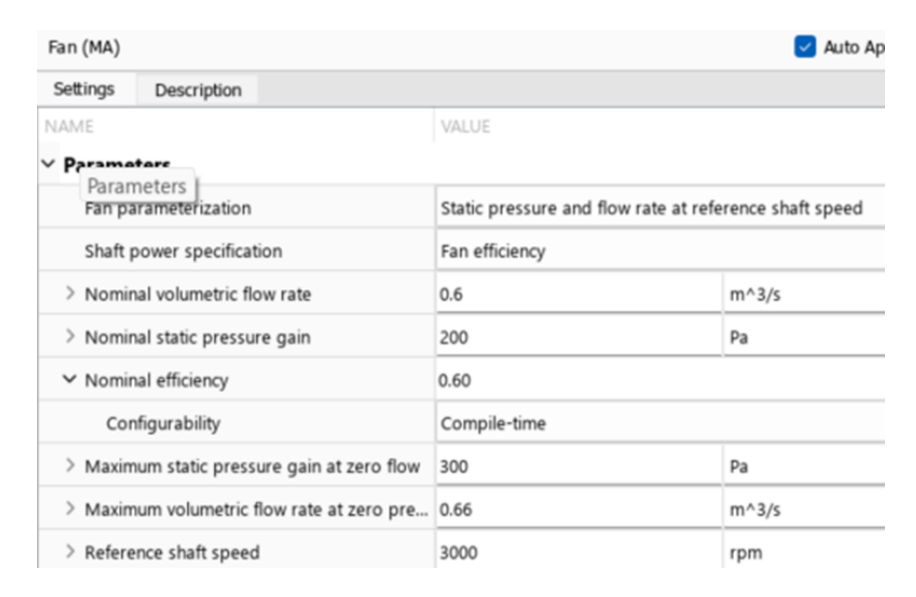


Figure 20: Simulink External Fan characteristics

Parameterization by Nominal Pressure, Flow Rate, and Shaft Speed

When the Fan parameterization parameter is set to Static pressure and flow rate at reference shaft speed, the block uses the analytical fan affinity laws and reference pressure differential to calculate the pressure gain from port A to port B:

$$p_B - p_A = \Delta p_{\text{ref}} \left(\frac{\omega}{\omega_{\text{ref}}}\right)^2 \left(\frac{D}{D_{\text{ref}}}\right)^2$$
 (15)

where:

• Δp_{ref} is the reference pressure differential.





- ω is the shaft angular velocity, $\omega_R \omega_C$.
- ω_{ref} is the reference shaft speed.
- D and D_{ref} are the actual and reference fan diameters, respectively.

The block calculates the shaft torque τ using reference mechanical power and the fan affinity laws:

$$\tau = \frac{\Phi_{\text{ref}} \,\omega^2}{\omega_{\text{ref}}^3} \left(\frac{D}{D_{\text{ref}}}\right)^5 \tag{16}$$

The reference mechanical power Φ_{ref} is computed as:

$$\Phi_{\text{ref}} = \frac{q_{\text{ref}} \,\Delta p_{\text{ref}}}{\eta_{\text{ref}}} \tag{17}$$

where:

- q_{ref} is the reference volumetric flow rate.
- η_{ref} is the reference efficiency.

If the *Shaft power specification* parameter is set to *Fan efficiency*, the block fits a quadratic curve for efficiency from the peak performance η_{nom} to 0. If it is set to *Brake power*, then nominal efficiency is computed as:

$$\eta_{\text{nom}} = \frac{q_{\text{nom}} \, \Delta p_{\text{nom}}}{\Phi_{\text{nom}}} \tag{18}$$

The efficiency is assumed to be zero when there is no flow or when the flow reaches its maximum value at zero pressure.

The reference flow rate q_{ref} is computed from current flow q as:

$$q_{\text{ref}} = q \cdot \frac{\omega_{\text{ref}}}{\omega} \left(\frac{D_{\text{ref}}}{D}\right)^3 \tag{19}$$

Power and Efficency You can specify shaft power as either fan efficiency or brake power. The block calculates efficiency as:

$$\eta = \frac{\Phi_{\text{fluid}}}{\Phi_{\text{brake}}} \tag{20}$$

where:

- $\bullet \ \Phi_{fluid}$ is the fluid power.
- Φ_{brake} is the brake (mechanical) power.

The brake power is computed as:

$$\Phi_{\text{brake}} = \tau \cdot \omega \tag{21}$$

The fluid power is calculated from flow rate and pressure differential:

$$\Phi_{\text{fluid}} = q \cdot (p_B - p_A) \tag{22}$$

Rearranging Equation (21), the torque is given by:

$$\tau = \frac{\Phi_{\text{brake}}}{\omega} \tag{23}$$





5.4 Condenser and Evaporator

The condenser and evaporator are the two primary components that physically exchange heat with the indoor and outdoor environments, forming the foundation of a heat pump's operation.

This thesis focuses on cooling the house by expelling heat from the indoor air to the outdoors. So specifically in this case the condenser is located in the outdoor unit. Its job is to transfer the heat contained in the refrigerant to the outside air, causing the refrigerant to change state from a vapor to a liquid. Conversely, the evaporator extracts heat from the warm indoor air and transfers it to the refrigerant, causing it to change from a liquid to a vapor.

In Simulink, the same block, called the *System-Level Condenser Evaporator* (2P-MA), can be configured to function as either a condenser or an evaporator. This is done by setting the 'Nominal operating condition' parameter to specify its role.

Figure 21 shows the System-Level Condenser Evaporator (2P-MA) block as found in the Simulink library used as an Evaporator.

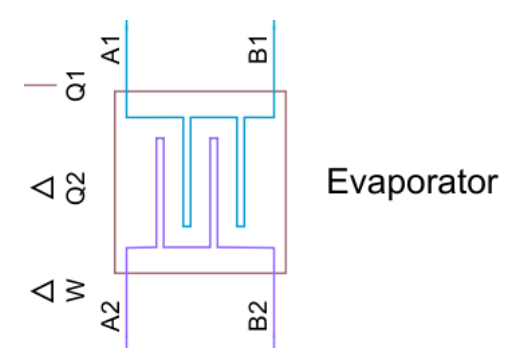


Figure 21: System-Level Condenser Evaporator (2P-MA) Simulink's block

The description done by Matlab about the working principle of this block it's here presented: "The System-Level Condenser Evaporator (2P-MA) block models a heat exchanger between a two-phase fluid network and a moist air network.

The block can act as a condenser or as an evaporator in a refrigeration system, depending on the direction of heat transfer. The block uses performance data from the heat exchanger datasheet, rather than the detailed geometry of the exchanger. You can adjust the size and performance of the heat exchanger during design iterations, or model heat exchangers with uncommon geometries. You can also use this block to model heat exchangers with a certain level of performance at an early design stage, when detailed geometry data is not yet available.

You parameterize the block by the nominal operating condition. The heat exchanger is sized to match the specified performance at the nominal operating condition at steady state.

The Two-Phase Fluid 1 side approximates the liquid zone, mixture zone, and vapor zone based on the change in enthalpy along the flow path. The Moist Air 2 side models water vapor condensation based on convective water vapor mass transfer with the heat transfer surface. Condensed water is removed from the moist air flow" [90].





The specifications used in this study and implemented in this block for the Evaporator are listed below.

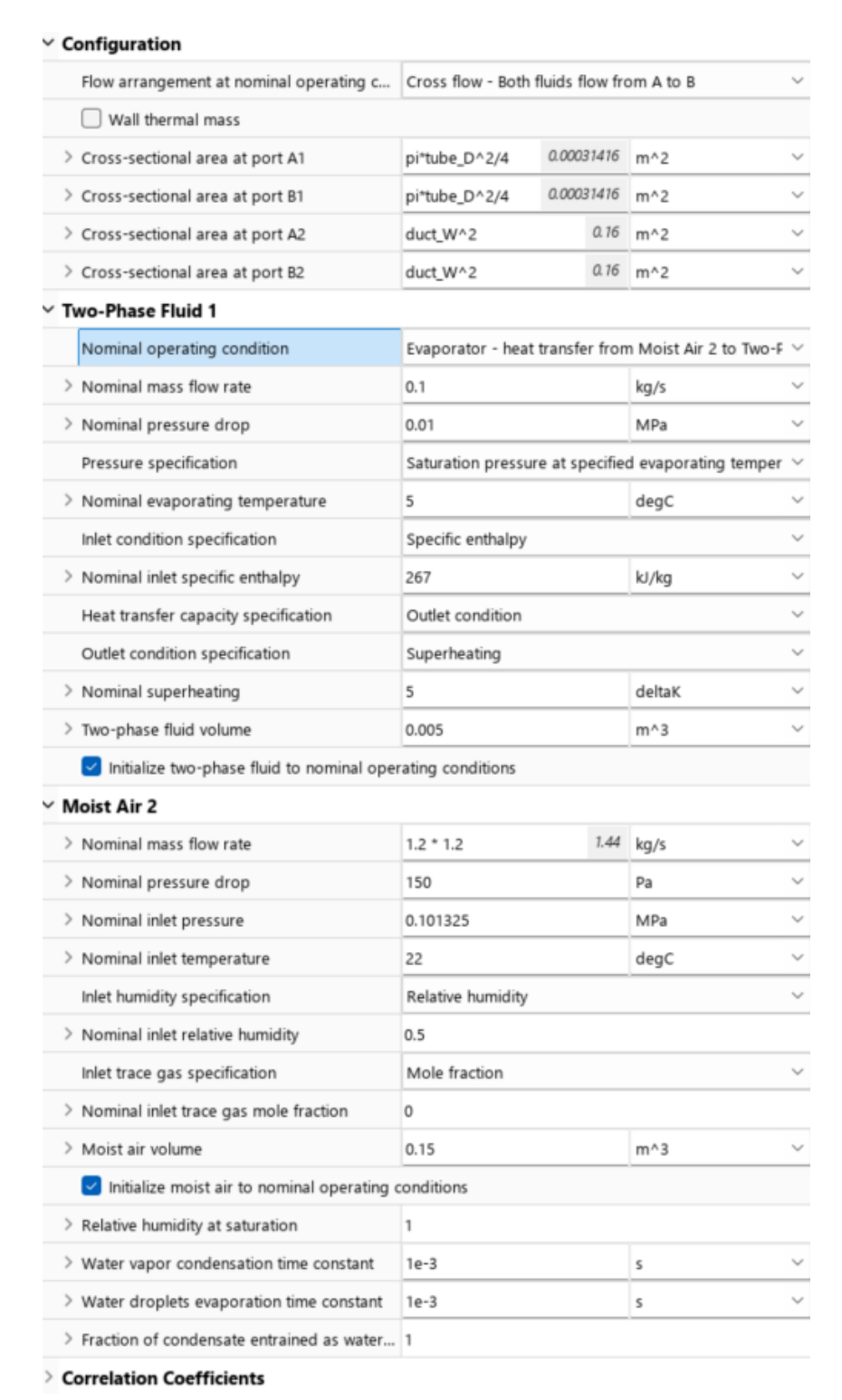


Figure 22: System-Level Condenser Evaporator (2P-MA) Simulink's block





The specifications used in this study and implemented in this block for the Condenser are listed below.

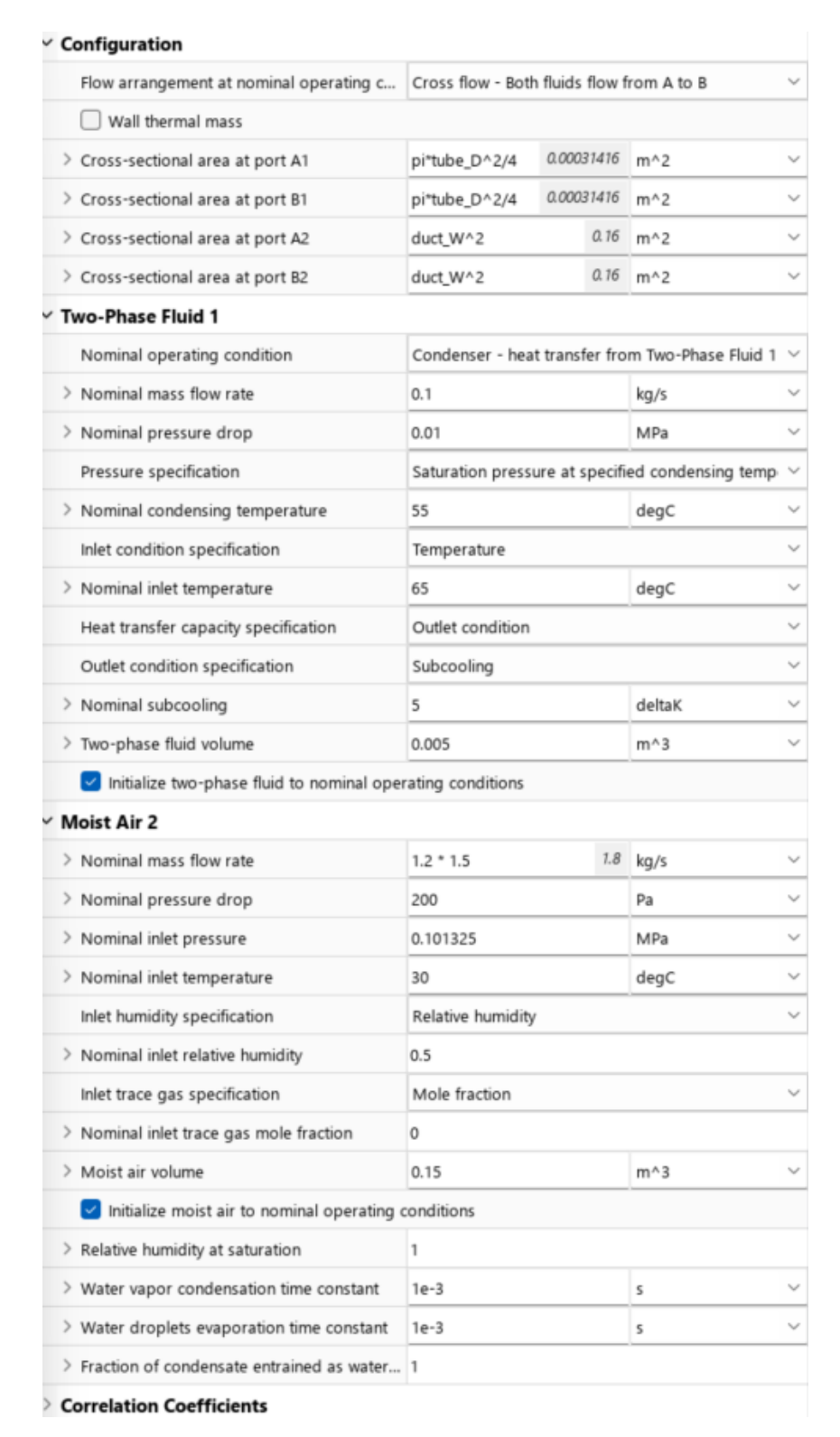


Figure 23: System-Level Condenser Evaporator (2P-MA) Simulink's block

The equations that govern this component will not be specified in this thesis, as they will not be addressed or modified during the study, and therefore are simply part of the system's dynamics. They can, however, be easily consulted at the following link: [90].





5.5 Liquid Receiver

This component is also essential for the proper operation of the heat pump (HP). In real-world applications, it is used to store refrigerant and, in the case of variable thermal loads, to manage the refrigerant's flow rate within the cycle. Furthermore, it is necessary to ensure a stable supply of fluid for efficient system operation. This also prevents refrigerant from backing up into the condenser coil and, finally, protects the compressor from the extremely dangerous phenomenon of "liquid slugging".

This component is especially important for reversible heat pumps, though this particular application is not the focus of this discussion.

In the Simulink model, the block identified as a "Liquid Receiver" serves a distinct modeling purpose. Its primary function is to completely eliminate any vapor at the condenser outlet, effectively enforcing a crucial boundary condition that ensures the rest. This block is on MatLab defined as a Receiver Accumulator (2P) [91] and is shown in Figure 24.

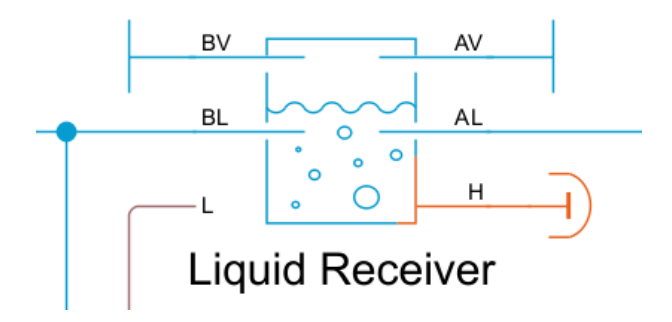


Figure 24: Receiver Accumulator (2P) Simulink's block

The description done by Matlab about the working principle of this block is here presented: "The Receiver-Accumulator (2P) block represents a tank with fluid that can undergo phase change. The liquid and vapor phases, referred to as zones, are modeled as distinct volumes that can change in size during simulation, but do not mix. The relative amount of space a zone occupies in the system is called a zone fraction, which ranges from 0 to 1. The vapor-liquid mixture phase is not modeled.

In an HVAC system, when this tank is placed between a condenser and an expansion valve, it acts as a receiver. Liquid connections to the block are made at ports AL and BL. When the tank is placed between an evaporator and a compressor, it acts as an accumulator. Vapor connections to the block are made at ports AV and BV. A fluid of either phase can be connected to either port, however the fluid exiting from a V port is in the vapor zone and an L port is in the liquid zone. There is no mass flow through unconnected ports.

The temperature of the tank walls are set at port H.

The liquid level of the tank is reported as a zone fraction at port L. If the liquid level reports 0, the tank is fully filled with vapor. The tank is never empty" [91].





Pressure above critical pressure check

> Vapor heat transfer coefficient

> Liquid heat transfer coefficient

Effects and Initial Conditions

> Initial liquid volume fraction

Initial liquid fraction specification

✓ Initial liquid and vapor volumes fully saturated

> Vaporization and condensation time const... 1

Heat Transfer

> Initial pressure

🚹 Block Parameters: Liquid Receiver Receiver Accumulator (2P) Auto Apply Settings Description VALUE ∨ Main 0.0088357 m^3 > Total tank volume pi*0.15^2/4 * 0.5 0.017671 m^2 > Tank cross-sectional area pi*0.15^2/4 0.00031416 m^2 > Cross-sectional area at port AV pi*tube_D^2/4 > Cross-sectional area at port BV pi*tube_D^2/4 0.00031416 m^2 0.00031416 m^2 > Cross-sectional area at port AL pi*tube_D^2/4 > Cross-sectional area at port BL pi*tube_D^2/4 0.00031416 m^2 Liquid volume fraction out of range check > Volume fraction threshold for transition to...

Warning

W/(K*m^2)

W/(K*m^2)

MPa

s

20

100

2.734

Liquid volume fraction

The specifications used in this study and implemented in this block are listed below.

Figure 25: Receiver Accumulator (2P) Simulink's block specifications

The equations that govern this component will not be specified in this thesis, as they will not be addressed or modified during the study, and therefore are simply part of the system's dynamics. They can, however, be easily consulted at the following link: [91].





5.6 Thermostatic Expansion Valve

This final component is crucial to a heat pump's refrigeration cycle. Its primary purpose is to regulate the flow of refrigerant entering the evaporator.

The valve's objective is to take the high-pressure, high-temperature refrigerant leaving the condenser and, by using a throttling effect, transform it into a cold, low-pressure fluid. This process is essential for ensuring the refrigerant is in the correct state to absorb heat in the evaporator. This process was previously defined by the following points:

 $3 \rightarrow 5$: Joule–Thomson expansion through the throttling valve

In Simulink the block is called *Thermostatic Expansion Valve* (2P) and it is possible to see it in Figure 26.

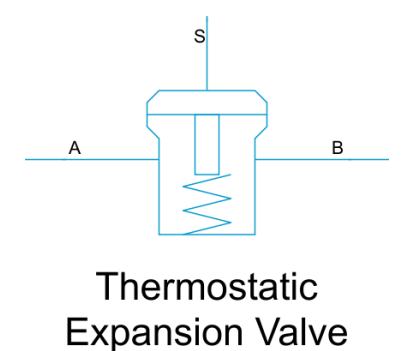


Figure 26: Thermostatic Expansion Valve (2P) block

The description done by Matlab about the working principle of this block is here presented: "The Thermostatic Expansion Valve (2P) block models a valve with a pressure drop that maintains an evaporator superheat in a two-phase fluid network. You typically place this valve between a condenser and an evaporator in a refrigeration system to maintain a specific temperature differential by moderating the flow into the evaporator.

The valve behavior depends on the superheat, which is the difference in temperature between the vapor at the evaporator outlet and the fluid evaporating temperature. The valve opens if the superheat increases to let more flow through, and the valve closes if the superheat decreases to let less flow through. When the superheat drops to or below the value of the Static (minimum) evaporator superheat parameter, then the valve is fully closed. The closed valve reduces the flow through the evaporator, which reduces the heat transfer and increases the outlet temperature. When you use the MOP limit parameter to enable a maximum pressure or temperature limit, the valve closes when the temperature or pressure exceeds the limit" [92].





> Laminar flow pressure ratio

> Inlet phase change time constant

> Cross-sectional area at ports A and B

Block Parameters: Thermostatic Expansion Valve Thermostatic Expansion Valve (2P) Auto Apply Settings Description VALUE Parameters Valve parameterization Nominal capacity, superheat, and operating conditions Capacity specification Evaporator heat transfer > Nominal evaporator heat transfer 16 kW 16 * 1.5 kW > Maximum evaporator heat transfer Pressure at specified saturation temperature Nominal pressure specification > Nominal condensing (saturation) tempera... 45 degC > Nominal evaporating (saturation) temper... degC > Nominal condenser subcooling deltaK > Nominal (static + opening) evaporator su... 5 deltaK > Static (minimum) evaporator superheat 2 deltaK MOP limit Pressure equalization Internal pressure equalization Bulb temperature dynamics > Leakage flow fraction 1e-6 > Smoothing factor 0.01

The specifications used in this study and implemented in this block are listed below.

Figure 27: Thermostatic Expansion Valve (2P) block specifications

pi*tube_D^2/4

0.00031416 m^2

0.999

0.1

The equations that govern this component will not be specified in this thesis, as they will not be addressed or modified during the study, and therefore are simply part of the system's dynamics. They can, however, be easily consulted at the following link: [92].





5.7 House model

The House subsystem developed on Simulink is constructed as shown in Figure 28. The purple lines identify the moist air circulation system due to the internal fan, which is driven by the mechanical system (Fan Drive) already explained. The orange lines, on the other hand, identify the thermal network and, consequently, all the heat exchanges that take place.

In general, the house is shaped like a parallelepiped topped by a sloping roof. The dimensions of the parallelepiped are: one side 20 m long; one side 10 m long; height 6 m. As for the roof, the two sides have a 40° slope from the horizontal, intersecting at the midpoint of the 10 m side.

The house is therefore modelled differently in the two networks: in the thermal network, the House Thermal Network block is used; in the moist air network, the House Air Volume block is used instead.

The block named House Air Volume is a Simulink *Constant Volume Chamber (MA)* block and is mainly characterised by a chamber volume of $1200 \,\mathrm{m}^3$ with an initial temperature and pressure of 295.15 K and 0.101325 MPa. The other specifications are the standard ones initialised by Simulink itself.

This block is connected to two pipes (area 0.16 m^2 , hydraulic diameter 0.4 m and length 30 m) which represent the fresh air entering the system and the warmer air extracted to circulate in the evaporator. As can be seen, points 1 (A2) and 2 (B2) are the connection points with the evaporator in the main Simulink system.

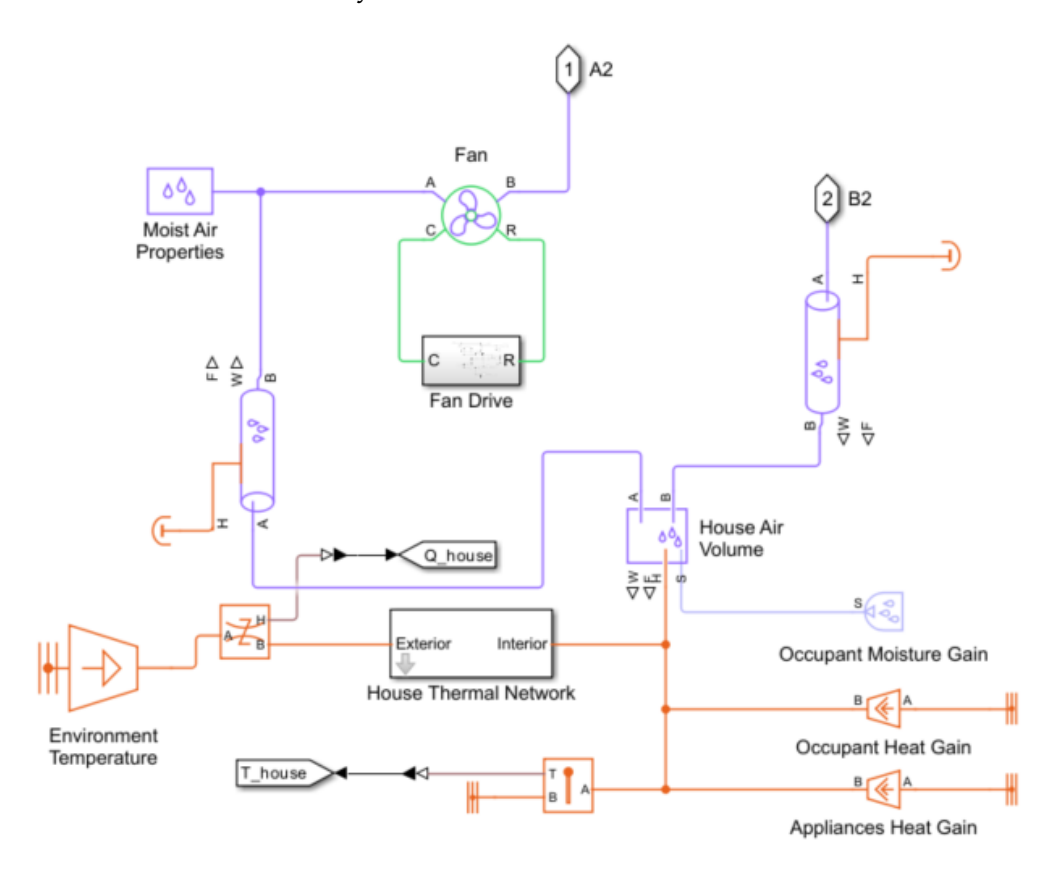


Figure 28: House Model

From the House Thermal Network block, we can extrapolate more information about the house model. Figure 29 shows all the variables needed to accurately calculate all the heat exchanges, that occur through the roof, windows, internal and external walls and due to the presence of





300 m³ of furniture, according to the laws of thermodynamics, specifically using conduction and convection (irradiation is not included).

Roof			
Parameter	Value	Unit	
Average thickness	0,2	m	
Average density	32	kg/m³	
Average specific heat	835	J/(kg·K)	
Average conductivity	0,038	W/(m·K)	
Interior heat transfer coeff.	12	W/(m ² ·K)	
Exterior heat transfer coeff.	38	W/(m²·K)	
Initial temperature	30	°C	

Exterior Walls		
Parameter	Value	Unit
Average thickness	0,2	m
Average density	1920	kg/m³
Average specific heat	835	J/(kg·K)
Average conductivity	0,038	W/(m·K)
Interior heat transfer coeff.	24	W/(m²⋅K)
Exterior heat transfer coeff.	34	W/(m²·K)
Initial temperature	30	°C

Furniture			
Parameter	Value	Unit	
Total surface area	300	m²	
Total mass	3000	kg	
Average specific heat	2000	J/(kg·K)	
Interior heat transfer coeff.	18	W/(m ² ·K)	
Initial temperature	22	°C	

Windows			
Parameter	Value	Unità	
Total area	12	m²	
Average thickness	0,01	m	
Average density	2700	kg/m³	
Average specific heat	840	J/(kg·K)	
Average conductivity	0,78	W/(m·K)	
Interior heat transfer coeff.	25	W/(m²⋅K)	
Exterior heat transfer coeff.	32	W/(m²⋅K)	
Initial temperature	30	°C	

Interior Walls				
Parameter Value Unità				
Average thickness	0,15	m		
Average density	10	kg/m³		
Average specific heat	1000	J/(kg·K)		
Average conductivity	0,2	W/(m·K)		
Interior heat transfer coeff.	24	W/(m²⋅K)		
Initial temperature	22	°C		

Figure 29:	House	parameters
------------	-------	------------

For the sake of clarity, the block mentioned above is a new feature in Simulink and, in a schematic and quicker way, models the following subsystem shown in Figure 30 created in previous versions [77].

House Thermal Network Subsystem

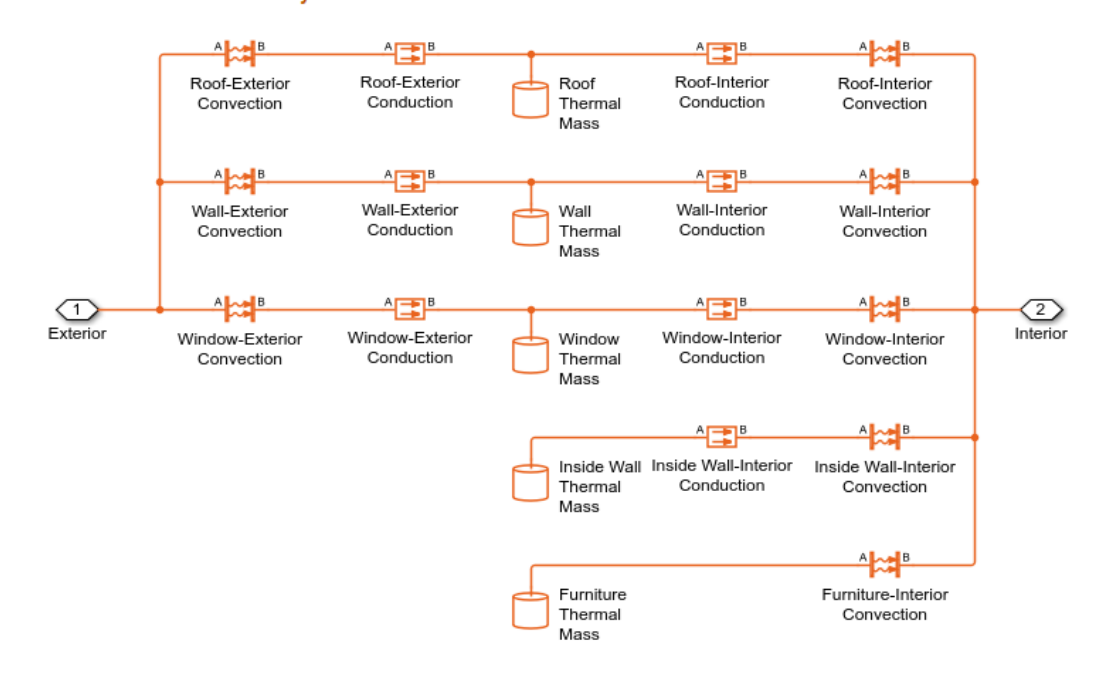


Figure 30: House thermal network subsystem [77]





Below will be explained how the blocks relating to 'Convective Heat Transfer' and 'Conductive Heat Transfer' work.

"The Convective Heat Transfer block represents heat transfer by convection between two bodies by means of fluid motion. The Newton law of cooling describes the transfer,

$$Q = kA(T_A - T_B) (24)$$

where Q is the heat flow, k is the convection heat transfer coefficient, A is the surface area and T_A and T_B are the temperatures of the two bodies.

The heat transfer coefficient, k, can be either constant, which you specify by using the Heat transfer coefficient parameter, or variable, which you specify by using the physical signal at port K'' [93].

"The Conductive Heat Transfer block represents heat transfer by conduction between two layers of the same material. For a flat surface, the Fourier law describes the transfer,

$$Q = k \frac{A}{D} (T_A - T_B) \tag{25}$$

where Q is the heat flow, k is the thermal conductivity of the material, A is the area normal to the heat flow direction, D is the distance between layers, that is, the thickness of material, T_A is the temperature of layer A and T_B is the temperature of layer B" [94].

Finally, the last block to highlight is the one representing Thermal Mass, which explains how thermal inertia is studied in relation to the components that model the house.

"The Thermal Mass block represents a thermal mass that reflects the ability of a material, or a combination of materials, to store internal energy. The mass of the material and its specific heat characterize this property. The thermal mass is described by

$$Q = c_p m \frac{dT}{dt} \tag{26}$$

where Q is the heat flow, c_p is the specific heat of the mass material ,m is the mass, T is the temperature and finally t is time" [95].





5.7.1 Legiferation on HVAC system

Every energy-related product circulating in Europe is required to meet certain parameters, which must be defined in various documents certifying their compliance with European rules. These are defined in various laws, including the new law "Ecodesign for Sustainable Products Regulation (ESPR), which entered into force on 18 July 2024 and that is the cornerstone of the Commission's approach to more environmentally sustainable and circular products. The ESPR is part of a package of measures that are central to achieving the aims of the 2020 Circular Economy Action Plan and fostering the transition to a circular, sustainable, and competitive economy. It will contribute to helping the EU reach its environmental and climate goals, double its circularity rate of material use and achieve its energy efficiency targets by 2030" [96].

This law defines the various general requirements for several categories of products. Specifically, with regard to air conditioners, reference is made to Regulation (EU) 206/2012 [97], which specifically covers only air conditioners with "rated capacity of 12 kW for cooling, and comfort fans with an electric fan power input 125 W". The law identifies an 'air conditioner' as "a device capable of cooling or heating, or both, indoor air, using a vapour compression cycle driven by an electric compressor, including air conditioners that provide additional functionalities such as dehumidification, air-purification..." [97].

Specifically, limits are defined with regard to:

- Minimum energy efficiency
- Maximum sound power level
- Maximum power consumption

More specifically, Table 3 shows the **Requirements for minimum energy efficiency** which depends solely on the summer efficiency or cooling (EER) and winter efficiency or heating (COP) levels, as well as the GWP (Global Warming Potential) index of the refrigerant fluid used.

Table 3: Minimum energy efficiency requirements for portable air conditioners (EU Regulation)

GWP del refrigerante	Double duct		Singl	e duct
	EER _{rated}	COP _{rated}	EER _{rated}	COP _{rated}
GWP > 150	2.40	2.36	2.40	1.80
GWP 150	2.16	2.12	2.16	1.62

Regarding the **Requirements for maximum sound power level**, this settles on a single, defined in Table 4.

Table 4: Indoor sound power level

Parameter	Value
Indoor sound power level	65 dB(A)





The last limits in Table 5 express what the Requirements are for maximum power consumption in off-mode and standby mode for single duct and double duct air conditioners and comfort fans.

Table 5: Power consumption limits for off and standby modes (EU Regulation No. 206/2012)

Mode	Power Consumption Requirement
Off mode	Power consumption of equipment in any off-mode condition shall
	not exceed 1.00 W.
Standby mode (reacti-	The power consumption of equipment in any condition provid-
vation only)	ing only a reactivation function, or providing only a reactivation
	function and a mere indication of enabled reactivation function,
	shall not exceed 1.00 W .
Standby mode (infor-	The power consumption of equipment in any condition provid-
mation display)	ing only information or status display, or providing only a combi-
	nation of reactivation function and information or status display,
	shall not exceed 2.00 W .
Availability of standby	Equipment shall, except where this is inappropriate for the in-
and/or off mode	tended use, provide off mode and/or standby mode, and/or an-
	other condition which does not exceed the applicable power con-
	sumption requirements for off mode and/or standby mode when
	the equipment is connected to the mains power source.

The calculation of all these values relating to the cooling phase, from 1 January 2013, must be carried out in accordance with Annex 2 of the same document [97], which specifies the operating limits of the standard conditions for measuring the COP for single and double duct air conditioners (Table 6):

Table 6: Nominal operating conditions for air conditioners (excluding single duct air conditioners)

Appliance Function	Indoor Air Temperature (°C)	Outdoor Air Temperature (°C)
	dry bulb / (wet bulb)	dry bulb / (wet bulb)
Cooling	27 / (19)	35 / (24)

This means that the legislation requires the manufacturer to declare the actual energy values of the machine up to this operating range and for all lower ranges. Only if the external or internal temperature conditions exceed 35° C or 27° C, respectively, a certain degree of deviation from the performance values declared by the manufacturer is permitted.

As regards thermal comfort requirements, regulations are somewhat more flexible when it comes to maintaining the temperature set point requested by the user. The ASHRAE (American Society of Heating, Refrigerating and Air-Conditioning Engineers) committee, in its ASHRAE 55-2020 standard (Thermal Environmental Conditions for Human Occupancy), establishes precise limits on acceptable temperature variations over time to ensure the thermal comfort of occupants. In Section 5.3.4.3, it defines the following for residential and commercial spaces:

- ± 2.2 °C during a 1 hour time period
- ± 1.1 °C during a 0.25 hour time period (15 minutes)





At the European level, EN 15251:2007 is the standard used by HVAC manufacturers for the selection and sizing of systems. In particular they refer to the paragraph — Indoor environmental input parameters for design and assessment of energy performance of buildings [98], which does not set limits for air conditioning systems but rather for user comfort, defining indoor environmental conditions relating to:

- Air temperature
- Humidity
- Air velocity
- Indoor air quality (CO₂, VOCs, etc.)
- Lighting and acoustics

and divide thermal comfort into four performance categories (from I= high to IV= acceptable). In residential or work environments where the category is identified as III or IV, the standard allows for variations of $\pm 2\,^{\circ}\mathrm{C}$ from the setpoint without causing too much discomfort to the user.





6 Characterization of the Heat Pump

The characterization of the heat pump used as air conditioning in this study is based on the primary objective for which this thesis aims to introduce an innovation: providing energy support to the electrical grid due to the decreasing of the electrical inertia provided by the increasing in the renewable energy share. As extensively discussed, the goal is to investigate how small units can contribute to ensure stability and security of the power system during destabilizing events through mechanisms such as Primary, Secondary, Tertiary Control Reserve or Replacement Reserve.

Each of these control strategies requires different response times and power levels, depending on the severity and complexity of the disturbance. Regarding the power contributions involved, it is clear that these will not be comparable in magnitude to those of the traditional power system (unless future widespread coordination is achieved), precisely because the underlying concept of this study is to shift the regulation capability to small-scale devices.

However, the required response times must be consistent with those of conventional systems, ranging from rapid responses—such as those required for Fast Frequency Response (FFR), typically under 30 seconds—to broader, long-duration support in the event of more critical contingencies.

What will be required of the proposed heat pump model is the ability to reduce the power input to the compressor for a defined period of time, without causing excessive discomfort to the user in the cooled room, and therefore without deviating significantly from the target temperature setpoint.

The proposed tests will vary in nature and methodology.

The first test aims to evaluate the energy performance of the air conditioning system developed in *Simulink*, by varying the power supplied to the compressor while respecting predefined limits on both time and temperature increase. Based on the previously introduced concept, the test is outlined as follows:

- 1. Impose a desired indoor setpoint temperature and a constant outdoor temperature over time
- 2. Allow the indoor environment to reach and maintain the setpoint temperature for a sufficiently long period, ensuring that all relevant variables thermodynamic, mechanical, and system-related are in steady-state conditions
- 3. Reduce the compressor power to a lower, constant value
- 4. Verify that, under this reduced power condition, the indoor temperature does not exceed the setpoint by more than $+0.5^{\circ}$ C over a period of 2 hours
- 5. Gradually decrease the compressor power between the identified upper and lower limits in order to assess the heat pump's performance over the defined operating range

Within the first test, a further characterization will be proposed in which a single outdoor temperature will be used, while the indoor set-point temperature will be varied.





The second test, on the other hand, is designed to make full use of the thermal capacity and thermal inertia of the modeled house, in order to support the electrical grid as much as possible. To this end, the procedure will be structured as follows:

- 1. Impose an indoor set-point temperature and a constant outdoor temperature over time
- 2. Allow the indoor environment to reach and maintain the setpoint temperature for a sufficiently long period, ensuring that all relevant variables thermodynamic, mechanical, and system-related are in steady-state conditions
- 3. Completely shut down the power input to both the compressor and the fans, effectively halting the operation of the heat pump
- 4. Observe how long it takes before thermal comfort for the user is no longer met, according to the current regulatory standards [99] [100]

One important specification to make is that, in an air conditioning system, there are two power inputs that can be controlled: the power supplied to the compressor and the power supplied to the fans. In this study, the fan power is assumed to be fixed at all times — a choice made also because their contribution to total power consumption is relatively low — while control is applied only to the compressor power.

Since the fans power is constant, the compressor must adjust its power dynamically based on the outdoor air temperature and the selected set-point temperature. The goal is to determine, over time, the appropriate compressor power needed to bring the system from a dynamic to a quasi-static state to start the study proposed. To achieve this, a mathematical approach was adopted using a Proportional-Integral-Derivative (PID) controller.





6.1 PID Controller

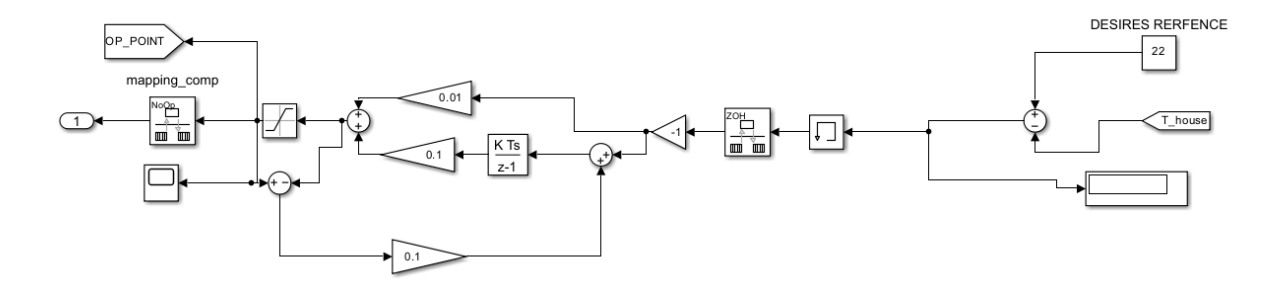


Figure 31: PID Controller on Simulink

This discrete incremental digital PID controller is applied to the indoor air temperature of the house, $T_{\rm house}$, which must be brought toward the set-point temperature ($T_{set} = 22^{\circ}\text{C}$) defined by the user.

The error $(T_{set}-T_{
m house})$ is gradually reduced based on three components:

- how far the actual temperature is from the target (Proportional)
- how long the error has persisted (Integral)
- and how the error is changing over time (Derivative)

The entire control strategy is implemented digitally using the *Z-transform*, making it well-suited for implementation on microcontrollers or in simulation environments [31].

The basic formula describing the behavior of a continuous-time PID controller is given by:

$$u(t) = K_p \cdot e(t) + K_i \int_0^t e(\tau) d\tau + K_d \cdot \frac{d}{dt} e(t)$$
(27)

where:

- u(t) is the control signal
- \bullet e(t) is the error between the set-point and the measured value
- K_p is the proportional gain
- K_i is the integral gain
- K_d is the derivative gain

Subsequently, the actual formula used in the implemented PID controller is introduced, which





takes into account the discretization of time:

$$e[k] = r[k] - y[k] \tag{28}$$

$$P[k] = K_p \cdot e[k] \tag{29}$$

$$I[k] = I[k-1] + K_i \cdot T_s \cdot e[k] \tag{30}$$

$$D[k] = K_d \cdot \frac{e[k] - e[k-1]}{T_s}$$
(31)

$$u[k] = P[k] + I[k] + D[k]$$
(32)

Writing it explicitly in a single formula:

$$I[k] = I[k-1] + K_i \cdot T_s \cdot (r[k] - y[k])$$
(33)

$$u[k] = K_p \cdot (r[k] - y[k]) + I[k] + K_d \cdot \frac{(r[k] - y[k]) - (r[k-1] - y[k-1])}{T_s}$$
(34)

Figure 32 clearly shows how the PID controller operates by progressively reducing the error and settling at a constant input value, and how this control principle interacts with the indoor temperature (Figure 33).

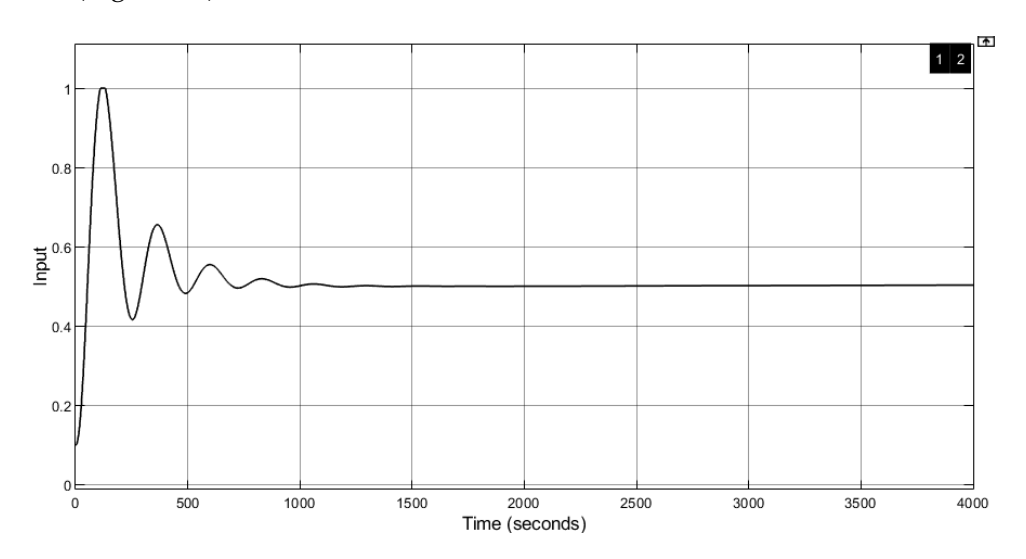


Figure 32: PID Controller working principle

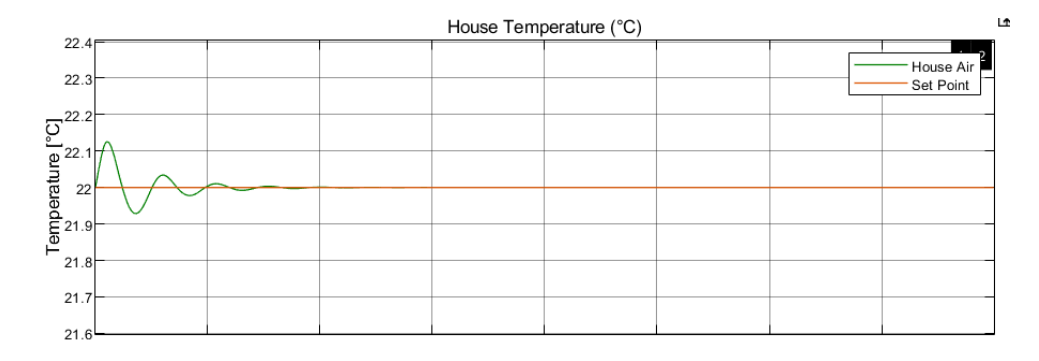


Figure 33: PID Controller working principle on the Temperature of the house





6.2 Steady State

Bringing the system to a steady-state condition is crucial for the purposes of the study being conducted. Achieving this objective does not simply mean that the indoor temperature reaches the set-point value; rather, it implies that all the variables involved in the heat pump model maintain a high degree of stability over time.

As previously mentioned, the only variable actively controlled in this study is the angular velocity supplied to the shaft of the compressor. It is precisely here that the PID controller, starting from the error between the indoor temperature and the set-point, determines a specific power trajectory (Figure 32) to be followed by the *Ideal Angular Velocity* block connected to the Compressor one.

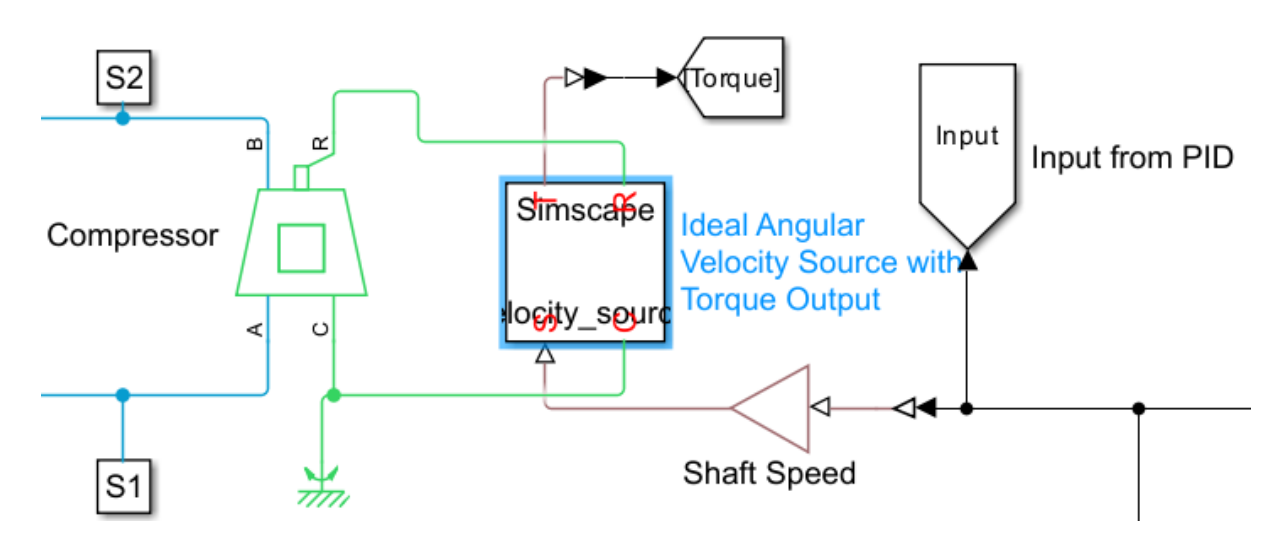


Figure 34: Ideal Angular Velocity block connected to the Compressor

What happens, therefore, is that the input provided by the PID controller at each time step is multiplied by the nominal shaft speed of the compressor (3900 rpm), which in turn generates a certain amount of mechanical power applied to the refrigerant circulating within the heat pump.

This certain quantity of refrigerant mass flow rate is then responsible, operating within the condenser and evaporator in counter flow with the air supplied by the two fans, for introducing into the house a stream of air, colder or warmer depending on the operating conditions, which interacts with the existing indoor air and causes a variation in the indoor temperature.

This updated indoor temperature is then used as the reference value in the next sampling instant to calculate the new error, allowing the PID controller to continue operating.

There are several variables involved that must reach a steady-state behavior, starting with the mechanical power applied by the compressor to the refrigerant fluid:





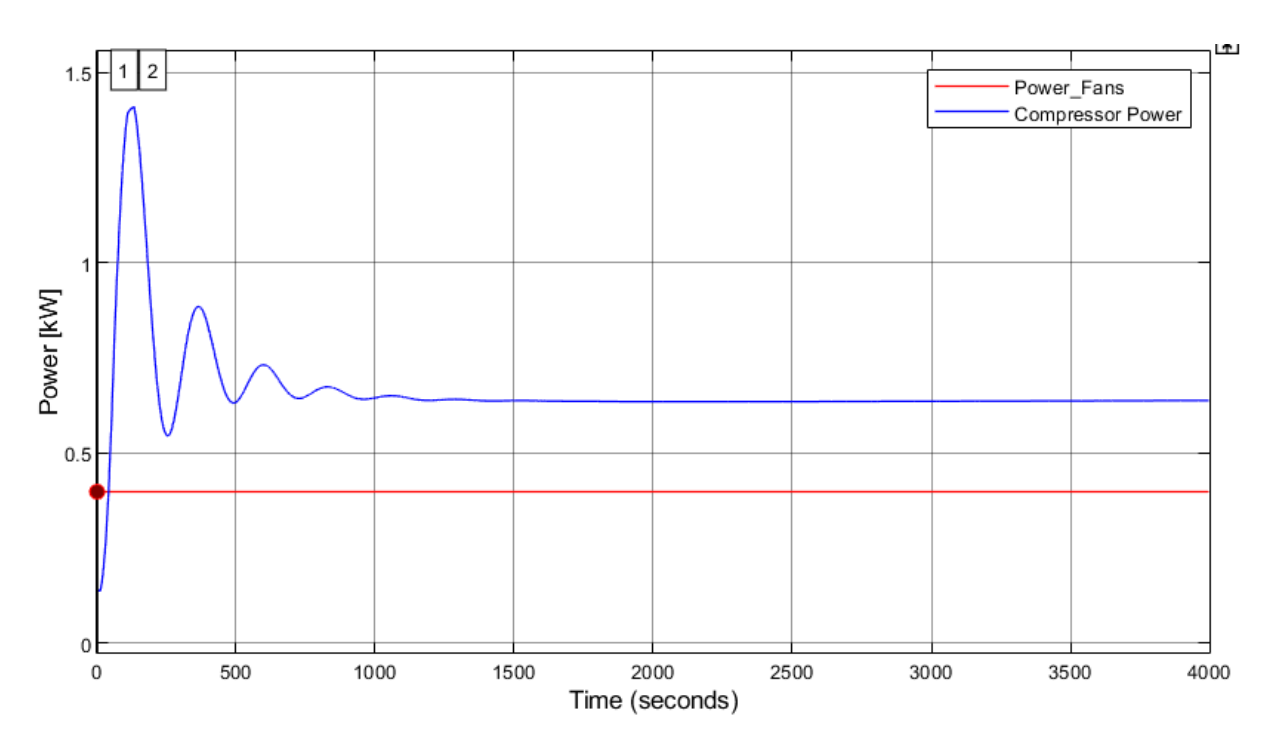


Figure 35: Compressor and Fans powers

Obviously, reaching a condition of constant power also implies achieving a constant operating frequency and a constant angular velocity at the three shafts (compressor and two fans). The frequency [Hz] was simply calculated based on the rotational speed of the shaft, which results from the normalized input provided by the PID controller.

$$f = \frac{\text{PID Input} \cdot (3900 \text{ rpm})}{60} \tag{35}$$

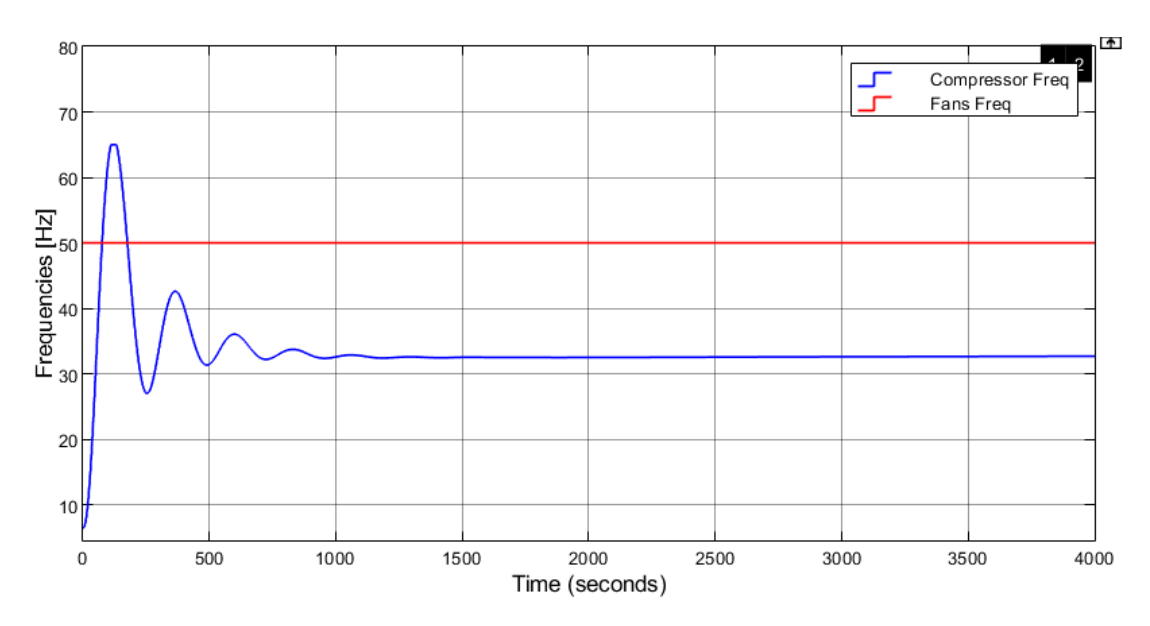


Figure 36: Compressor and Fans frequency

As discussed in Section (5.2), it is mathematically shown how the power applied to the compressor — or, more precisely, the angular velocity ω — is directly responsible for the refrigerant





mass flow rate within the heat pump (see Equation 8). This relationship is also visually demonstrated in Figure 37:

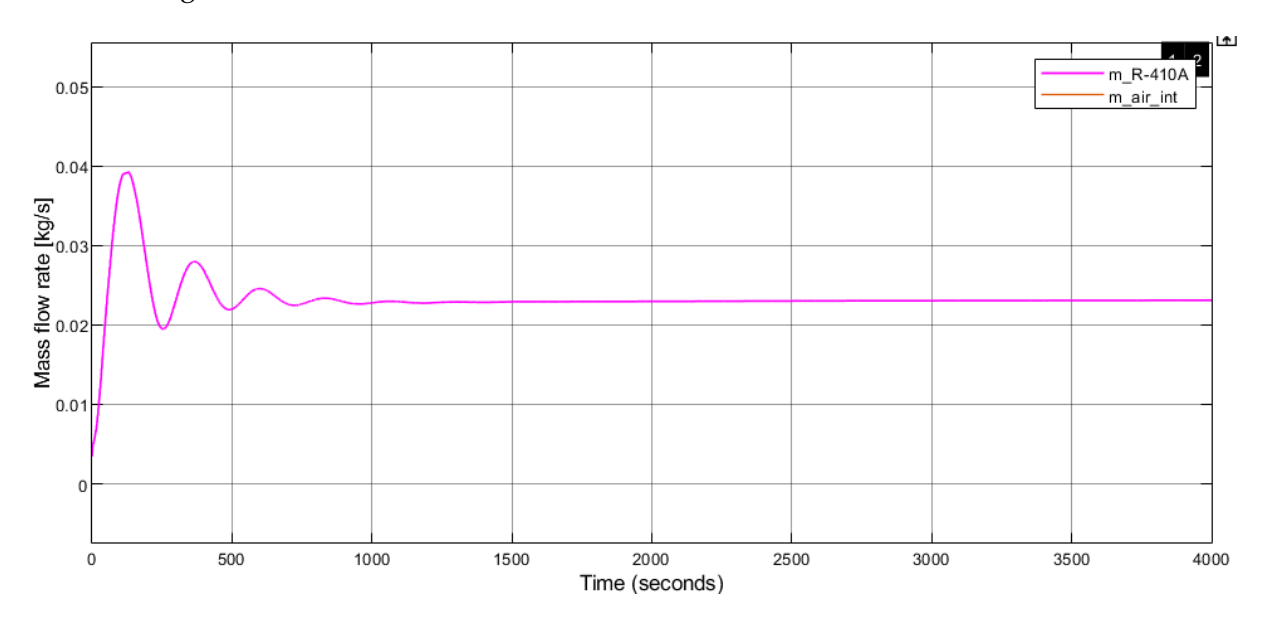


Figure 37: Mass flow rate of R-410A

Following the chain of interactions among variables, the mass flow rate of the R-410A refrigerant is directly responsible for the amount of heat exchanged in both the evaporator and the condenser, given that the mass flow rate of air supplied to these two components remains nearly constant at all times.

On the other hand, the heat entering the house from the outdoor environment is entirely independent of the refrigerant mass flow rate. Instead, it depends solely on various building-related coefficients and parameters (such as insulation, thermal conductivity, surface area, etc.) as well as the outdoor air temperature.

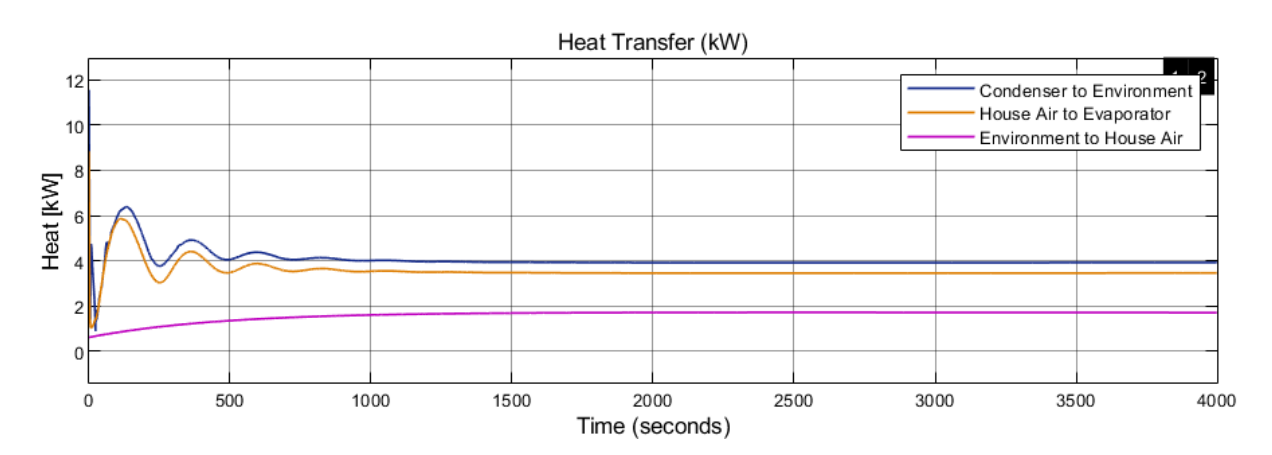


Figure 38: Heats exchanged in the system

To provide a general overview, it is useful to graphically observe the basic energy balance of a refrigeration cycle in a heat pump. Below, the general equation is reported:

$$\dot{Q}_{\text{Evaporator}} - \dot{Q}_{\text{Condenser}} = \dot{W}_{\text{Compressor}}$$
 (36)

A clarification must be made regarding why the energy balance does not exactly equal zero:





this is due to the fact that the compressor power used in the calculation refers to the mechanical power at the shaft, rather than the thermodynamic power actually transferred to the refrigerant, which would naturally be lower.

Moreover, pressure losses and other intrinsic inefficiencies of the modeled cycle are not fully accounted for. Nonetheless, it can be observed that this imbalance stabilizes over time and remains negligible in magnitude (10^{-1}) compared to the main heat flows in the system (10^0) .

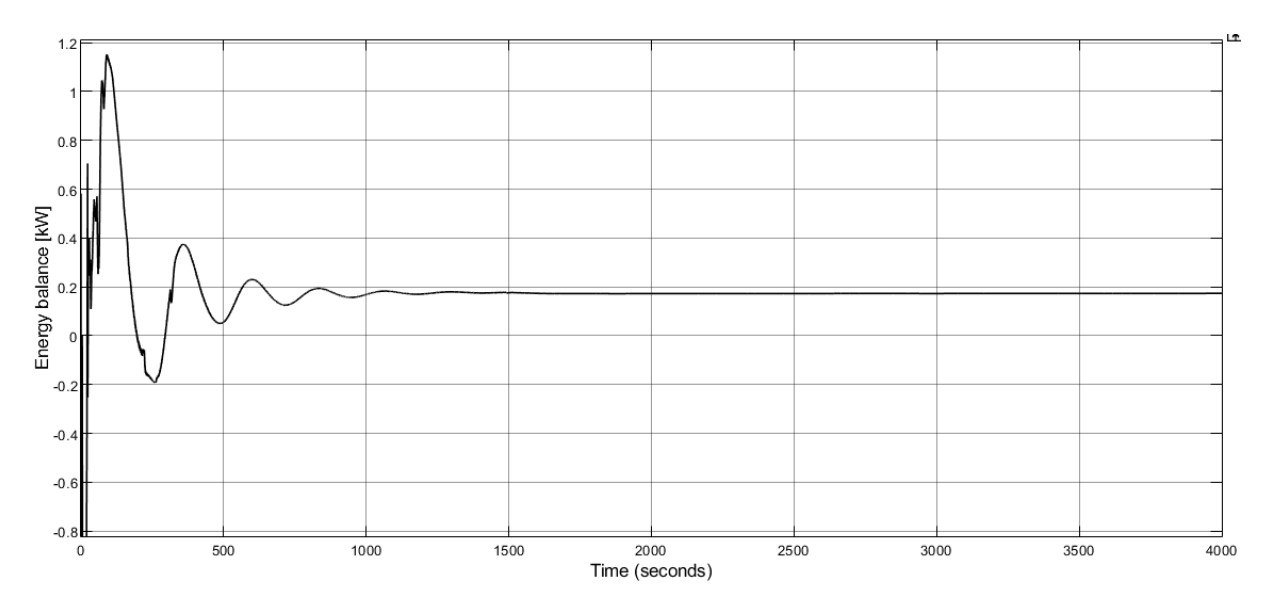


Figure 39: Energy balance of a Heat Pump





7 Results of the First Test

This first characterization of the heat pump (air conditioning system) consisted of analyzing how a reduction in compressor power — or more specifically, in its angular velocity ω — would propagate throughout the system parameters, with particular focus on energy performance and efficiency indicators.

For each selected outdoor temperature (proportional to the amount of heat entering the house) and a fixed indoor set-point temperature, the first step was to determine the **minimum compressor power** required to ensure that the indoor temperature **did not increase by more than 0.5 °C over a 2-hour period**. This threshold is significantly more restrictive than the comfort tolerances typically accepted by European [98] and U.S. [99] standards.

Recalling that the **maximum power** required to stabilize the system was determined using the *PID controller*, the **minimum power** was instead identified through an iterative process, by progressively observing the behavior of the indoor temperature over time while instantaneously changinh the power supplied to the compressor.

As well shown in Figure 40 (T_{ext} =27°C; T_{set} =22°C), a *step-wise behavior* was applied between the nominal and minimum power values. This approach was used to trigger the time evolution of all variables in the system, starting from a **Steady-State conditions**.

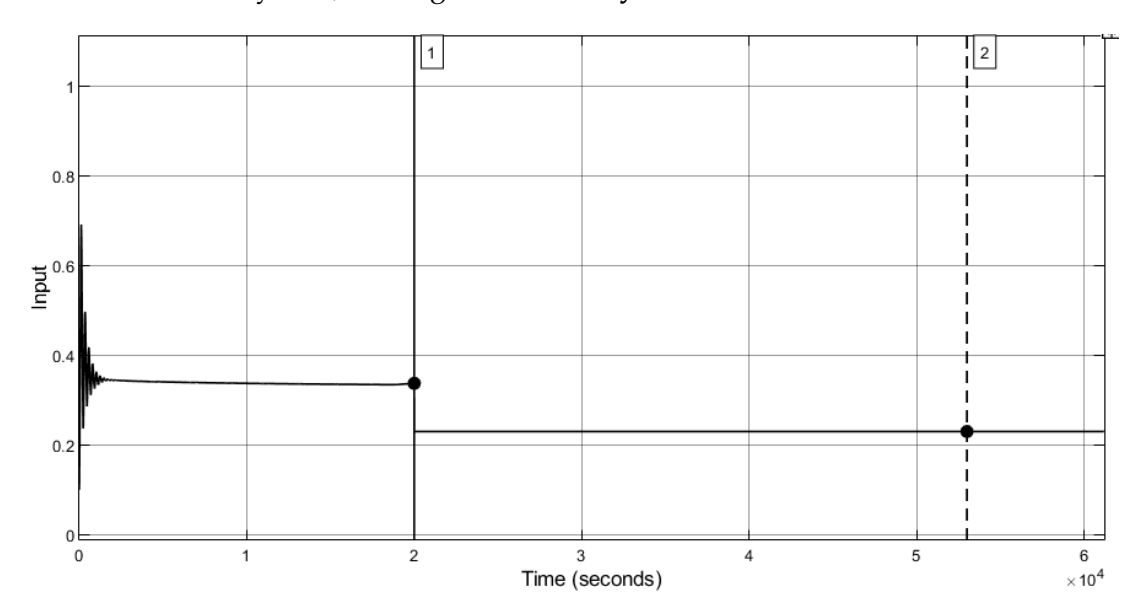


Figure 40: Normalized Input for the Compressor angular velocity to obtain the +0.5°C

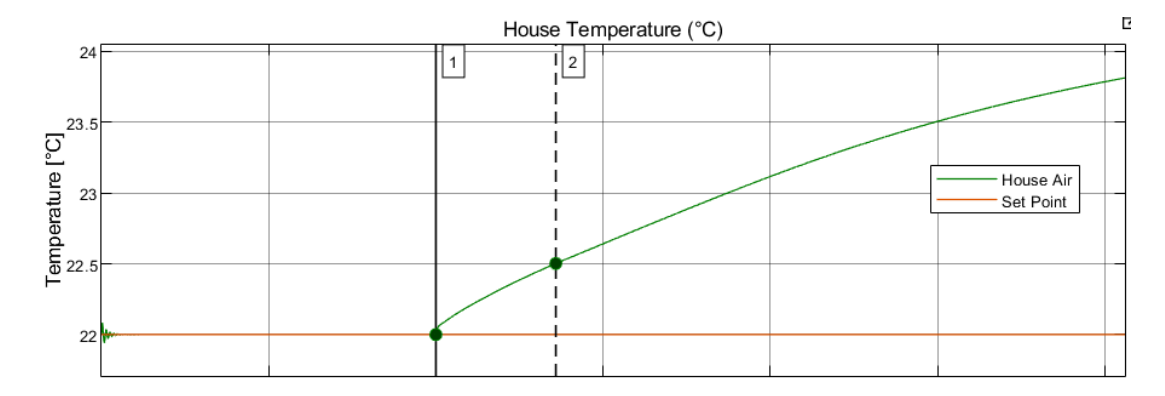


Figure 41: Temperature increase due to minimum Compressor power





Once the minimum input value at which the temperature constraint $(+0.5^{\circ}\text{C})$ in a 2 hours period is no longer satisfied (Figure 42) has been identified, the angular velocity of the compressor is gradually decreased (from the nominal to the minimum), in order to allow a controlled evolution of the system. To do so it was used a *Ramp block* (mask)(link) on Simulink. Typically, the slope set within the block is: -0.000007.

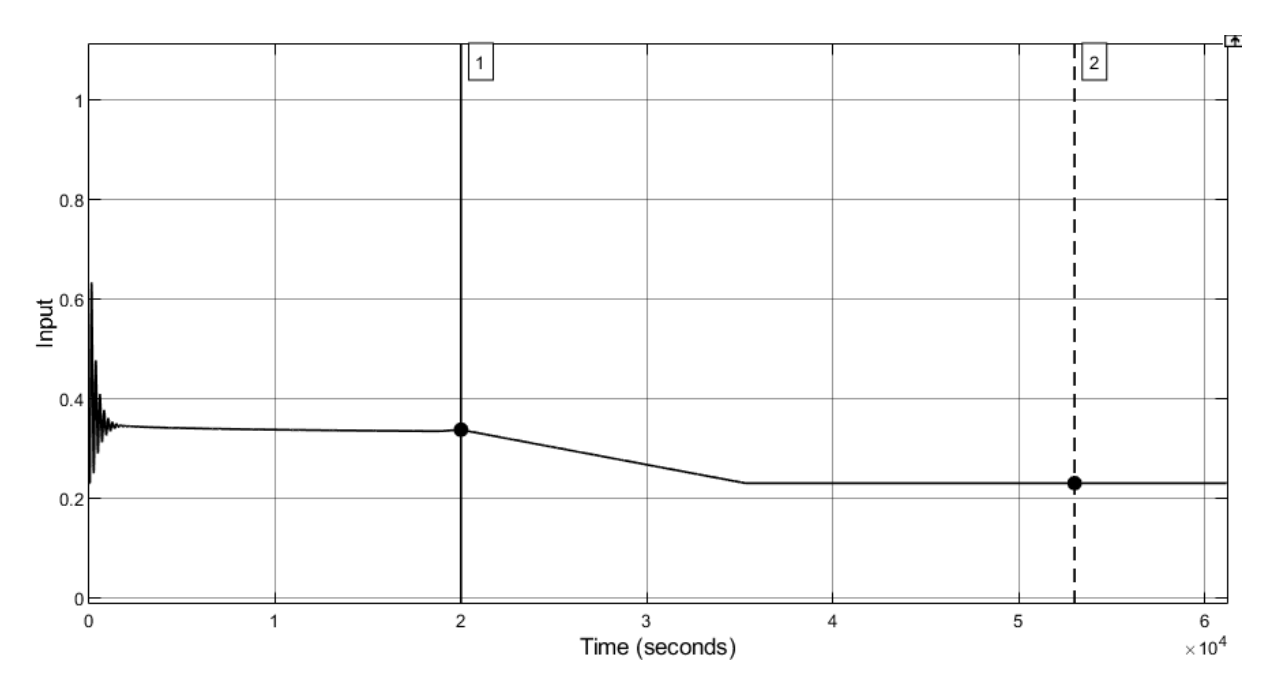


Figure 42: Input for the First test

By observing how the system evolves, decreasing the angular velocity at the compressor, within the range defined by the nominal and minimum power values, it is possible to understand the interactions among the various variables involved.

This allows the development of a grid support-oriented system design that takes into account as many relevant parameters as possible.

As previously mentioned, the components that draw electrical power from the grid are two: the *fans* and the *compressor*. This initial study focuses solely on varying the compressor power (angular velocity), while keeping the fan power constant throughout the test.

Figure 43 lists in a table the fan frequency settings corresponding to each external temperature, assuming a fixed indoor set-point temperature of 22 °C.

T_setpoint = 22°C		
External temperature [°C] Fans Frequency [Hz]		
35	60	
32	50	
30	50	
27	40	
25	40	

Figure 43: Fans frequencies for each External temperature





The choice of fan frequencies and so powers is not arbitrary and is based on several considerations: it aims to reflect a realistic and practical reduction pattern consistent with the typical operating behavior of an air conditioning system; it results from a comparative analysis across individual scenarios (as it possible to see in the next paragraph 7.0.1); and it has always the objective of ensuring compliance with the critical temperature limit of the refrigerant fluid at the compressor outlet, which must not exceed $71.3\,^{\circ}\text{C}$ (Table 2).

In the case where $T_{\rm ext}=35^{\circ}{\rm C}$, the power levels of both the fan and the compressor were set as if they were operating at their maximum capacity, while still fully complying with all the specifications previously outlined.

It is important to note that the Simulink model also provides an additional graphical and mathematical verification of the cycle operation, the pressure–enthalpy (p-h) state diagram for each seconds of the working model. At any operating point of the refrigeration machine, this must comply with the four key stages of the refrigeration cycle, remaining below the saturation curve of the R-410A refrigerant, as shown in the following figure. The diagram (Figure 44) refers to the most critical operating condition among all the tests performed, with an external temperature of 35 °C and maximum angular velocity of both the compressor and the fans.

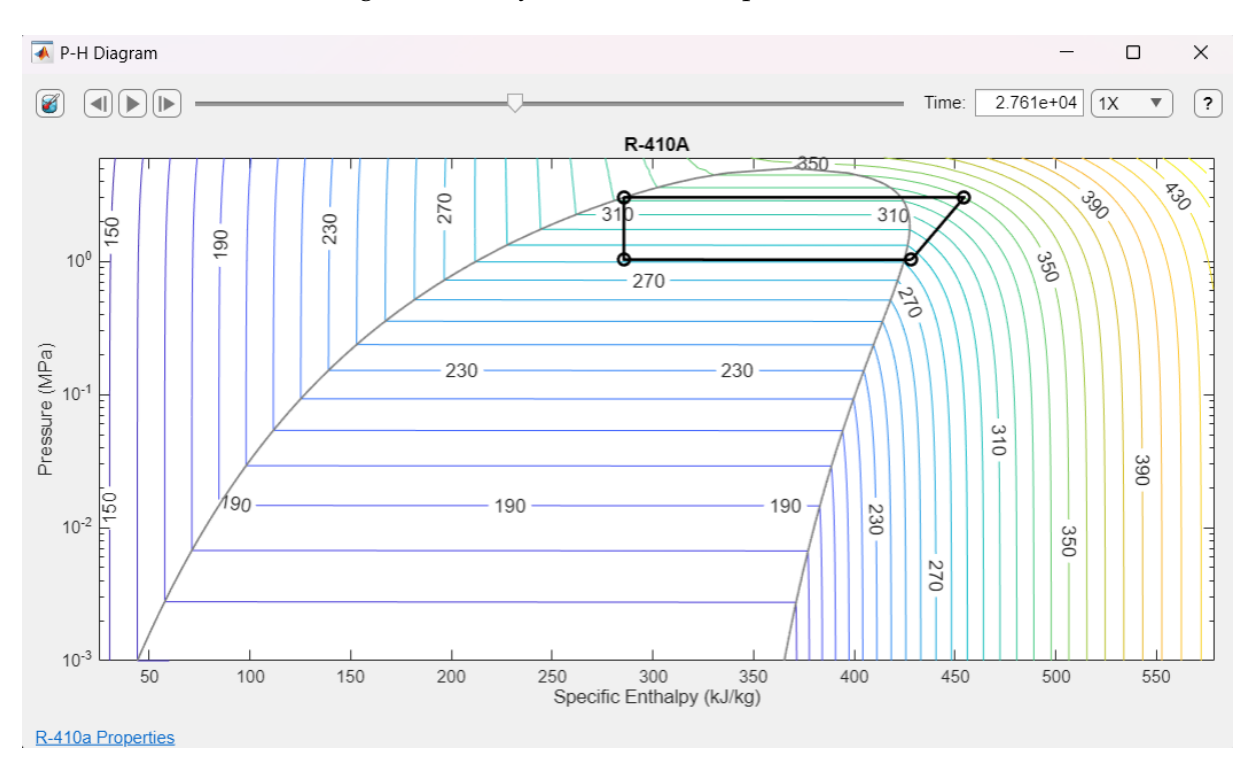


Figure 44: (p-h) state diagram for T_{ext} =35°C

As can be observed, taking into account the theoretical framework on heat pumps previously analyzed, the system also satisfies the fundamental points of the cycle in this 'extreme' operating condition. It might appear logical to assume that, if the cycle is respected under this limiting case, it would consequently hold true for all other conditions as well. However, based on extensive practical experience, it is always recommended to verify the validity of the cycle at every instant, since the variables involved are numerous and not always entirely predictable.





7.0.1 Comparative analysis in the case where $T_{\rm ext}=30^{\circ}{\rm C}$, in which the fan operating frequency was varied — once set to 60 Hz, once to 50 Hz and once to 40 Hz

The following section outlines the energy analysis conducted for the case with an outdoor temperature (T_{ext}) of 30°C to facilitate the correct selection of the system's fan frequency. While this analysis was performed across all the range of outdoor temperatures, for the sake of brevity, the discussion will be confined to this specific case.

Figure 45 illustrates the resulting dependency between the selected fan frequency and power, and the compressor's power for the system under study.

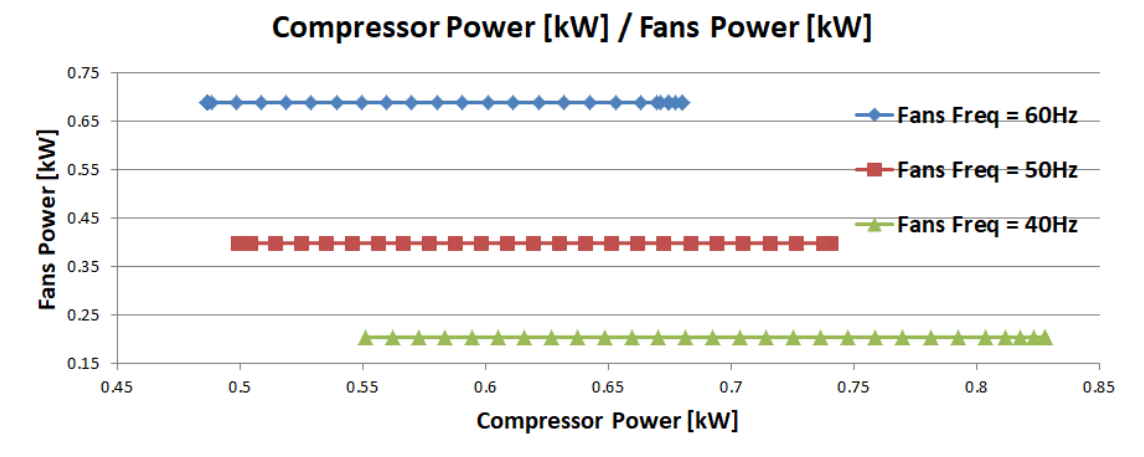


Figure 45: Text=30°C Power comparison between fans frequencies

The first parameter on which this comparative energy study is based is the EER (Energy Efficiency Ratio) that is a dimensionless performance indicator used to assess the cooling efficiency of heat pump and refrigeration systems and is defined here as:

$$EER_{M} = \frac{Cooling Capacity}{Electrical Power Input} = \frac{Q_{evaporator}}{W_{compressor} + W_{fans}}$$
(37)

In this study both the compressor and fan power refer to the *mechanical power*, not the electrical one as typically required by the standard EN 14511 [100]. This choice is due to the fact that mechanical power is the only value that can be extracted directly from the Simulink model used in this study.

$$Wcompressor/fans [kW] = \frac{T \cdot 2\pi \cdot w}{60 \cdot 1000}$$
 (38)

where:

- *W* is the mechanical power in kilowatt [kW],
- *T* is the torque in Newton-meter [Nm],
- w is the angular velocity in revolutions per minute [rpm].

Taking into account the EER as defined above, this parameter can now also be included in the comparative analysis.





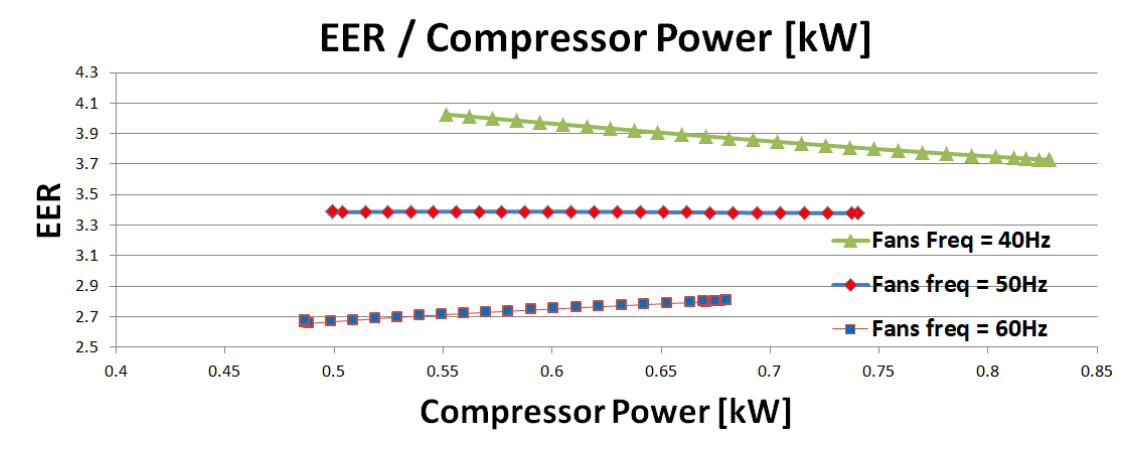


Figure 46: Text=30°C EER comparison between fans frequencies

From this comparison, several observations can be made. The first (Figure 46) is that the compressor power range in the case where the fans operate with the lowest frequency of 40 Hz (referred to as Case 1) is shifted to the left compared to the 50 Hz (Case 2) and 60 Hz configurations (Case 3). This result is fully consistent with the analysis carried out, as it confirms that the compressor in Case 1 requires more power initially to stabilize the system—due to the lower airflow provided by the fans. Furthermore, as the angular velocity decreases, the system in Case 1 fails to meet the indoor temperature constraint more quickly, since it struggles to maintain the thermal balance (see Equation (36)).

The second observation (Figure 46) —arguably the most significant—is that within the range of power values common to all the cases, the EER, i.e., the system's efficiency, is significantly higher in **Case 1** and furthermore, it increases as the power supplied to the compressor decreases.

This indicates that, for an equal reduction in compressor power, when the fans operate at 40 Hz, the system achieves a much more efficient and energy-saving performance compared to Case 2 and Case 3. This outcome can also be explained from a thermodynamic perspective: increasing the fan power means increasing the airflow to the heat exchangers (evaporator and condenser), but this air has a lower heat transfer capacity than the refrigerant gas. As a result, for an equal increase in power applied to the compressor (and thus refrigerant mass flow rate) or to the fans (airflow rate), the system will exchange more heat when compressor power is increased. Consequently, efficiency (EER) is also improved in that case. It is important to note, however, that if there is insufficient airflow available to exchange heat—on either the indoor (house) or outdoor side of the circuit—the temperature of the refrigerant will increase, potentially causing serious issues related to its critical temperature limit.

In this example, it is worth pointing out that the temperature at the compressor outlet (T_2) , at maximum compressor power, is approximately 330 K in the case with the fan operating at 60 Hz, whereas it reaches 335 K in the case with the fan at 50 Hz and it reaches 341 K in the case of 40 Hz.

Keeping in mind that the critical temperature limit for the refrigerant is $\bf 344.8~K$ a choice was therefore made that took into account both the efficiency of the system and its structural and technical limitations.





7.1 First Test — the desired indoor temperature is fixed (in this case, $T_{\rm set\,point}=22\,^{\circ}\text{C}$)—the behavior of the modeled heat pump parameters is observed as the angular velocity of the compressor decreases. The study is performed for five different outdoor temperatures

The various results obtained from this analysis are presented below.

The first point to clarify is that the following results are presented as lines on graphs. However, these lines are composed of discrete operating points, and it is in this form that they must be evaluated. At each of these operating points, corresponding to a specific outdoor temperature, the heat pump is capable of operating for a minimum duration of 2 hours without causing the indoor temperature to rise by more than 0.5°C.

As a first result, the power ranges at the compressor are shown as a function of the selected fans frequencies and external temperatures that ensure compliance with the constraint on the allowable increase of the indoor air temperature.

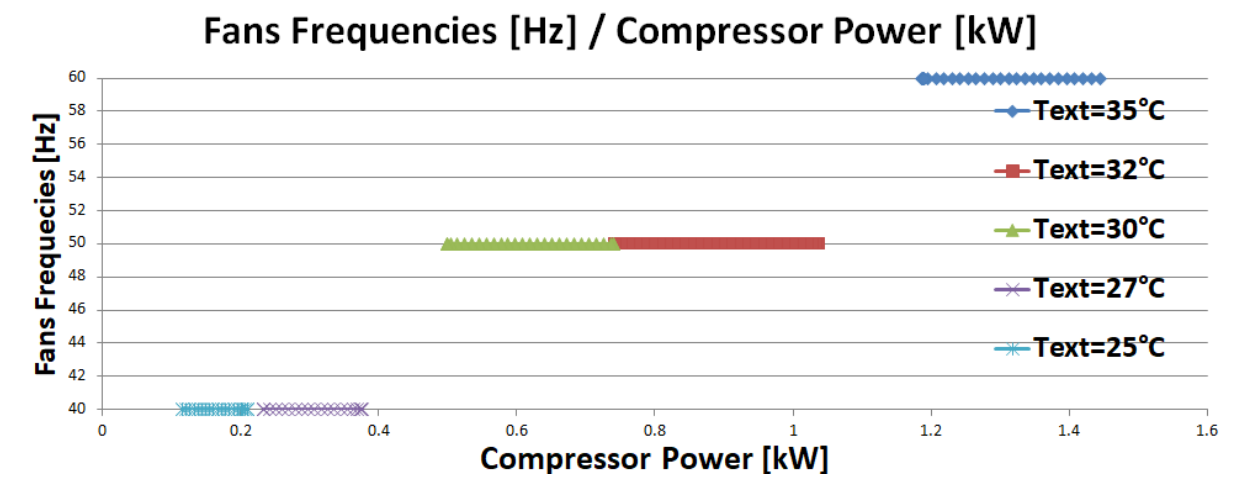


Figure 47: Fans Frequency/ Compressor Power

Figure 48 shows the relationship between the compressor mechanical power and frequency for various outdoor temperatures. As expected, these two variables exhibit a fully proportional behavior, since they are functions of one another and both are directly proportional to the angular velocity.

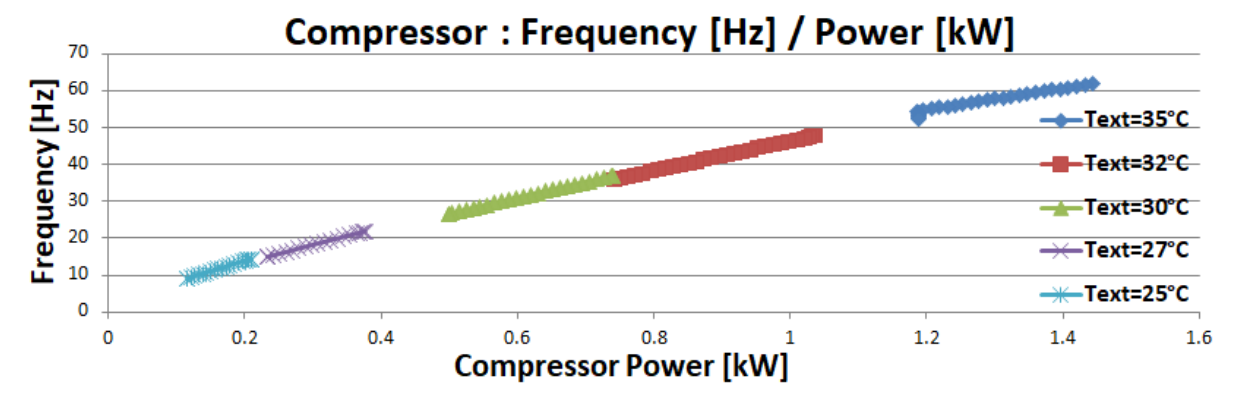


Figure 48: Fans Frequency/ Compressor Power

It is also possible to observe (Figure 49) how the capacity of the evaporator to extract heat—given





a constant airflow rate through the house and external environment circuit—is proportional to the power supplied to the compressor, which in turn determines the mass flow rate of refrigerant circulating within the heat pump (Figure 50). By reducing the latter, the amount of heat exchanged in the evaporator (as well as in the condenser) naturally decreases accordingly.

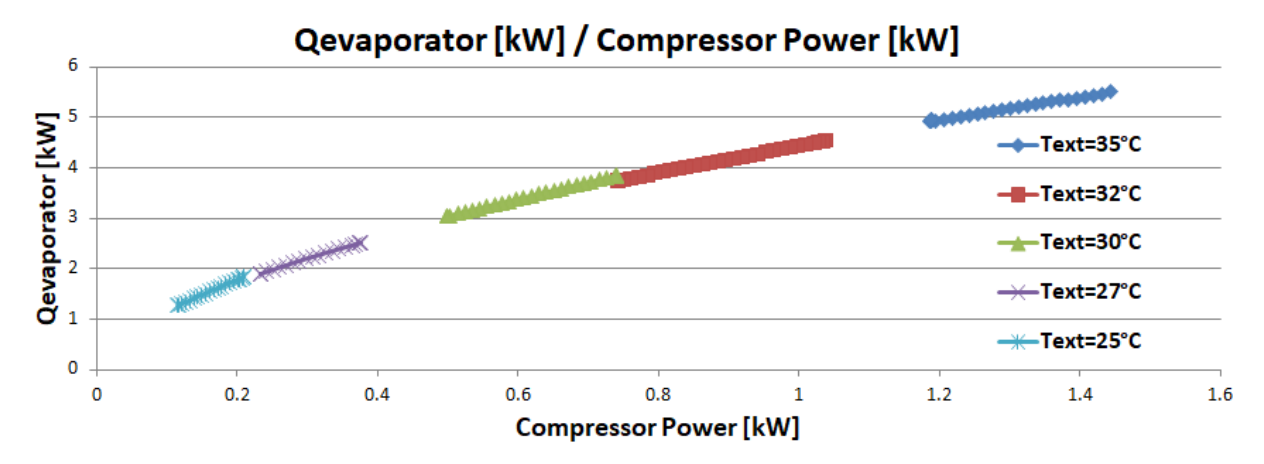


Figure 49: $Q_{evaporator}$ / Compressor Power

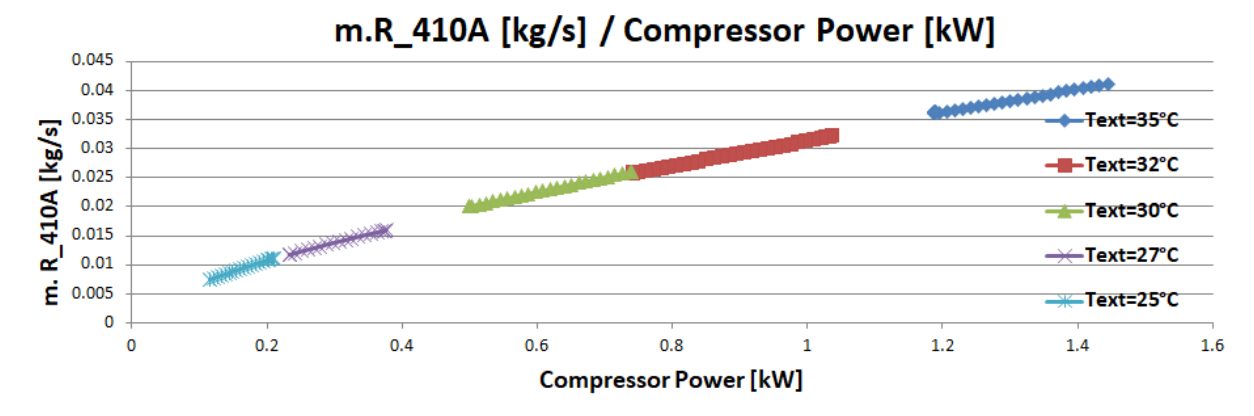


Figure 50: mass flow rate R-410A depending on the Compressor power

Recalling the formula of EER_M reported below, it is possible to analyze, from an energy efficiency perspective, the effect of the power reduction at the compressor:

$$EER_M = \frac{Q_{\text{evaporator}}}{W_{\text{compressor}} + W_{\text{fans}}}$$
(37)

It is important to note that $W_{\rm fans}$ remains constant throughout all the tests; consequently, the only variables in play are $Q_{\rm evaporator}$ and $W_{\rm compressor}$ which, as shown in Figure 49, are proportional and behave as illustrated. It is clearly visible that during the reduction of the compressor power, whose delta between the maximum and minimum power, regarding each test, is on the order of 0.25–0.1 kW, the corresponding delta in the useful effect, i.e., the power extracted from the evaporator, is on the order of 0.5–1 kW. These different orders of magnitude obviously make the results rather detailed and nuanced (Figure 51).





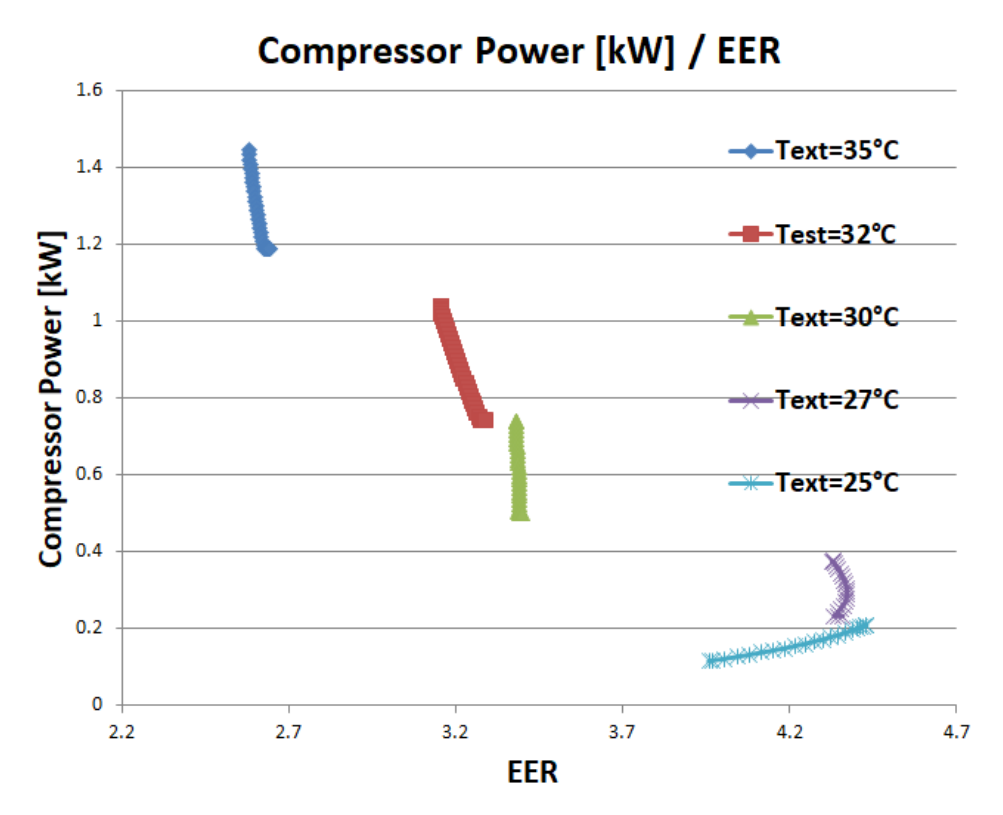


Figure 51: Compressor Power / EER_M

From a visual analysis, it can be easily observed that the slopes of the curves vary significantly depending on the external temperature. When the external temperature is 35° C, 32° C, or 30° C, it is evident that reducing the compressor power enhances the First Law efficiency of the refrigeration system.

Consequently, from the perspective of supporting the grid through an automatic demand reduction response, two main effects are produced: first, the electrical power consumption of the system decreases, contributing to peak shaving and grid stabilization; second, the efficiency improvement allows the system to operate more sustainably, minimizing energy losses while still providing the required cooling performance.

Regarding the case in which the external temperature is $27\,^{\circ}$ C, it can be clearly observed that there is a reversal in the slope when the compressor power is approximately 0.2977 kW. This indicates that below this power level, the heat exchanged by the evaporator decreases more rapidly than the total power absorbed by the heat pump (i.e., $W_{\text{compressor}} + W_{\text{pump}}$). This change in trend can be easily explained, as both $Q_{\text{evaporator}}$ and $W_{\text{compressor}}$ are relatively low, and the power consumed by the fans begins to have a significant impact on the overall energy balance.

Thus, from the previously mentioned point, namely $W_{\rm compressor} \approx 0.2977$ kW, it can be inferred that reducing the compressor power for potential grid support purposes also leads to a decrease in the energy performance of the analyzed heat pump.

Finally, attention is drawn to one last detail regarding these $W_{\rm compressor}/EER_M$ curves, namely the change in slope before and after the reversal point. Reducing the compressor power above this point, i.e., for the three higher external temperatures, increases the EER_M , but only relatively slightly.





- T_{ext} =35°C: EER_M increase from \approx 2.579 to \approx 2.641
- T_{ext} =32°C: EER_M increase from \approx 3.152 to \approx 3.287
- T_{ext} =30°C: EER_M increase from \approx 3.377 to \approx 3.395

In the case of $T_{\rm ext}=27\,^{\circ}{\rm C}$, moreover, for a variation in compressor power of approximately half compared to the other three cases, the EER_M decreases from about 4.429 to 3.965, resulting in a delta that is roughly five times larger than the others.

The last noteworthy result to be reported concerns the extent to which the mechanical power supplied to the compressor varies in the extreme cases, the Steady State and Minimum Power in order to be compliant with the $+0.5^{\circ}$ C in 2h, compared to each individual case analyzed.

	COMPRESSOR		
External temperature	Steady State Power [kW]	Minimum Power [kW]	delta Power [kW]
Text=35°C	1.445	1.189	0.255
Text=32°C	1.037	0.742	0.295
Text=30°C	0.740	0.499	0.241
Text=27°C	0.375	0.233	0.142
Text=25°C	0.210	0.115	0.094

Figure 52: First test: results on the maximum ΔP for each external temperature

7.2 First Test second part - results concerning the characterization of the air conditioning system, keeping the outdoor temperature constant (set at $T_{\rm ext}=30^{\circ}{\rm C}$) while varying the indoor set-point temperature of the house

A clarification to be made is that in this second test the frequency and power supplied to the fans are kept equal and constant for all three setpoint temperatures. The fans are therefore operated at $50\,\mathrm{Hz}$, at which they absorb approximately $0.3983\,\mathrm{kW}$ of total "mechanical" power.

In this second test as well, a remarkable result is the linear dependence between the mechanical power supplied to the compressor and its operating frequency, as can be clearly observed in Figure 53. It also emerges that, in order to satisfy a lower indoor temperature setpoint, a greater power input is required compared to when the setpoint temperature is higher.

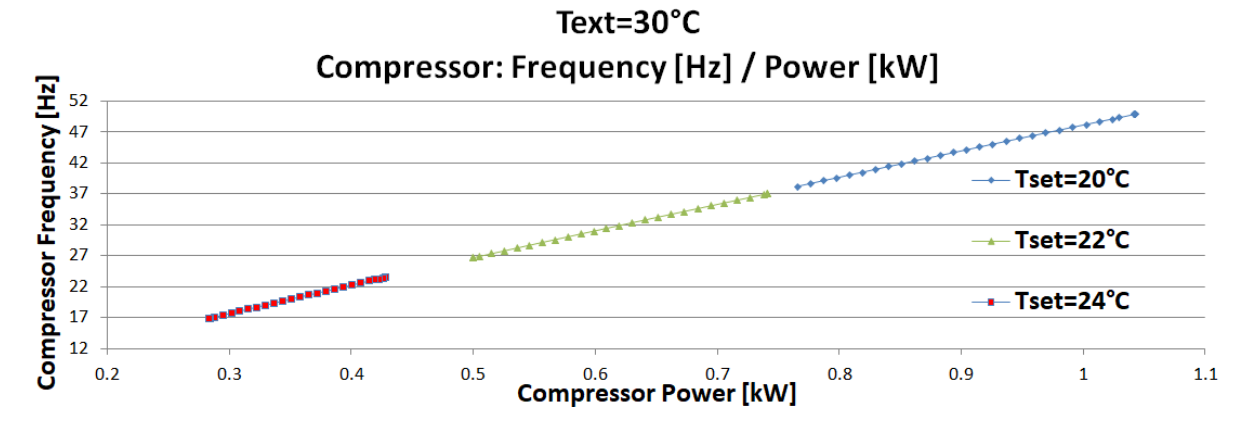


Figure 53: Fans Frequency/ Compressor Power





Continuing along the line of interdependent variables, it can also be observed here that a lower power supplied to the compressor results in a lower thermal power exchanged at the evaporator, which is obviously also due to a reduced flow of refrigerant circulating in the heat pump circuit (concepts already discussed previously). However, Figure 54 illustrates an additional theoretical aspect that was not previously observable. Increasing the setpoint temperature, under the same external conditions, naturally leads to a decrease in the temperature difference between the indoor and outdoor environments and, consequently, to a reduction in the actual amount of thermal power that must be extracted by the evaporator from the house before being rejected into the outdoor environment. The results obtained are therefore consistent with this concept, since as $T_{\rm setpoint}$ decreases, the value of $Q_{\rm evaporator}$ increases.

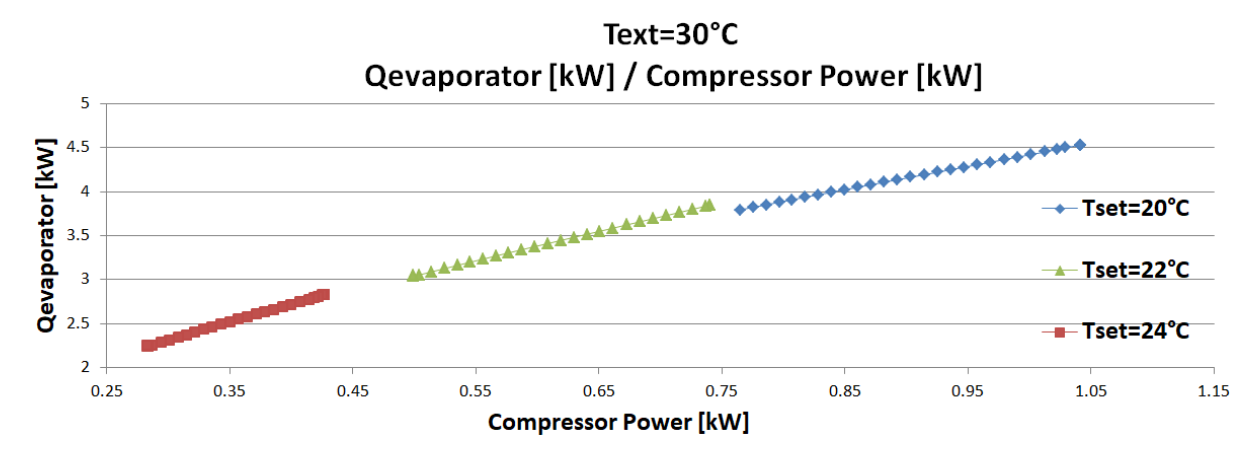


Figure 54: $Q_{evaporator}$ / Compressor Power

The last graph presented illustrates the relationship between the power supplied to the compressor and the coefficient of performance (EER_M) .

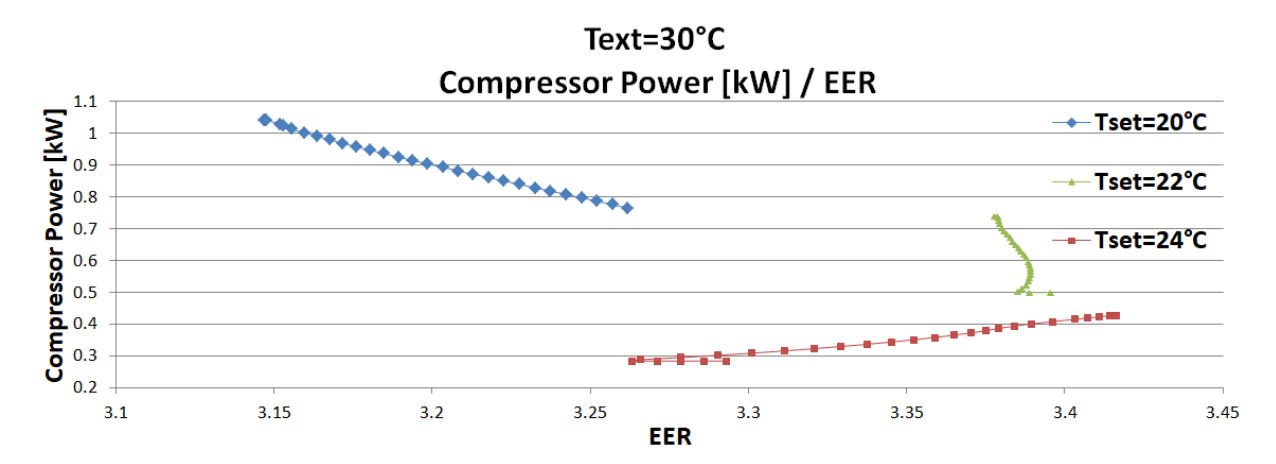


Figure 55: Compressor Power / EER_M

It can also be observed in this case that when the compressor power demand is relatively high $(T_{\rm setpoint}=20\,^{\circ}{\rm C})$, the curve exhibits a negative slope, indicating that a reduction in the power supplied to the heat pump compressor results in an improvement in the overall energy efficiency of the system.

For $T_{\rm setpoint}=22\,^{\circ}{\rm C}$, on the other hand, a variable behavior can be observed depending on whether the operating point lies above or below the inversion threshold at $W_{\rm compressor}=0.566\,{\rm kW}$. This inversion point is associated with a different balance established between the numerator





and the denominator of the EER_M , and more specifically with the relative weight that W_{fans} assumes within the overall energy balance.

It is nevertheless important to observe that, as the compressor power decreases, the EER_M values do not diverge significantly from one another, suggesting a certain degree of indifference in terms of First Law efficiency with respect to variations in the power absorbed by the system.

Finally, we consider the curve corresponding to $T_{\rm setpoint} = 24\,^{\circ}\text{C}$ which, as already discussed, requires the least energy input to the heat pump in order to achieve equilibrium between the thermal exchanges within the analyzed system, given its proximity to the external temperature. In this case, several aspects can be observed.

First, reducing the compressor power leads to a decrease in the EER_M of the heat pump. Moreover, the slope of the curve is nearly twice as steep as in the case of $T_{\rm setpoint}=20\,^{\circ}\text{C}$. Despite these two negative effects, it is evident that the EER_M values remain consistently higher than those at $T_{\rm setpoint}=20\,^{\circ}\text{C}$, indicating that operating at this higher temperature is, in any case, more advantageous from an energy efficiency perspective.

The final result to be extracted from this test is the maximum delta on the power applied to the compressor, bearing in mind that any power within the Steady State-Minimum Power range is capable of satisfying the primary constraint, i.e. the limitation on the temperature increase $(+0.5^{\circ}\text{C})$ over a 2-hour interval.

	External temperature 30°C COMPRESSOR		
T set point [°C]	Steady State Power [kW]	Minimum Power [kW]	delta Power [kW]
20	1.041	0.765	0.277
22	0.740	0.499	0.241
24	0.428	0.283	0.144

Figure 56: First test second part: results on maximum ΔP

For both parts of the first test, it was observed that the input power can generally be reduced by approximately 30% compared to the nominal power required to maintain the steady state.

The most interesting aspect related to this power reduction is the speed with which the load can be modulated. The compressor modelled in this heat pump utilizes a variable speed (inverter) compressor, which provides two key advantages. Firstly, it is already operating during the power modulation, which completely avoids the overcoming of start-up mechanical inertia (the slowest and most energy-intensive phase). Secondly, given the domestic scale of the system, it is characterized by a reduced rotating mass and therefore a relatively low mechanical inertia, which renders the compressor's response time almost instantaneous.

This combination of factors leads to the conclusion that, while adhering to the limits imposed by the test, all these power reductions (ΔP_{HP}) can be achieved practically instantaneously.





8 Results of the Second Test

By reintroducing the fundamentals of the second test, it was designed to fully exploit the thermal inertia of the house by instantly cutting off the mechanical power supplied to the compressor and fans, thereby stopping the refrigeration cycle and its useful work of cooling the house.

For this test as well, the same fan frequencies used in the first test were applied (Figure 57). The only difference is that, since the PID value necessary to reach the system's equilibrium point was already known, it was directly set as the input to the compressor for each case. Therefore, all the inputs for this second test were constant for both the compressor and the fans.

T_setpoint = 22°C			
External temperature [°C]	Fans Frequency [Hz]		
35	60		
32	50		
30	50		
27	40		
25	40		

Figure 57: Fans frequencies for each External temperature

Figure 58 shows that at t=20,000 s, when the power to the compressor and fans is cut off, heat exchanges associated with the heat pump cease immediately. The evaporator stops absorbing heat from the indoor air, and the condenser no longer rejects heat to the exterior. The only remaining heat transfer is due to the natural thermal flow from the external environment into the house, governed by the indoor–outdoor temperature gradient. The graph clearly shows an initial steady-state period prior to heat pump shutdown, corresponding to the established thermal equilibrium, followed by a decline in exchanged heat as the indoor temperature rises.

The total heat transfer $Q_{enviroment-to-house}$ can be expressed as the sum of convective and conductive contributions:

$$Q_{environment-to-house} = \sum_{i} h_i A_i (T_{s,i} - T_{\infty,i}) + \sum_{j} \frac{k_j A_j}{d_j} (T_{\text{inside},j} - T_{\text{outside},j})$$
(39)

where h_i and A_i are the convective heat transfer coefficient and surface area of surface i, $T_{s,i}$ and $T_{\infty,i}$ are the surface and ambient temperatures for convection, and k_j , d_j , A_j , $T_{\text{inside},j}$, and $T_{\text{outside},j}$ are the thermal conductivity, thickness, cross-sectional area, and interior and exterior temperatures of wall j, respectively.

It is therefore easily observed, even from the formula, that the heat flux exchanged between two environments is directly proportional to the temperature difference between them. The greater this ΔT , the higher the exchanged heat flux.





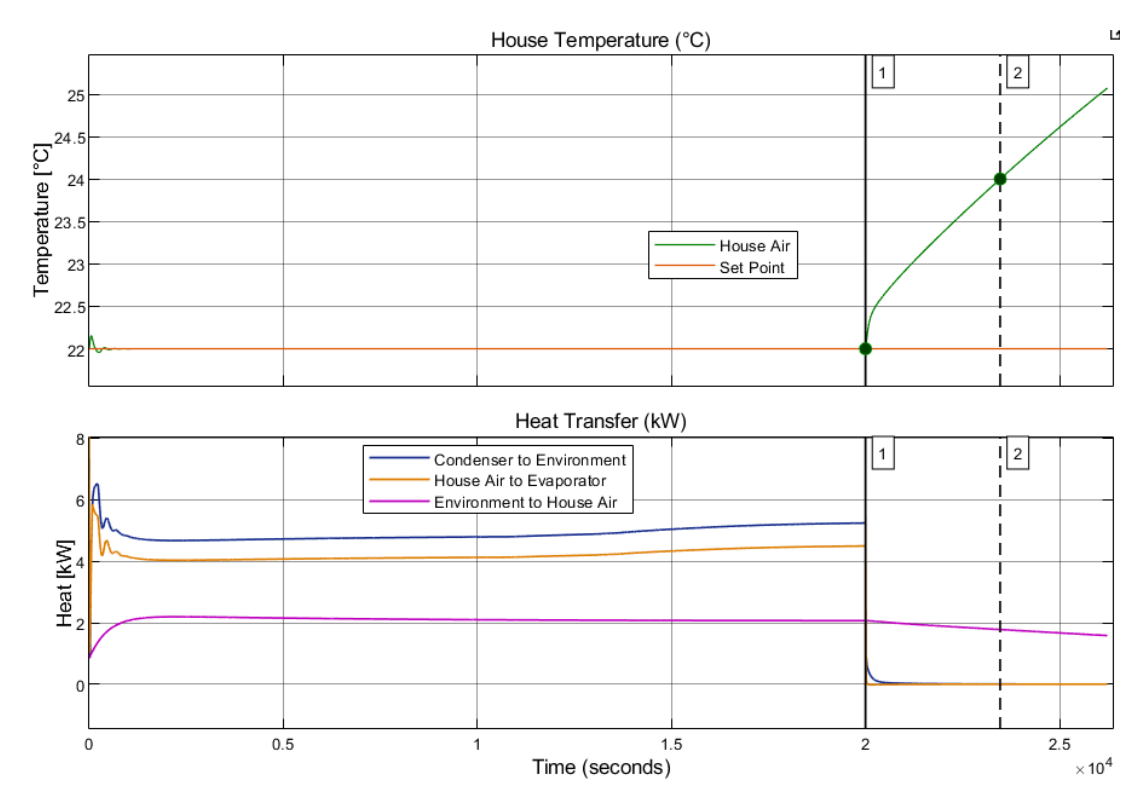


Figure 58: Text=32°C temperature and heat exchange behaviour stopping the system

A novel theoretical framework is hereby introduced to rigorously define the concept of thermal inertia.

In building physics, thermal inertia is often quantified using the **thermal inertia index**, which reflects the ability of building elements (such as walls, floors, or entire rooms) to absorb and release heat over time.

$$I_t = \sum_{i} (\rho_i \cdot c_i \cdot d_i) \tag{40}$$

where ρ_i , c_i , and d_i are, respectively, the density [kg/m³], the specific heat capacity [J/(kg·K)], and the thickness [m] of material layer i. This index is calculated by summing the contributions of each individual layer that composes a building element. The higher the value of I_t , the greater the thermal inertia of the structure [31]. Numerical calculation of this index is not required for the scope of this thesis and will therefore not be performed.

Thermal inertia, instead, will be assessed using a temporal value expressed in seconds or minutes. Specifically, it will be defined as the time elapsed, from the instant the heat pump is completely turned off, until the indoor temperature (set at $T_{\text{setpoint}} = 22^{\circ}\text{C}$) increases by either +0.5°C or +2.0°C. This approach, analogous to ON–OFF control, provides the greatest support to grid stability, albeit over a shorter time interval.

Figure 59 presents, for each analyzed outdoor temperature, the maximum decrease in power that can be drawn from the heat pump and the duration for which this reduction to 0 kW can be sustained.





Temperature set point = 22°C									
	+(0.5°C	+2	2.0°C	Fans Power [kW]	Compressor Power [kW]	Total Power [kW]		
Text [°C]	time[s]	time [min]	time[s]	time [min]					
25	1470	24.50	10000	166.67	0.204	0.210	0.414		
27	850	14.17	7050	117.5	0.204	0.375	0.579		
30	400	6.67	4450	74.17	0.398	0.740	1.138		
32	260	4.33	3490	58.17	0.398	1.037	1.435		
35	110	1.83	2460	41	0.688	1.445	2.133		

Figure 59: Thermal inertia of the house in [s] and the resulting power capacity that can be gained

The interdependence of the variables at play is easy to see. The higher the outdoor temperature, the greater the amount of heat that must be expelled to maintain the setpoint temperature. This results in a direct proportionality between the outdoor temperature and the amount of instantaneous power the compressor uses.

Consequently, the higher the outdoor temperature, the greater the amount of curtailable power from the unit. However, at the same time, the less time it will take for the indoor temperature to exceed the limits set in the test.

To conclude, this second test also aims to highlight the clear distinction between the system's electrical rapidity and its thermal slowness.

Completely curtailing the power supply to the heat pump's compressor, which possesses very low mechanical inertia, results in measurable changes, first in the compressor's angular speed and subsequently on the electrical grid, within extremely short timescales (seconds or milliseconds).

Conversely, the thermal system (comprising indoor air, walls,thermal mass/supplies ...) exhibits high thermal inertia, which, as demonstrated, takes minutes if not hours to register a violation of the study's imposed temperature limits.





9 Results on the support provided

The potential support to the grid provided by this type of heat pump control and management will be assessed solely on the basis of their frequency support capability, which derives from their reduced power consumption, hypothetically regulated autonomously by a microprocessor that detects deviations of the grid frequency around 50 Hz.

To delve deeper into the local primary frequency control strategy, a flowchart is provided to illustrate its operation.

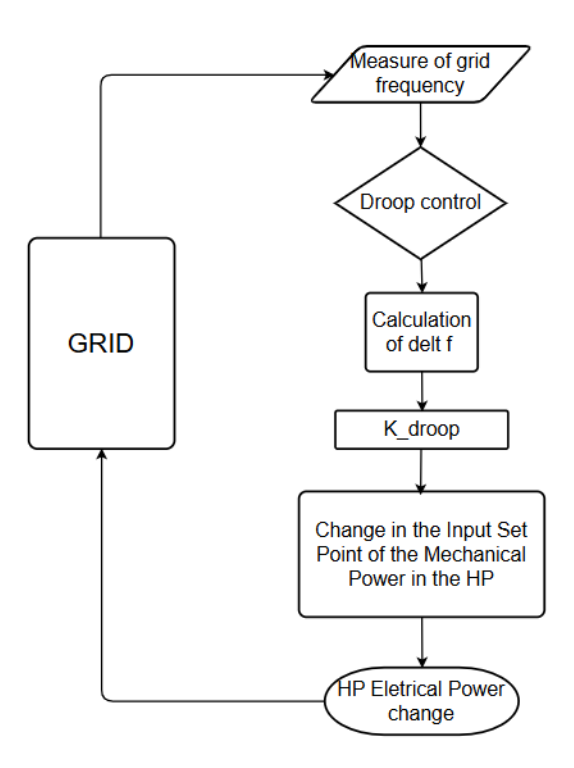


Figure 60: Local primary frequency control algorithm flowchart

The Droop Control setting is the same as the one used in the report [101] and it is based on principles of primary control for synchronous generators.

This control method adjusts the electrical power adsorbed from the heat pump based on observations of frequency variations in the electrical network Δf_{grid} . "The droop control follows a linear relationship between adjusted power consumption ΔP_{HP} and Δf_{grid} , where the droop k_{droop} describes the control sensitivity according to:

$$\Delta P_{HP} = k_{droop} * \Delta f_{grid} \tag{41}$$

The droop parameter k_{droop} must be small enough for the controlled device to ignore small imbalances or measurement errors, but large enough to improve the frequency response after a disturbance" [101]. Once the ΔP_{HP} of the heat pump imposed by the microprocessor or controller has been found due to the change in frequency in the network, it is also possible to study how this difference in energy absorption affects, in the opposite way, the frequency of the network itself.

Subsequently, the basic equation for frequency variation Δf_{HP} in the grid analyzed, due to a difference in absorption by the loads ΔP_{HP} , is recalled, which can be approximately estimated





by the following formula:

$$\Delta f_{HP} = \frac{\Delta P_{HP}}{2HS_{\text{base}}} \tag{42}$$

where:

- Δf_{HP} is the frequency support to the network due to the Heat Pump droop control [Hz]
- ΔP_{HP} : sudden change in power of the heat pump [MW]
- *H*: system inertia constant which represents the capability of rotating machines to withstand frequency deviations (in seconds)
- S_{base}: system base power (typically in MW)

The proposed study aims to analyze only the final step of the control algorithm within a Fast Frequency Response (FFR) framework. Specifically, once the microcontroller's response to the heat pump's power consumption difference (ΔP_{HP}) is known, the study evaluates its impact on the grid frequency.

The use of the term FFR is justified by the system's ability to change its power consumption virtually instantaneously, rather than by the actual duration for which this type of response is implemented.

It is important to remember that the first test allowed the system to maintain power consumption below its nominal value for at least 2 hours, whereas in the second test, the maximum duration for which power to the HPs could be completely curtailed was the primary variable. The results for this complete curtailment fell within a range of 2 to 24 minutes for a set temperature limit of +0.5°C, and between 41 and 167 minutes for a limit of +2.0°C.

Some preliminary clarifications regarding the study's assumptions must be made in order to understand how this formula will be applied.

Uniform Frequency Variation: The frequency variation in the grid is considered uniform across the entire area under study. This first assumption means that the grid is considered 'stiff,' meaning it is a well-interconnected network, and that the primary response is linear, i.e., without the activation of all the intrinsic control and protection mechanisms present in a real power system.

Identical Unit Size: Contrary to the reality where heat pumps have diverse nominal power ratings, all units will be assumed to be of the same size (the one set in the first and second tests). It is also important to note that the formula is valid only for relatively small power variations with respect to the total system power; therefore, it will be used for theoretical order-of-magnitude estimates rather than for actual and detailed assessments, which would require more complex simulations, including a complete system simulation rather than focusing solely on loads.

Coordinated Control: All units are assumed to be coordinated or, more simply, equipped with the same droop control scheme. This remark, although self-evident, is that in order to observe a significant contribution, a synchronous coordination of multiple units must be considered, since the effect of a single residential unit on system frequency would be negligible—both in the context of a microgrid and even more so in the context of a national grid.

Uniform distribution of the HP over the territory: The actual distribution of heat pumps is complex and non-uniform. Including all these variables would render the study analytically intractable and computationally prohibitive. Therefore, the assumption of a uniform distribution creates a manageable model, allowing the study to focus on the core phenomenon.





Uniform external and set point temperature over the whole area under study: Since the results from the first test are valid for only one set of temperatures at a time, it's important to consider a collective response from the HP fleet. Consequently, all units must be operating under uniform boundary conditions.

It is also important to remember that this formula can only express a single moment in time for which the system is characterised by a specific system base S and system inertia H.





9.1 European Scenario

Carrying out the proposed study under the aforementioned conditions at a European level is obviously an over-simplification of the concept to be analyzed. The most strained assumption is certainly that of a uniform frequency variation across the entire continent, which is known to be a paradox given the vastness of the electrical grid and the numerous voltage level decompositions (HHV, HV, MV, LV).

However, it remains interesting to qualitatively assess the potential contribution of coordinating these heat pumps to the grid's frequency.

To obtain the system base power (S), which reflects the sum of the rated power of all generators connected to the grid, we chose to look at the European load curve, which, obviously, except for transmission losses, must be equal in value at every moment in time to our S (as expressed in the Equation (5)). This choice was made because S is not explicitly known at every moment at the European level.

Figure 61 shows the maximum and minimum European load curves in 2024 for a single day provide by the ENTSO-E [27] (of course, this does not imply that these days hold the yearly peak and trough in energy demand). As already discussed, the maximum load curve generally is in winter, while the minimum load curve is in summer. It is also important to remember that during the summer, the share of renewables is much higher than in winter (lower contribution from solar energy), which also leads to a practical reduction in system inertia during this period.

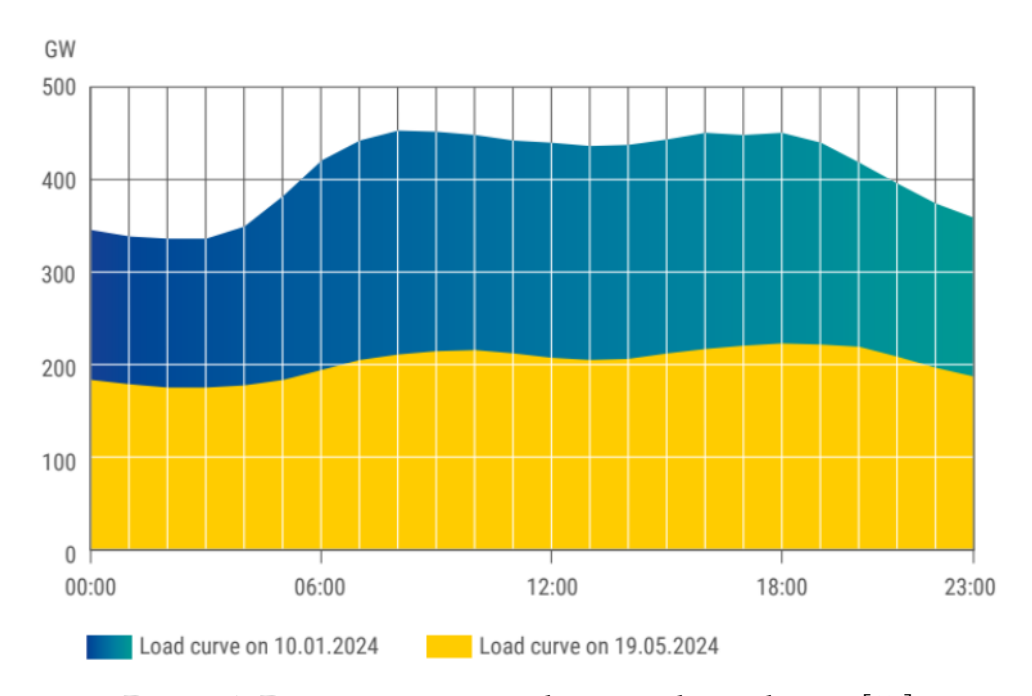


Figure 61: European maxima and minima demand curve [27]

The second piece of data we need is to understand how many units are present at the European level that can actually take part in the study we are conducting.

The European Heat Pump Association (EHPA), now in its 25th year, states that by 2024 there will be a stock of 25.5 million heat pumps in Europe, almost half of which will be air-to-air. The countries leading sales are those in the north, with Norway at the top of the list, where 48.1 heat pumps will have been purchased per 1,000 households by 2024. Italy stands at 13.2 units, and last is the United Kingdom with 3.5 units per 1,000 households [102].





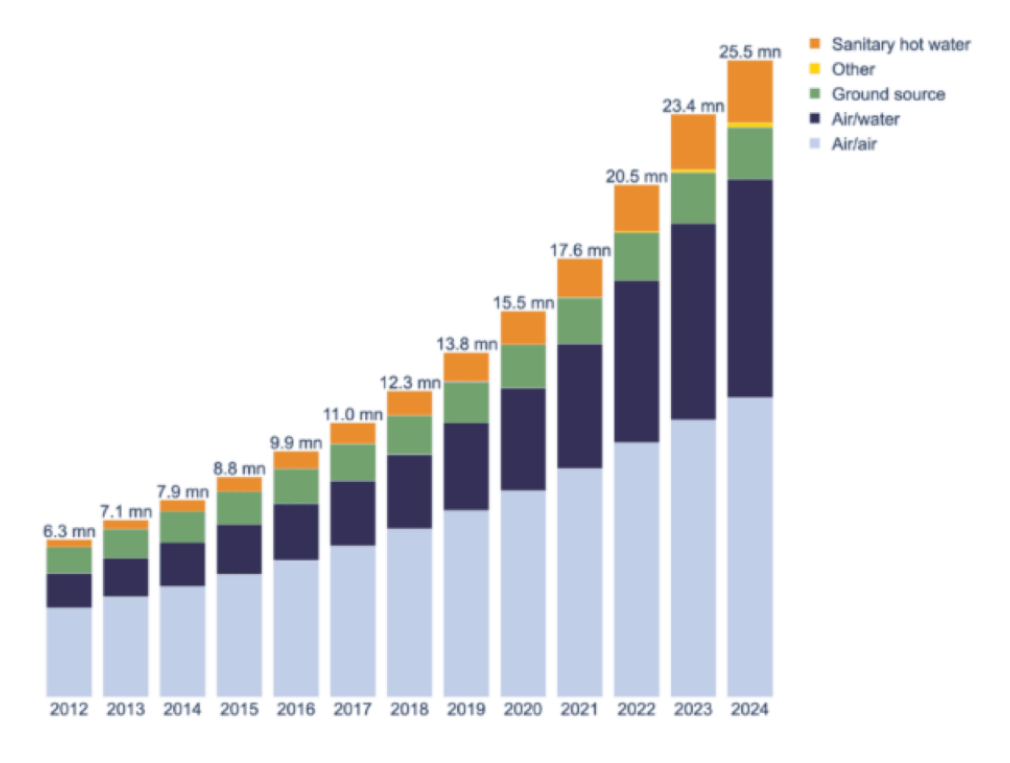


Figure 62: Heat pump units in Europe [27]

The final data point relevant to our study is the system's inertia. Referring to the study conducted by ENTSO-E [103] and considering the TYNDP2022-NT2030 scenario (i.e., the perspective from 2022 for achieving the 2030 targets), the maximum and minimum points of System Inertia can be identified.

To facilitate a more practical reading, Figure 7 containing the overall European inertia values analyzed in the report is once again presented.

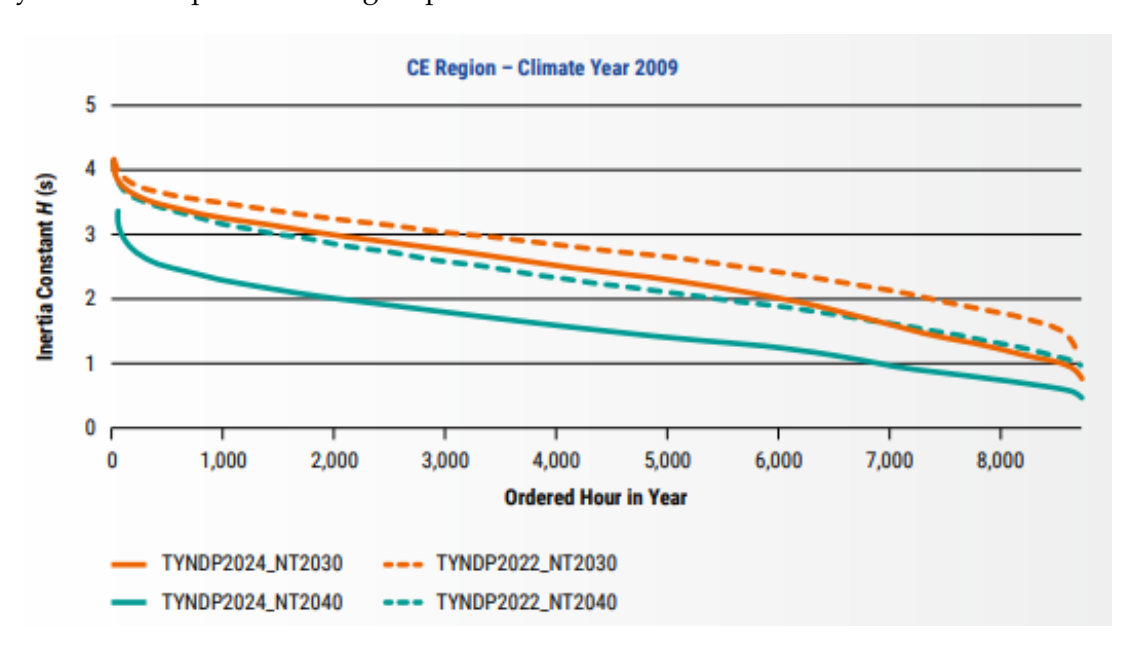


Figure 7. Inertia duration curve of the Continental Europe Synchronous Area (Replica of Figure 7 from page 16)

With all the necessary data available and by setting the ΔP_{HP} values equal to those found in





the first and second tests, it is possible to calculate the frequency support that N_{HP} heat pump units, operating in unison, can introduce into the European interconnected grid. Upon further refinement of the Equation (42), the new formulation to be utilized is obtained.

$$\Delta f_{HP} = \frac{\Delta P_{HP} * N_{HP}}{2HS_{\text{base}}} \tag{43}$$

Only two extreme cases will be studied, with the results subdivided based on whether all heat pumps operating in Europe are considered or only the air-to-air units discussed in this thesis. The two extreme cases will be referred to as *max* and *min*.

The *max* case will address the European winter scenario at 8:00 o'clock. This period is characterized by the highest demand for power (S_{max}) (Figure 61) and hypothetically also the highest system inertia (H_{max}) , given the lowest contribution from inverter-based energy sources.

This choice is supported by the fact that at this time of day, the sunrise has broken only in the southernmost European nations, such as Italy and Greece, less than half an hour ago, while in all other countries, the sun has not yet appeared. This, of course, results in a near-total absence of solar power generation and, consequently, an obvious need for power compensation from traditional power plants.

Conversely, the *min* case will focus on the summer period at 12 o'clock. During this time, instantaneous power demand is at its lowest (Figure 61), but a large portion for sure is produced by renewable sources. This leads to a reduction in the overall system inertia.

By cross-referencing the values between the maximum and minimum load curves and the maximum and minimum system inertia values, the following cases are presented.

1.
$$H_{max} = 4.1 \text{ s and } S_{max} = 450 \text{ GW}$$

2.
$$H_{min} = 1.2 \text{ s} \text{ and } S_{min} = 210 \text{ GW}$$

A table will subsequently be presented, which summarizes the results from the first test. In this test, for each specific outdoor temperature analyzed, the mechanical input power was decreased from the nominal operating power absorbed by the heat pump—which is used to perpetually maintain an indoor setpoint temperature of 22°C.

The power was decreased to a minimum value that, if held constant, was still able to prevent the setpoint temperature from being exceeded by more than $+0.5^{\circ}$ C over a 2-hour period.

For each outdoor temperature, this maximum ΔP_{HP} will therefore be presented. Using this data and the Equation (43), the maximum frequency support to the grid will be calculated for both the *max* and *min* cases, considering the number of heat pump units under analysis.

			air/air heat pumps		
		25500000	12750000	25500000	12750000
		Case H a	nd S max	Case H and S min	
External temperature delta Power [kW]		[mHz]	[mHz]	[mHz]	[mHz]
Text=35°C	0.255	1.765	0.883	12.926	6.463
Text=32°C	0.295	2.035	1.018	14.900	7.450
Text=30°C	0.241	1.664	0.832	12.185	6.093
Text=27°C	0.142	0.979	0.489	7.167	3.583
Text=25°C	0.094	0.653	0.326	4.780	2.390

Figure 63: First Test: Frequency support to the grid due to ΔP_{HP}





A careful analysis of the reported results immediately shows that as the maximum ΔP_{HP} increases, the possible frequency support to the grid also increases. It is also observed, in both the *max* and *min* cases, that the grid frequency results when considering all heat pumps versus only the air-to-air units are exactly half in value. This is due to the assumption that air-to-air units constitute 50% of the total installed fleet. These results are entirely consistent with what was expected using Equation (43).

A subsequent significant finding is the difference in values obtained in the max and min cases. It can be clearly seen in Figure 63 that these values differ by approximately an order of magnitude in every case, indicating that the support provided by these heat pumps in a Fast Frequency Response context is much more pronounced when the grid has low stability (H_{min}) and generation is also quite low (S_{min}) .

Figure 64 graphically shows the difference between the usage of S and H maximum or minimum for the $T_{ext}=35\,^{\circ}\text{C}$ and $T_{ext}=25\,^{\circ}\text{C}$ cases, considering all heat pumps in use. It is easy to note that for the same reduction in power provided to the compressor (ΔP_{HP}) , there is an enormous difference in the effect this produces on the grid.

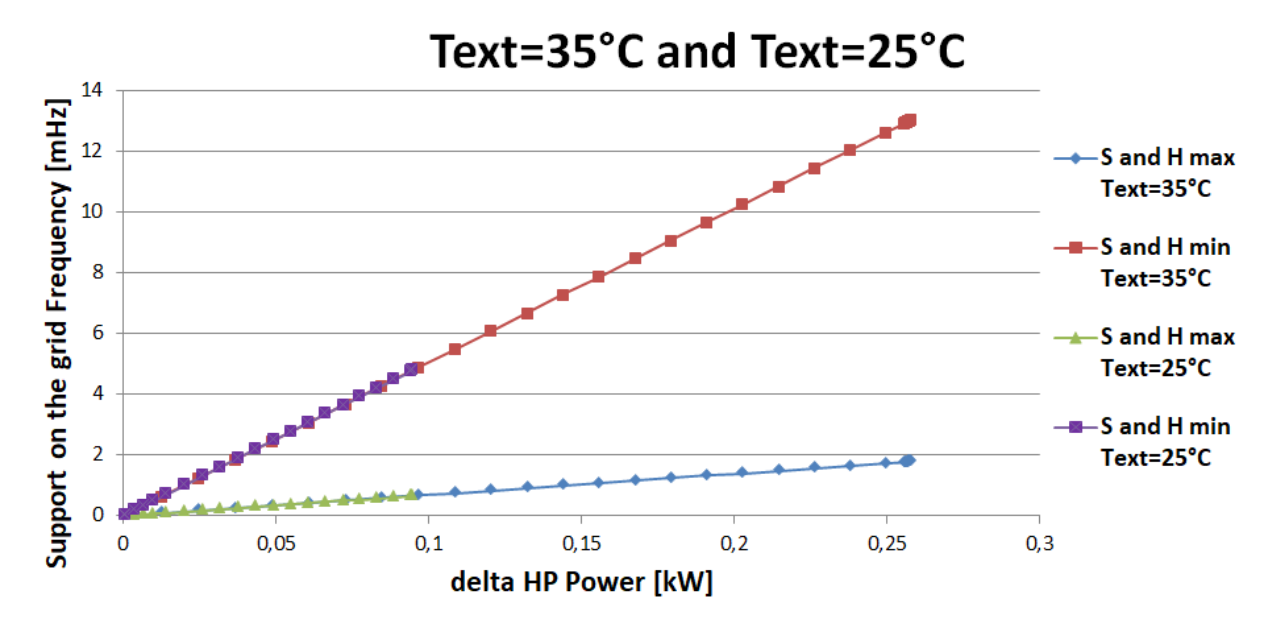


Figure 64: Difference in max and min case for T_{ext} =35°C and T_{ext} =25°C

This result is also valid for all other outdoor temperatures. This is entirely consistent with the theory introduced in this thesis, as well as being fully mathematically coherent with the formula used (43).

In contrast to the results just described, it is crucial to recall that a part of the first test involved the systematic reduction over time of the power supplied to the compressor, from its nominal value down to a minimum. This, of course, means that the ΔP_{HP} changes over time, increasing until it reaches its maximum value.

It is therefore also of interest to examine how the frequency support to the grid varies as ΔP_{HP} increases for different outdoor temperature scenarios. Figure 65 wants to highlight this phenomenon taking into account the cases where $T_{ext}=35^{\circ}\text{C}$ and $T_{ext}=25^{\circ}\text{C}$, showing also how the effect changes with the number of units considered.





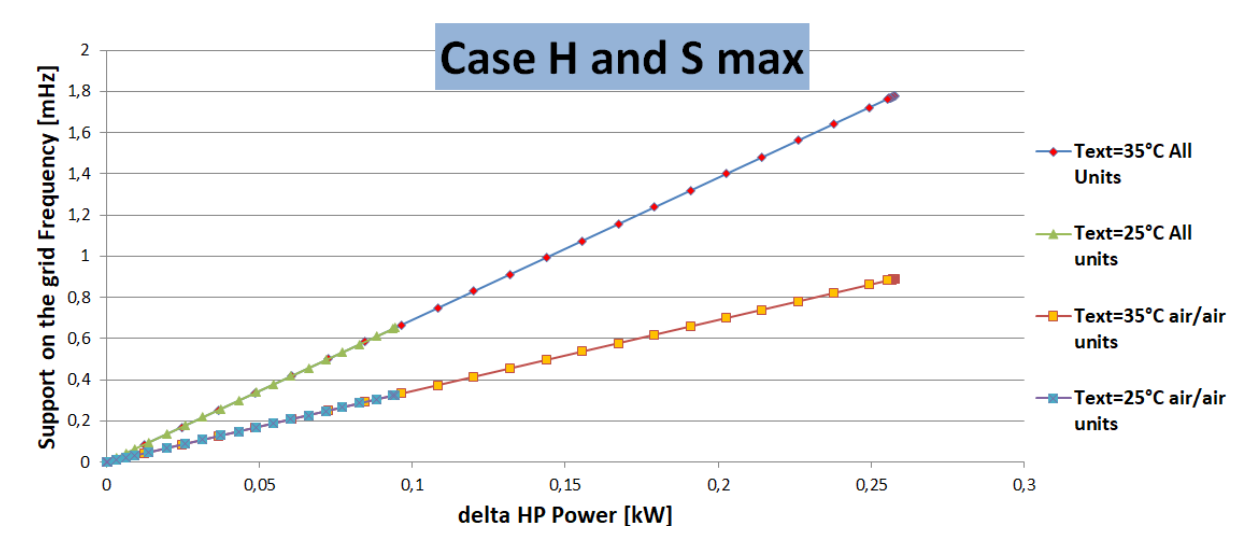


Figure 65: Inertia results of the second test

Upon analysis, it's clear that in all four cases, the frequency support provided to the grid increases linearly with the increasing of the ΔP_{HP} . Naturally, for the same ΔP_{HP} , the frequency response is exactly double when all heat pump units are considered, as opposed to only the air-to-air units. This is consistent with the earlier finding that air-to-air units make up 50% of the total fleet.

The second part of the first test involved setting the outdoor temperature at 30°C and varying the indoor setpoint temperature. The results from this portion of the study are presented below (Figure 66):

		all the heat pumps	air/air heat pumps	all the heat pumps	air/air heat pumps
		25500000	12750000	25500000	12750000
External temperature 30°C		Case H and S max		Case H and S min	
T set point [°C]	delta HP Power [kW]	[mHz]	[mHz]	[mHz]	[mHz]
20	0.277	1.912	0.956	13.997	6.999
22	0.241	1.664	0.832	12.185	6.093
24	0.144	0.998	0.499	7.307	3.653

Figure 66: Inertia results of the second test

While the final result to be presented concerns the second test (Figure 67) , which involved completely eliminating the power supply to all heat pump components connected to the grid—namely the compressor and the two fans. The time required for the indoor temperature to exceed predefined limits was then observed. Specifically, the two limits were $+0.5^{\circ}$ C and $+2.0^{\circ}$ C relative to the setpoint temperature.

				all the heat pumps	air/air heat pumps	all the heat pumps	air/air heat pumps
		Temperture set point= 22°C		25500000	12750000	25500000	12750000
		+0.5°C	+2.0°C	Case H and S max		Case H and S min	
Text [°C]	Total HP Power [kW]	time [min]	time [min]	[mHz]	[mHz]	[mHz]	[mHz]
35	2.133	1.8	41.0	14.740	7.370	107.917	53.958
32	1.435	4.3	58.2	9.917	4.959	72.607	36.303
30	1.138	6.7	74.2	7.867	3.934	57.598	28.799
27	0.579	14.2	117.5	3.998	1.999	29.271	14.636
25	0.414	24.5	166.7	2.860	1.430	20.937	10.469

Figure 67: Inertia results of the second test





The entire discussion from the preceding analysis is equally applicable to these cases. In particular, the key findings are thus reaffirmed:

- A direct, linear relationship is observed between the increasing of the ΔP_{HP} and the capacity for frequency support to the grid
- The *min* case demonstrates a capacity for frequency response that is approximately an order of magnitude greater than that of the *max* case

The final observation to be made relates to the fact that in the second test (where the power supply is completely cut off), the greatest capacity for grid support is achieved, albeit for a shorter duration.

What makes this second test so compelling is the potential for a coordinated HP fleet to respond very quickly to frequency fluctuations, thereby providing a Fast Frequency Service. What's more, by considering the less restrictive $+2.0^{\circ}$ C temperature limit, the system could also provide long-duration frequency support, fitting within the scope of Secondary or Tertiary Frequency Response.

Additionally, keeping in mind that this involves a complete curtailment of power consumption, this technology could also be considered for use in contexts such as Load Shedding (LS) or Interruptible Load Management (ILM) when much more dangerous grid-level contingencies occur.





9.2 Italian Scenario

The same methodology will be applied to calculate the frequency support that heat pump units distributed across Italy can provide. The System Base will be taken from the specific ENTSO-E report for each nation [27], while the System Inertia will be assumed to be the same as the European-level value, given that it is an interconnected environment that should theoretically operate in a synchronous manner.

Highest and lowest hourly load values for 2024 in MW¹

	HIGH	EST LOAD	VALUE	LOWE	ST LOAD	VALUE
	Date	Time ²	(in MW)	Date	Time ²	(in MW)
AL	31.12.24	16:00 - 17:00	1 659	18.09.24	21:00 - 22:00	419
AT ³	08.01.24	10:00 - 11:00	10 268	04.08.24	02:00 - 03:00	4 177
BA	17.01.24	16:00 - 17:00	2 233	01.01.24	06:00 - 07:00	0
BE	19.01.24	10:00 - 11:00	13 206	28.07.24	03:00 - 04:00	6 194
BG ⁴	23.01.24	07:00 - 08:00	6 899	27.10.24	02:00 - 03:00	2 331
CH	06.12.24	08:00 - 09:00	10 437	05.12.24	22:00 - 23:00	2 743
CY	31.12.24	17:00 - 18:00	928	12.12.24	05:00 - 06:00	567
CZ	11.01.24	08:00 - 09:00	10 561	04.08.24	03:00 - 04:00	3 850
DE	15.01.24	10:00 - 11:00	75 508	22.09.24	01:00 - 02:00	32 413
DK	22.10.24	14:00 - 15:00	9 070	14.07.24	03:00 - 04:00	2 520
EE	04.01.24	09:00 - 10:00	1 595	22.09.24	12:00 - 13:00	463
ES	11.01.24	19:00 - 20:00	37 937	27.10.24	00:00 - 01:00	4 707
FI	03.01.24	17:00 - 18:00	14 993	23.06.24	01:00 - 02:00	5 780
FR	10.01.24	12:00 - 13:00	82 800	12.05.24	04:00 - 05:00	29 575
GB	27.11.24	18:00 - 19:00	1 443	20.10.24	03:00 - 04:00	413
GE	23.08.24	11:00 - 12:00	2 299	19.04.24	02:00 - 03:00	1 003
GR	22.07.24	11:00 - 12:00	11 034	05.05.24	03:00 - 04:00	3 074
HR	17.07.24	17:00 - 18:00	3 363	31.03.24	02:00 - 03:00	1 213
HU	22.01.24	16:00 - 17:00	7 148	01.04.24	11:00 - 12:00	2 701
IE	27.11.24	17:00 - 18:00	5 642	06.08.24	03:00 - 04:00	2 672
IT	19.07.24	12:00 - 13:00	50 046	01.01.24	03:00 - 04:00	17 312

Figure 68: European maxima and minima demand curve [27]

What we are observing, however, represents a shift from the total European curve. The two maximum and minimum cases are highlighted again:

- On July 19, 2024, during the summer period, the peak power demand occurs between 12:00 and 13:00. This is a time when a significant amount of renewable energy is certainly connected to the grid decreasing the value of the system inertia.
- On January 1, 2024, the minimum peak is found between 03:00 and 04:00. During this period, the renewable contribution is very limited, as evidenced by the complete absence of solar power in the middle of the night.

Upon reintroducing the two maximum and minimum European H values [103] and inversely correlating them with the two S values for Italy, the following two cases are observed:





- 1. $H_1 = 4.1 \text{ s}$ and $S_1 = 17.312 \text{ GW}$
- 2. $H_2 = 1.2 \text{ s}$ and $S_2 = 50.046 \text{ GW}$

Regarding Italy, the report produced by the European Commission, 'ITALY: STATUS OF THE HEAT PUMP MARKET' [104], states: "heating and cooling account for 79% of the country's residential final energy consumption, with renewables supplying 19% of the total energy used for heating and cooling across all sectors" while the European Heat Pump Market Report 2025 produced by EHPA descrives Italy as a pivotal player in the European market, solidifying its position as the second-largest market by sales volume. The country's cumulative stock of nearly 4.2 million installed heat pumps demonstrates its key position, as it is a figure second only to France

However, the report highlights that Italy's market penetration remains limited relative to its household count. In 2024, the country registered fewer than 15 sales per 1,000 households, a figure that falls significantly short of the levels seen in Scandinavian countries [102].

It is estimated that approximately 97% of the heat pumps in operation are air-source units, meaning they draw energy from the ambient air (air-to-air or air-to-water). Furthermore, drawing from various sources, it will be assumed that the share of only air-to-air systems in Italy is around 70%.

Consequently, the following values will be used:

- Total heat pumps: 4.2 million units
- Air-to-air heat pumps: 4.2 million \times 97% \times 70% = 2.8518 million units

The initial results from the first test, contextualized for the Italian case, are presented in Figure 69.

It should be noted that the test comprised two distinct test conditions: one where a fixed indoor setpoint temperature ($T_{\rm setpoint}=22^{\circ}{\rm C}$) was maintained while the outdoor temperature was varied, and a second where a fixed outdoor temperature ($T_{\rm ext}$ =30°C) was maintained while the indoor setpoint temperature was varied.

It must also be recalled that for both cases, the ΔP_{HP} values represent the maximum power reduction that can be drawn from the HP's power supply, while still ensuring that the established setpoint temperature does not exceed an increase of $+0.5^{\circ}$ C over a 2-hour period.

		all the heat pumps	air/air heat pumps	all the heat pumps	air/air heat pumps
		4200000	2851800	4200000	2851800
		Case H_1	and S_1	Case H_2 and S_2	
External temperature	delta HP Power [kW]	[mHz]	[mHz]	[mHz]	[mHz]
Text=35°C	0.255	7.558	5.132	8.933	6.066
Text=32°C	0.295	8.713	5.916	10.298	6.992
Text=30°C	0.241	7.125	4.838	8.421	5.718
Text=27°C	0.142	4.191	2.846	4.953	3.363
Text=25°C	0.094	2.795	1.898	3.304	2.243
External temp	erature 30°C				
T set point [°C]	delta Power [kW]				
20	0.277	8.185	5.558	9.674	6.569
22	0.241	7.125	4.838	8.421	5.718
24	0.144	4.273	2.901	5.050	3.429

Figure 69: Results of the First Test for the Italian area





Consistent with the European case, the initial result shows that the greater the maximum achievable ΔP_{HP} from the heat pump, the larger the maximum frequency support that the analyzed system can contribute to the grid.

It can also be easily seen that the greater the number of heat pumps controlled in a coordinated manner, the greater their frequency support capacity. Therefore, in both $Case\ 1$ and $Case\ 2$, when the entire fleet of heat pumps is considered rather than just the air-to-air units, the frequency support increases.

Regarding the differentiation between $Case\ 1$ and $Case\ 2$, the results do not show as pronounced a difference as they did in the European case. This can be attributed to the initial H and S values selected to reflect two real-world, extreme scenarios for the Italian grid. It can be said that these values fortuitously compensate for each other. This allows for a homogenization of the grid support capacity, even though the boundary conditions are entirely different.

The final results presented here (Figure 70) are from the second test, which involved completely disconnecting the power supply to the heat pump at various outdoor temperatures. The time elapsed until the indoor temperature increased by $+0.5^{\circ}$ C and $+2.0^{\circ}$ C relative to the setpoint temperature ($T_{\text{setpoint}} = 22^{\circ}$ C) was then measured.

				all the heat pumps	air/air heat pumps	all the heat pumps	air/air heat pumps
		Temperture s	et point= 22°C	4200000	2851800	4200000	2851800
		+0.5°C	+2.0°C	Case H_1 and S_1		Case H_2 and S_2	
Text [°C]	Total Power [kW]	time [min]	time [min]	[mHz]	[mHz]	[mHz]	[mHz]
35.0	2.133	1.8	41.0	63.11	42.85	74.58	50.64
32.0	1.435	4.3	58.2	42.46	28.83	50.18	34.07
30.0	1.138	6.7	74.2	33.68	22.87	39.81	27.03
27.0	0.579	14.2	117.5	17.12	11.62	20.23	13.74
25.0	0.414	24.5	166.7	12.24	8.31	14.47	9.83

Figure 70: Results of the Second Test for the Italian area

The findings from the first test in the Italian context also apply to this second set of results.

A key point to add is the trade-off between the magnitude and duration of frequency support. Higher outdoor temperatures require greater instantaneous power consumption to maintain the indoor setpoint temperature. This increased power draw implies that a larger amount of power can be reduced, thus providing a greater frequency support contribution to the grid. However, this support is maintained for a more limited period of time before the indoor temperature limits are exceeded.





10 Grid Flexibility and Energy Efficiency: An Integrated Assessment of Heat Pump Performance

The final section of this thesis examines the energy performance of the previously coordinated and modeled HP fleet and how it would behave in both the European and Italian contexts when used in a Fast Frequency Response (FFR) scheme. This is based on the assumption that these units would be the "first" to deviate from their nominal operating pattern.

Building on the results from the first part of the study, it was previously shown that a decrease in compressor power does not always correspond to an increase in the analyzed EER_M . Consequently, achieving the dual positive outcome of both an increased EER_M and frequency support to the grid is not always guaranteed. It is crucial to remember, however, that using these heat pumps in this context always implies some level of thermal discomfort for the user, even if it is limited and controllable.

This final analysis on the heat pump's performance relies on two key equations, which are recalled here: the one for EER_M (37) and the one for frequency support (43).

$$EER_M = \frac{Q_{\text{evaporator}}}{W_{\text{compressor}} + W_{\text{fans}}}$$
(37)

$$\Delta f_{HP} = \frac{\Delta P_{HP} * N_{HP}}{2HS_{\text{base}}} \tag{43}$$

Crucially, the change in heat pump power, denoted as ΔP_{HP} , is defined as the difference between the nominal compressor power and the new, lower power absorbed. This relationship is expressed by the following equation:

$$\Delta P_{HP} = W_{\text{compressor}} - W_{\text{compressor,i}} \tag{44}$$

where $W_{\text{compressor}}$ is the nominal power required to maintain the set point temperature (T_{setpoint}) , and $W_{\text{compressor},i}$ is the reduced power absorbed during the transient period.

This first section presents the results of the first test, which was conducted to evaluate the heat pump's performance during transient operation. The study began with the compressor running at a nominal power ($W_{\text{compressor}}$) to maintain the indoor setpoint temperature considering a specific constant external temperature. The power was then gradually ramped down to the minimum level that could keep the indoor temperature increase below the +0.5°C limit over a 2-hour period. The study was then conducted by considering five different outdoor temperatures.

The results will be presented for all the four cases: two for the European context (max and min) and two for the Italian context $(Case\ 1 \text{ and } Case\ 2)$. This analysis focuses exclusively on the coordinated use of air-to-air heat pumps.

The two European cases considered in this study were:

- 1. $H_{max} = 4.1$ s and $S_{max} = 450$ GW; the data was collected on January 10, 2024, at 8:00 AM. The ambient conditions at this time, with sunrise just beginning in the southernmost regions of Europe, allow for the hypothesis of significant system inertia due to the higher share of power produced by the traditional power plants.
- 2. $H_{min} = 1.2$ s and $S_{min} = 210$ GW; this was obtained on May 19, 2024, at 12:00 PM. In this case, it can be easily hypothesized that there was significant production of renewable energy, especially solar, which in turn suggests a weaker system inertia.





Two Italian cases considered in this study were:

- 1. $H_1 = 4.1$ s and $S_1 = 17.312$ GW; the data was collected on January 1, 2024, between 3:00 and 4:00 AM. During this period, the renewable contribution is very limited, as evidenced by the complete absence of solar power in the middle of the night.
- 2. $H_2 = 1.2$ s and $S_2 = 50.046$ GW; the data was collected on July 19, 2024, between 12:00 and 13:00. This is a time when a significant amount of renewable energy is certainly connected to the grid decreasing the value of the System Inertia

Solar energy is specified due to its inherent predictability. Unlike wind power—which is the leading inverter-based renewable—solar generation can be effectively forecasted or at least approximated, as it is not subject to the same high degree of variability as wind.

Figure 71 thus represents the combination of the heat pump's efficiency as a function of absorbed power and its ability to support grid frequency for the two European cases analyzed where 12,750,000 units of HP work together.

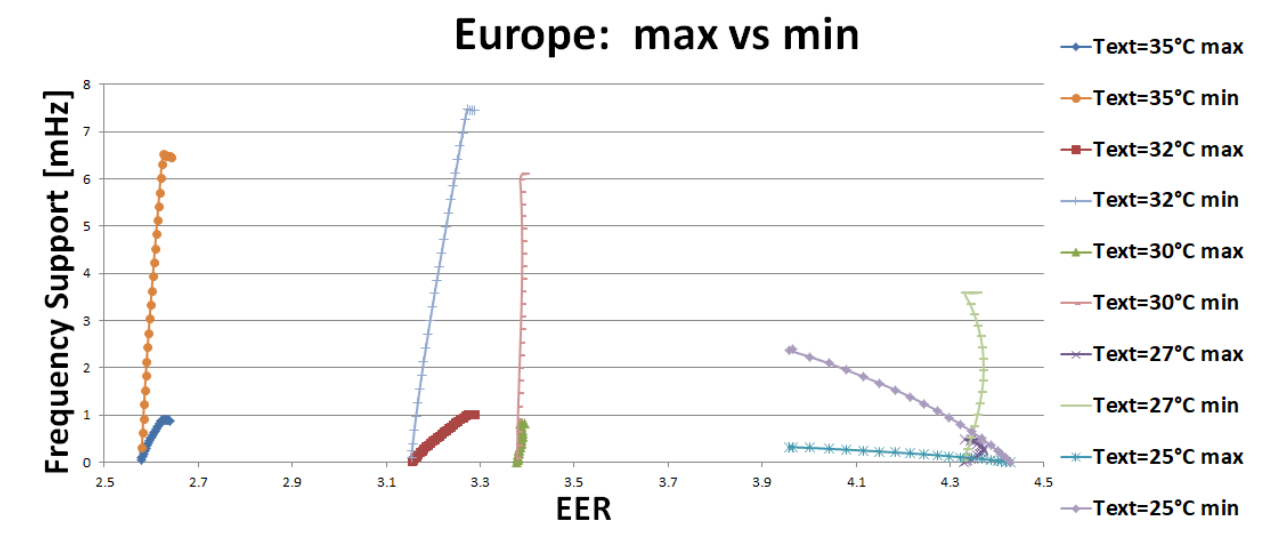


Figure 71: First Test: Heat Pump performance vs frequency response in Europe

The first result, consistent across all outdoor temperatures analyzed, shows a clear difference in the capacity and effective support that the fleet of heat pumps can provide for grid frequency balance, depending on whether the max or min case is considered.

It is evident that the heat pumps have a significantly greater capacity (nearly 7 times higher) in the min case. This is because the min case corresponds to a rather low grid inertia, which is a result of a high level of energy production from inverter-based generation.

The second key finding, which applies to both the max and min cases, is how the heat pump's efficiency behaves as power consumption decreases, and consequently, as its grid support capacity increases.

For outdoor temperatures set at 35°C and 32°C, the results show that as frequency support increases, the EER of the unit also rises slightly. This is undoubtedly the most compelling result of the study. The same trend is observed for the outdoor temperature set at 30°C, although only a very slight increase in EER is achieved.

In contrast, for an outdoor temperature of 27°C, the behavior is not uniform. Initially, as the frequency support increases, the EER also rises. However, at approximately half of the total capacity, the trend in the EER reverses, and it begins to decrease.





The last outdoor temperature analyzed was 25° C, which showed the worst overall performance. First, this configuration had the lowest grid support capacity, reaching a maximum of 0.362 mHz in the max case and 2.390 mHz in the min case. Furthermore, it was the only one characterized by an operating curve with a negative slope. This indicates that as absorbed power decreases—and thus grid frequency balancing capacity increases—the heat pump's efficiency also deteriorates.

Next, we present the results of the study as applied to the Italian scenario, which considered a fleet of 2.851.800 air-to-air heat pumps (Figure 72).

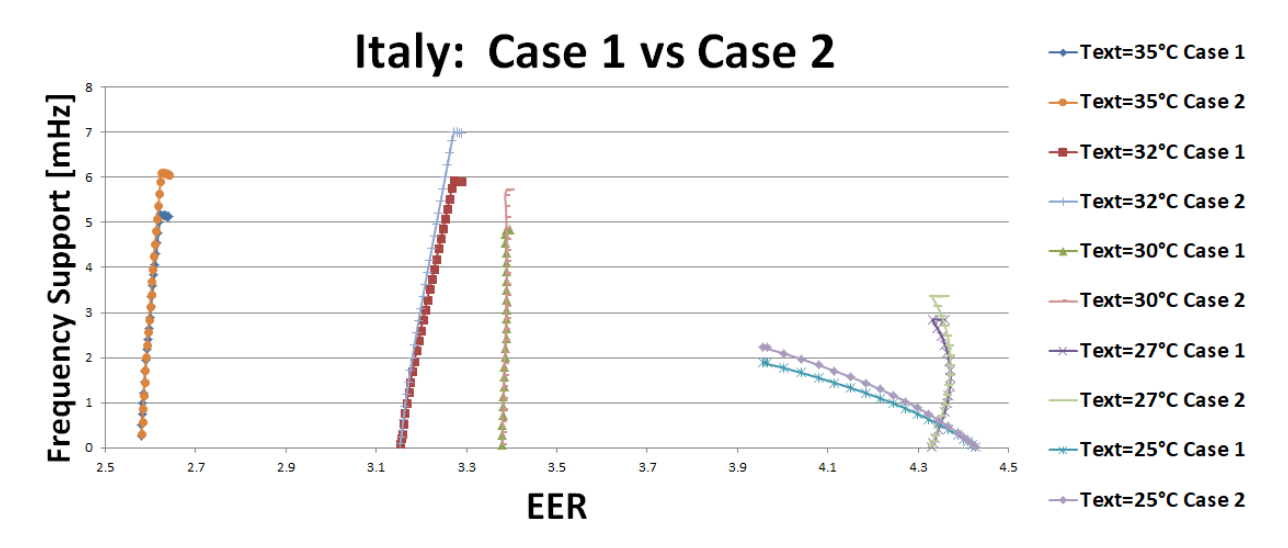


Figure 72: First Test: Heat Pump performance vs frequency response in Italy

In the Italian context, it is immediately evident that there is not a significant difference in grid support capacity between $Case\ 1$ and $Case\ 2$. This indicates that, even in these two extreme scenarios, a balance exists among the factors that influence grid stability.

Specifically, H and S are the variables that counterbalance each other in the frequency response formula (43). This is because the power decrement and the number of heat pump units are the same in both cases.

Regarding the behavior of first-law efficiency as frequency support increases, the same considerations from the European case apply when varying the outdoor temperature.

As a reminder, the second part of the first test used the same methodology as the first part. The key difference was that the outdoor temperature was held constant while the indoor setpoint temperature was varied.

Specifically, the outdoor temperature was set at 30°C, while the indoor temperature assumed the values of 20°C, 22°C, and 24°C across the three tests.

Also here the results will be presented for all the four cases: two for the European context (max and min) and two for the Italian context $(Case\ 1 \text{ and } Case\ 2)$. This analysis focuses exclusively on the coordinated use of air-to-air heat pumps.

The results regarding the study in the European context are shown in Figure 73.





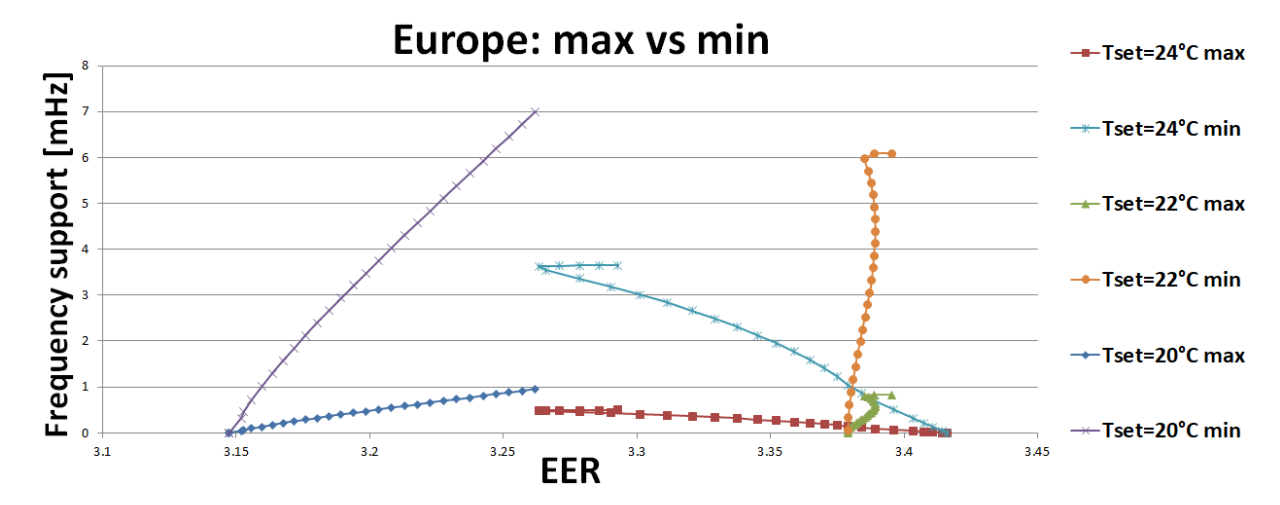


Figure 73: First Test (second part): Europe

Similar to the European case, the first thing to note is the significant difference in grid support capacity when considering the max and min cases.

The value of the system inertia H_{min} is very low and is not compensated for by a correspondingly large value of the system base S_{min} . This results in a more pronounced lack of stability in the electrical grid during the min case, which in turn allows the coordinated HP fleet to offer a greater contribution to the system's frequency balancing.

A more accurate categorization of the three responses based on the setpoint temperature leads to the following conclusions.

When the setpoint temperature is 24° C, a negative slope is observed in the operating curve. It is first important to recall that the closer the setpoint temperature is to the outdoor temperature, the lower the nominal power required by the compressor to stabilize the system. Consequently, setting the indoor temperature to 24° C means a relatively low power draw compared to the other two cases.

When the power supplied to the compressor is decreased in this case—and the frequency support capacity is increased—the heat pump's efficiency performance deteriorates, with the nominal value dropping from 3.42 to a minimum of 3.26.

For the case with an indoor setpoint temperature of 22°C, an almost vertical trend is observed. Relative to a nominal COP of 3.378, the efficiency reaches a maximum value of 3.388. This implies that the reduction in power to the heat pump has a negligible effect on the machine's efficiency.

The final setpoint temperature was 20°C. This particular condition requires the highest power consumption from the heat pump to maintain equilibrium.

The results show that in this case, a reduction in power to the compressor positively impacts the system's efficiency. Therefore, this final temperature setting demonstrates that the ability to provide a frequency response to the grid is also linked to achieving better energy performance from the machine.





Italy: Case 1 vs Case 2

—Tset=24°C Case 1

—Tset=22°C Case 1

—Tset=22°C Case 1

—Tset=22°C Case 1

—Tset=20°C Case 2

—Tset=20°C Case 2

The results regarding the study in the Italian context are shown in Figure 74.

Figure 74: First Test (second part): Italy

It's immediately clear that the capacity of the coordinated HP fleet to support grid frequency management is quite similar in the two extreme cases studied. The reason for this is the same as the one previously explained for the Italian scenario.

Regarding the relationship between EER and frequency support for each analyzed setpoint temperature, the same considerations made for the aforementioned European context also apply to this case.

What we have demonstrated in this paragraph is that, depending on the operational conditions of the HP fleet in interconnection with the electrical system (defined by specific values of the system base power S and system inertia H), the modulation of the absorbed power in favor of a frequency service strategy produces different results in terms of energy performance.

It is fundamental to recall that the capability of these Heat Pumps to participate in FFR (Fast Frequency Response) or PFR (Primary Frequency Response) services is due to two key characteristics:

- The very low mechanical inertia of the compressor, which allows for almost instantaneous modulation of the power
- A thermal system that, conversely, possesses high thermal inertia, capable of storing energy and mitigating power variations, essentially acting as a thermal battery

Utilizing these two specifications, it has been shown that under certain conditions, power modulation can even improve the HP's EER (Energy Efficiency Ratio), thereby strengthening the potential Demand Response business model that could be integrated. This result provides a powerful incentive that goes beyond the simple capability of providing flexibility to the system, making participation in DR programs desirable for both the TSO (Transmission System Operator) and the end-user.





11 Conclusion

The thesis aimed to investigate and quantify the role of heat pumps as flexible resources, capable of making a significant contribution to the stability of a rapidly evolving electrical grid. In an energy context increasingly dominated by intermittent renewable sources, which reduce system inertia, the ability to proactively manage the demand side emerges as a fundamental pillar to ensure grid resilience and reliability.

Through the development of a detailed model on Matlab/Simulink and the simulation of European and Italian scenarios, this research has unequivocally demonstrated that a coordinated fleet of heat pumps is not a simple load, but a true strategic resource. The results of the first test confirmed that the ability to provide instantaneous frequency support (Fast Frequency Response) is not only feasible but becomes particularly relevant when system stability is critical, acting as an essential "cushion" to mitigate frequency fluctuations and prevent instability. The analysis highlighted how the magnitude of this support is directly proportional to the maximum power that heat pumps can reduce, showing a remarkable potential that scales with their widespread adoption. Another significant finding to take into account, emerging from the second test, is the complex but crucial relationship between the magnitude of frequency support and the duration of the service.

In addition, under certain operating conditions, it was found that power modulation to provide grid support can even lead to an improvement in the energy performance of the heat pump, as demonstrated by the EER values. This result debunks the myth that grid support necessarily involves a compromise on efficiency, paving the way for a "win-win" model where the end-user benefits from both system stability and more efficient energy consumption.

The contributions of this thesis extend beyond technical results. They highlight the potential of heat pumps as catalysts for the transformation of consumers from passive entities to active prosumers, capable of interacting dynamically with the grid. This vision of "Demand-Side Management" is no longer a theoretical concept but a concrete and scalable solution that can accelerate the transition towards a cleaner and more decentralized energy future. At a regulatory and political level, the results underline the importance of creating frameworks and incentive programs that recognize and reward the value of the flexibility services provided by these technologies, encouraging their adoption and system-level integration.

For the future, research in this field can focus on several directions. It will be essential to develop even more sophisticated control algorithms that are not limited to responding to frequency signals but also integrate real-time price signals and market conditions, optimizing economic benefits for consumers and operators. Furthermore, to obtain more realistic predictive models, it will be necessary to conduct studies that consider a more heterogeneous fleet of heat pumps, taking into account different models, operating states and boundary conditions. Finally, a crucial step will be the analysis of the behavior of these fleets in more geographically localized grids, such as microgrids or residential areas connected to the same bus, where the impact of their action can be measured with greater precision and where their interaction with fundamental electrical parameters can be analyzed in a more controlled and realistic context. This thesis therefore represents a solid starting point for a new generation of studies aimed at unlocking the full potential of heat pumps in the ongoing energy revolution.





Bibliography

- [1] European Union. Regulation (EU) 2021/1119 of the European Parliament and of the Council of 30 June 2021 establishing the framework for achieving climate neutrality. Accessed on 14 April 2025. 2021. URL: https://eur-lex.europa.eu/legal-content/EN/TXT/?uri=CELEX:32021R1119.
- [2] IEA. Global Energy Review 2025, IEA, Paris. Visitato il 14 aprile 2025. 2025. URL: https://www.iea.org/reports/global-energy-review-2025, %20Licence: %20CC%20BY%204.0.
- [3] Hannah Ritchie, Pablo Rosado, and Max Roser. "Energy Production and Consumption". In: *Our World in Data* (2020). https://ourworldindata.org/energy-production-consumption.
- [4] International Energy Agency. Global Energy Review 2025 Electricity. Accessed on 14 April 2025. 2025. URL: https://www.iea.org/reports/global-energy-review-2025/electricity#electricity-generation.
- [5] Hannah Ritchie, Max Roser, and Pablo Rosado. "Renewable Energy". In: *Our World in Data* (2020). https://ourworldindata.org/renewable-energy.
- [6] Jianxue Wang et al. "Optimal Planning Strategy for Distributed Energy Resources Considering Structural Transmission Cost Allocation". In: *IEEE Transactions on Smart Grid* 9.5 (Sept. 2018), pp. 5236–5248. DOI: 10.1109/TSG.2017.2684160.
- [7] Red Eléctrica de España. Demanda Eléctrica Peninsular: 28 de abril de 2025. Ultimo accesso: 2 maggio 2025. Apr. 2025. URL: https://demanda.ree.es/visiona/peninsula/nacionalau/total/2025-04-28.
- [8] Paul Kirby. How Spain powered back to life from unprecedented national blackout. Ultimo accesso: 2 maggio 2025. Apr. 2025. URL: https://www.bbc.com/news/articles/c175ykvjxyeo.
- [9] Reuters. Sánchez pressed to explain Spain's blackout; grid says solar not to blame. Ultimo accesso: 2 maggio 2025. Apr. 2025. URL: https://www.reuters.com/world/europe/sanchez-pressed-explain-spains-blackout-grid-says-solar-not-blame-2025-04-30/.
- [10] H. Hui et al. "Operating reserve evaluation of aggregated air conditioners". In: *Applied Energy* 196 (June 2017), pp. 218–228. DOI: 10.1016/j.apenergy.2017.03.124.
- [11] Neil Weaver. Inertia (and rate of change of frequency): an introduction. https://modoenergy.com/research/system-inertia-grid-frequency-rocof-explainer. Accessed via Modo Energy Research. July 2022.
- [12] Hongxun Hui et al. "Dynamic and Stability Analysis of the Power System With the Control Loop of Inverter Air Conditioners". In: *IEEE Transactions on Industrial Electronics* 68.3 (Mar. 2020), pp. 218–228. doi: 10.1109/TIE.2020.2975465. URL: https://doi.org/10.1109/TIE.2020.2975465.
- [13] Manisa Pipattanasomporn et al. "Load Profiles of Selected Major Household Appliances and Their Demand Response Opportunities". In: *Smart Grid*, *IEEE Transactions on* 5 (Mar. 2014), pp. 742–750. DOI: 10.1109/TSG.2013.2268664.
- [14] Ruihao Song, Vladimir Terzija, and Thomas Hamacher. "Integrating Air-Source Heat Pumps into the Demand-Side Fast Frequency Response Service: A Study Based on Thermal Dynamic Uncertainty". In: *IEEE Transactions on Power Systems* (2023). Early Access. DOI: 10.1109/TPWRS.2023.XXXXXXXX.
- [15] Jacopo Famiglietti et al. "Environmental life cycle assessment of industrial high-temperature to residential small-size heat Pumps: A critical review". In: *Energy Conversion and Management: X* 26 (2025), p. 100947. ISSN: 2590-1745. URL: https://www.sciencedirect.com/science/article/pii/S2590174525000790.
- [16] P. Denholm et al. *Inertia and the Power Grid: A Guide Without the Spin*. Tech. rep. NREL/TP-6120-73856. Golden, CO, USA: National Renewable Energy Laboratory (NREL), 2020. URL: https://www.nrel.gov/docs/fy20osti/73856.pdf.

- [17] Terna SpA. *Partecipazione alla regolazione di frequenza e frequenza-potenza*. Tech. rep. Terna SpA, luglio 2008.
- [18] N. Hatziargyriou et al. "Definition and Classification of Power System Stability—Revisited & Extended". In: *IEEE Transactions on Power Systems* 36.4 (July 2021), pp. 3271–3281. DOI: 10.1109/TPWRS.2020.3041775. URL: https://doi.org/10.1109/TPWRS.2020.3041775.
- [19] P. Tielens and D. Van Hertem. "The relevance of inertia in power system". In: *Renewable and Sustainable Energy Reviews* 55 (2016).
- [20] International Energy Agency. *Harnessing Variable Renewables: A Guide to the Balancing Challenge*. Tech. rep. Accessed: 2025-05-13. Paris, France: International Energy Agency, 2011. url: https://www.iea.org/reports/harnessing-variable-renewables.
- [21] EURELECTRIC. Flexibility and Aggregation Requirements for Their Interaction in the Market. Tech. rep. Accessed: 2025-05-13. Brussels, Belgium: EURELECTRIC, 2014. url: https: //www.usef.energy/app/uploads/2016/12/EURELECTRIC-Flexibility-and-Aggregation-jan-2014.pdf.
- [22] Madeline Geocaris. Assessing Power System Reliability in a Changing Grid Environment. Accessed: 2025-05-13. 2022. URL: https://www.nrel.gov/news/detail/program/2022/assessing-power-system-reliability-in-a-changing-grid-environment.
- [23] O. Gomis-Bellmunt et al. "Grid-Forming Loads: Can the Loads Be in Charge of Forming the Grid in Modern Power Systems?" In: *IEEE Transactions on Smart Grid* 14.2 (2023), pp. 1042–1055. DOI: 10.1109/TSG.2022.3202646. URL: https://ieeexplore.ieee.org/document/9869743.
- [24] Vahan Gevorgian, Yingchen Zhang, and Erik Ela. "Investigating the impacts of wind generation participation in interconnection frequency response". In: *IEEE Transactions on Sustainable Energy* 6.3 (2015). Accessed: 2025-05-13, pp. 1004–1012. DOI: 10.1109/TSTE.2014.2343836. URL: https://ieeexplore.ieee.org/document/7150225.
- [25] Eldrich Rebello, David Watson, and Marianne P. Rodgers. "Performance analysis of a 10 MW wind farm in providing secondary frequency regulation: Experimental aspects". In: IEEE Transactions on Power Systems 34.4 (2019). Accessed: 2025-05-13, pp. 3090–3097. DOI: 10.1109/TPWRS.2019.2891962. URL: https://ieeexplore.ieee.org/document/8686980.
- [26] Shahil Shah and Vahan Gevorgian. Control, Operation, and Stability Characteristics of Grid-Forming Type III Wind Turbines: Preprint. Tech. rep. NREL/CP-5D00-78158. Accessed: 2025-05-13. National Renewable Energy Laboratory, 2020. url: https://www.nrel.gov/docs/fy20osti/78158.pdf.
- [27] ENTSO-E. Statistical Factsheet 2024. https://eepublicdownloads.blob.core.windows.net/public-cdn-container/clean-documents/Publications/Statistics/Factsheet/entsoe_sfs2024_web.pdf. 2025.
- [28] National Grid Electricity System Operator (NGESO). Frequency Risk and Control Policy December 2020. Tech. rep. National Energy System Operator (NESO), Dec. 2020. URL: https://www.neso.energy/document/183426/download.
- [29] ENTSO-E. Frequency Stability Evaluation Criteria for the Synchronous Zone of Continental Europe: Requirements and Impacting Factors. Tech. rep. Disponibile online. ENTSO-E, Mar. 2016.
- [30] Md Rabiul Islam, Fahad Alzahrani, and Hemanshu R. Pota. "Exploring the Utilization of Energy Storage Systems for Frequency Response Adequacy of a Low Inertia Power Grid". In: *IEEE Access* PP.99 (2021), pp. 1–1. DOI: 10.1109/ACCESS.2021.3114216. URL: https://doi.org/10.1109/ACCESS.2021.3114216.
- [31] OpenAI. ChatGPT (modello GPT-4). https://chat.openai.com. Large language model. 2025
- [32] RSE, ANIE ENERGIA. I sistemi di accumulo nel settore elettrico. Tech. rep. RSE, Mar. 2015.
- [33] D. P. Kothari and I. J. Nagrath. *Modern Power System Analysis*. McGraw Hill Higher Education, June 2011.





- [34] Prabha Kundur. *Power System Stability and Control*. New York: McGraw-Hill Inc., 1994.
- [35] Fabio Bignucolo, Martino Pettinà, and Roberto Caldon. "Stability of the power system in presence of low-inertia generation: evolution and new approaches". In: *Dipartimento di Ingegneria Industriale, Università di Padova* (2020).
- [36] ENTSO-E. *Inertia and Rate of Change of Frequency (RoCoF), Version 17.* 16 December 2020. SPD Inertia TF, Dec. 2020.
- [37] P. Tielens and D. Van Hertem. "Grid Inertia and Frequency Control in Power Systems with High Penetration of Renewables". In: *Young Researchers Symposium in Electrical Power Engineering*. Delft, Netherlands, 2012.
- [38] ENTSO-E. Continental Europe Operation Handbook. https://www.entsoe.eu.n.d.
- [39] Pierluigi Siano. "Demand response and smart grids—A survey". In: Renewable and Sustainable Energy Reviews 30 (2014), pp. 461–478. ISSN: 1364-0321. DOI: https://doi.org/10.1016/j.rser.2013.10.022. URL: https://www.sciencedirect.com/science/article/pii/S1364032113007211.
- [40] Q. Shi et al. "Dynamic demand control for system frequency regulation: Concept review, algorithm comparison, and future vision". In: *Electric Power Systems Research* 154 (Jan. 2018), pp. 75–87. DOI: 10.1016/j.epsr.2017.08.015.
- [41] Q. Hu et al. "A framework of residential demand aggregation with financial incentives". In: *IEEE Transactions on Smart Grid* 9.1 (Jan. 2018), pp. 497–505. DOI: 10.1109/TSG.2016. 2562678.
- [42] C. W. Gellings and J. H. Chamberlin. *Demand-side management: Concepts & Methods*. The Fairmont Press, Inc., 1993.
- [43] Gianfranco Chicco. "Users Participation and Demand Response". Politecnico di Torino corso Smart Electricity Systems. Mar. 2025.
- [44] Ji-Eun Han, Seung-Hwan Han, and Kaoru Sezaki. "Automated demand response from home energy management system under dynamic pricing and power and comfort constraints". In: *IEEE Transactions on Smart Grid* 6.5 (2015), pp. 2314–2322.
- [45] Lidong Huang et al. "Demand response with incomplete information: A systematic review". In: *Electric Power Systems Research* 246 (2025), p. 111720. ISSN: 0378-7796. DOI: https://doi.org/10.1016/j.epsr.2025.111720. URL: https://www.sciencedirect.com/science/article/pii/S037877962500313X.
- [46] Euronews Green. "Perché i combustibili fossili sono come pagare un affitto mentre le importazioni di pannelli". In: Euronews (2025). Consultato: 2025-06-02. URL: https://it.euronews.com/green/2025/04/23/perche-i-combustibili-fossili-sono-come-pagare-un-affitto-mentre-le-importazioni-di-pannel.
- [47] Arendse Huld. *Urbanization in China New Action Plan to Facilitate Urban Migration*. Accessed: 2025-06-03. 2024. URL: https://www.china-briefing.com/news/urbanization-in-china-action-plan-migration/.
- [48] Xiangyang Wu. "Reflections on building a low-carbon Beijing". en. In: *Science and Technology Innovation Herald* 07 (2011), pp. 212–213. doi: 10.16660/j.cnki.1674-098x. 2011.07.20.
- [49] Stephanie Alencar Braga dos Santos et al. "Demand response application in industrial scenarios: A systematic mapping of practical implementation". In: *Expert Systems with Applications* 215 (2023), p. 119393. ISSN: 0957-4174. DOI: 10.1016/j.eswa.2022.119393.
- [50] W. N. Silva et al. "Market models and optimization techniques to support the decision-making on demand response for prosumers". In: *Electric Power Systems Research* 210 (2022), p. 108059. ISSN: 0378-7796. DOI: 10.1016/j.epsr.2022.108059.
- [51] Catarina Araya Cardoso, Jacopo Torriti, and Mate Lorincz. "Making demand side response happen: A review of barriers in commercial and public organisations". In: *Energy Research & Social Science* 64 (2020), p. 101443. ISSN: 2214-6296. DOI: 10.1016/j.erss. 2020.101443.





- [52] Junfeng Xie et al. "A Survey of Blockchain Technology Applied to Smart Cities: Research Issues and Challenges". In: *IEEE Communications Surveys Tutorials* 21.3 (2019), pp. 2794–2830. por: 10.1109/COMST.2019.2899617.
- [53] Abubakar M. Hambali et al. "Review on Home Energy Management System Considering Demand Responses, Smart Technologies, and Intelligent Controllers". In: *IEEE Access* PP.99 (2018). License: CC BY-NC-ND 4.0, pp. 1–1. DOI: 10.1109/ACCESS.2018. 2831917.
- [54] G. Bianco et al. "A Building Energy Management System for demand response in smart grids". In: 2020 IEEE 16th International Conference on Automation Science and Engineering (CASE). 2020, pp. 1485–1490. DOI: 10.1109/CASE48305.2020.9216880.
- [55] J.W. Feltes, B.D. Gemmell, and D. Retzmann. "From Smart Grid to Super Grid: Solutions with HVDC and FACTS for Grid Access of Renewable Energy Sources". In: 2011 IEEE Power and Energy Society General Meeting. 2011, pp. 1–6. ISBN: 978-1-4577-1000-1. DOI: 10. 1109/PES.2011.6039820.
- [56] Electricity Demand-Side Response. Tech. rep. POST-PN-452. London: The Parliamentary Office of Science and Technology, Jan. 2014. url: http://researchbriefings.parliament.uk/ResearchBriefing/Summary/POST-PN-452#fullreport.
- [57] Sumit Nema, Vivek Prakash, and Hrvoje Pandžić. "The role of thermostatically controlled loads in power system frequency management: A comprehensive review". In: Sustainable Energy, Grids and Networks 42 (2025), p. 101680. ISSN: 2352-4677. DOI: https://doi.org/10.1016/j.segan.2025.101680. URL: https://www.sciencedirect.com/science/article/pii/S2352467725000621.
- [58] Yaxin Wang et al. "NSGA-II-based load resource management for frequency and voltage support". In: Global Energy Interconnection 8.2 (2025), pp. 258–268. ISSN: 2096-5117. DOI: https://doi.org/10.1016/j.gloei.2025.01.005. URL: https://www.sciencedirect.com/science/article/pii/S2096511725000271.
- [59] Xingzhao Yang et al. "Flexible Air Conditioning Loads as Voltage/Frequency-Responsive Sources in Microgrid". In: 2020 IEEE/IAS Industrial and Commercial Power System Asia (ICPS Asia). 2020, pp. 1739–1744. DOI: 10.1109/ICPSAsia48933.2020.9208569.
- [60] William Mendieta and Claudio A. Cañizares. "Primary Frequency Control in Isolated Microgrids Using Thermostatically Controllable Loads". In: *IEEE Transactions on Smart Grid* 12.1 (2021), pp. 93–105. DOI: 10.1109/TSG.2020.3012549.
- [61] R. Stamminger. *Synergy Potential of Smart Appliances*. EIE, D2.3 of WP 2 from the Smart-A project. Nov. 2008.
- [62] C. Vivekananthan et al. "Demand Response for Residential Appliances via Customer Reward Scheme". In: *IEEE Transactions on Smart Grid* 5.2 (2014), pp. 809–820.
- [63] Philip J. Douglass et al. "Smart Demand for Frequency Regulation: Experimental Results". In: *IEEE Transactions on Smart Grid* 4.3 (2013), pp. 1713–1720. DOI: 10.1109/TSG. 2013.2259510. URL: https://doi.org/10.1109/TSG.2013.2259510.
- [64] Jaqueline Litardo et al. "Air-conditioning life cycle assessment research: A review of the methodology, environmental impacts, and areas of future improvement". In: Energy and Buildings 296 (2023), p. 113415. ISSN: 0378-7788. DOI: https://doi.org/10.1016/j.enbuild.2023.113415. URL: https://www.sciencedirect.com/science/article/pii/S037877882300645X.
- [65] Commissione Europea. *Pompe di calore*. Accesso: 12 maggio 2025. 2025. URL: https://energy.ec.europa.eu/topics/energy-efficiency/heat-pumps_en.
- [66] M. González-Torres et al. "A review on buildings energy information: Trends, end-uses, fuels and drivers". In: *Energy Reports* 8 (2022), pp. 626–637.
- [67] D. Ürge-Vorsatz et al. "Advances toward a net-zero global building sector". In: *Annual Review of Environment and Resources* 45.1 (2020), pp. 227–269.
- [68] International Energy Agency. *The Future of Heat Pumps*. Licence: CC BY 4.0. Paris: IEA, 2022. URL: https://www.iea.org/reports/the-future-of-heat-pumps.





- [69] Electrification & Digital Decarbonization Software. https://www.gevernova.com/software/.
- [70] Paul Barter. "Cars are parked 95% of the time". Let's check! https://www.reinventingparking.org/2013/02/cars-are-parked-95-of-time-lets-check.html. Posted February 22, 2013; accessed 26 August 2025. 2013.
- [71] Vidya M. S. "Reduction of Frequency Deviation on Microgrid by Coordination of Electric Vehicles in a Charging Station". In: *International Journal of Innovative Technology and Exploring Engineering (IJITEE)* 14.4 (2025), pp. 14–20. DOI: 10.35940/ijitee.E4609.14040325.
- [72] Phoomat Jampeethong and Surin Khomfoi. "Coordinated Control of Electric Vehicles and Renewable Energy Sources for Frequency Regulation in Microgrids". In: *IEEE Access* 8 (2020), pp. 141967–141976. DOI: 10.1109/ACCESS.2020.3010276.
- [73] Raffaello Cozzolino and Gino Bella. "A review of electrolyzer-based systems providing grid ancillary services: current status, market, challenges and future directions". In: Frontiers in Energy Research 12 (Feb. 2024), pp. –. DOI: 10.3389/fenrg.2024.1358333.
- [74] M. G. Dozein, A. Jalali, and P. Mancarella. "Fast frequency response from utility-scale hydrogen electrolyzers". In: *IEEE Transactions on Sustainable Energy* 12.3 (July 2021), pp. 1707–1717.
- [75] Mehdi Ghazavi, Ahvand Jalali, and Pierluigi Mancarella. "Fast Frequency Response From Utility-Scale Hydrogen Electrolyzers". In: *IEEE Transactions on Sustainable Energy* (Feb. 2021). DOI: 10.1109/TSTE.2021.3063245.
- [76] CEI Comitato Elettrotecnico Italiano. CEI 0-16:2019 Norma italiana per la connessione di utenti finali alle reti di distribuzione in bassa tensione. https://www.ldreti.it/wp-content/uploads/2020/09/0-16_2019.pdf. Ultimo accesso: October 7, 2025. 2019.
- [77] Refrigeration Cycle (Air Conditioning). https://it.mathworks.com/help/hydro/ug/residential-refrigeration-unit.html. MathWorks MATLAB & Simulink Documentation; accessed 26 August 2025.
- [78] Chiara Silvi. "Tecnica del freddo e criogenia". Politecnico di Torino corso Tecnica del freddo e criogenia. Mar. 2025.
- [79] Ministero dell'Ambiente e della Sicurezza Energetica. *Il Protocollo di Montreal*. Consultato il 11 giugno 2025. 2025. URL: https://www.mase.gov.it/pagina/il-protocollo-di-montreal.
- [80] myclimate. Cos'è l'effetto serra antropico? Consultato il 11 giugno 2025. 2022. URL: https://www.myclimate.org/it-ch/informarsi/dettaglio-faq/effetto-serra-antropico/#:~:text=L'effetto%20serra%20antropico%20deriva, sorta%20di%20accumulo%20di%20calore..
- [81] Certifico Srl. GWP (Global Warming Potential) / Note e calcolo. Consultato il 11 giugno 2025. 2024. URL: https://www.certifico.com/chemicals/documenti-chemicals/221-documenti-riservati-chemicals/22781-gwp-global-warming-potential-note-e-calcolo.
- [82] Avinash Kumar et al. "Seasonal performance comparison of R-410A and R-454B in a variable-speed air-cooled scroll chiller". In: *Thermal Science and Engineering Progress* 56 (2024), p. 103050. ISSN: 2451-9049. DOI: https://doi.org/10.1016/j.tsep.2024. 103050. URL: https://www.sciencedirect.com/science/article/pii/S2451904924006681.
- [83] E.W. Lemmon, M.L. Huber, and M.O. McLinden. *NIST Standard Reference Database 23: Reference Fluid Thermodynamic and Transport Properties (REFPROP)*. Version 9.0. National Institute of Standards and Technology. 2010.
- [84] Engineers Edge. Saturated R410A Tables. https://www.engineersedge.com/thermodynamics/saturated_r410a_tables_14782.htm.
- [85] Arkadiusz Gużda and Norbert Szmolke. "Compressors in Heat Pumps". In: *Machine Dynamics Research* 39.2 (2015), pp. 71–83.
- [86] Ahmed Jasim Hamad, Abdul Hadi N. Khalifa, and Doaa Zaid Khalaf. "The Effect of Compressor Speed Variation and Vapor Injection on the Performance of Modified Re-





- frigeration System". In: *International Review of Mechanical Engineering (IREME)* 12.3 (Mar. 2018), p. 285. doi: 10.15866/ireme.v12i3.1419.
- [87] MathWorks. Positive Displacement Compressor (2P). Accessed: 2025-07-11. 2024. URL: https://www.mathworks.com/help/releases/R2024b/hydro/ref/positivedisplacementcompressor2p.html.
- [88] Autori non specificati. "Performance analysis of axial fans in unitary air-conditioning systems". In: 2002 37th Intersociety Energy Conversion Engineering Conference (IECEC). IEEE, Aug. 2002. DOI: 10.1109/IECEC.2002.1392099. URL: https://ieeexplore.ieee.org/document/1392099.
- [89] MathWorks. Fan MATLAB Simulink. 2024. URL: https://www.mathworks.com/help/releases/R2024b/hydro/ref/fanma.html.
- [90] MathWorks. System-Level Condenser Evaporator (2P-MA). Versione R2024b. url: https://ch.mathworks.com/help/releases/R2024b/hydro/ref/systemlevelcondenserevaporator2pma.html.
- [91] MathWorks. Receiver Accumulator (2P). Versione R2024b. url: https://ch.mathworks.com/help/releases/R2024b/hydro/ref/receiveraccumulator2p.html.
- [92] MathWorks. Thermostatic Expansion Valve (2P). Versione R2024b. url: https://ch.mathworks.com/help/releases/R2024b/hydro/ref/thermostaticexpansionvalve2p.html.
- [93] MathWorks. Convective. Accessed: 2025-07-11. 2024. URL: https://www.mathworks.com/help/releases/R2024b/simscape/ref/convectiveheattransfer.html.
- [94] MathWorks. Conduction. Accessed: 2025-07-11. 2024. URL: https://www.mathworks.com/help/releases/R2024b/simscape/ref/conductiveheattransfer.html.
- [95] MathWorks. Thermal mass. Accessed: 2025-07-11. 2024. url: https://www.mathworks.com/help/releases/R2024b/simscape/ref/thermalmass.html.
- [96] European Commission. Ecodesign for Sustainable Products Regulation (ESPR). 2024. URL: https://commission.europa.eu/energy-climate-change-environment/standards-tools-and-labels/products-labelling-rules-and-requirements/ecodesign-sustainable-products-regulation_en.
- [97] European Commission. Commission Regulation (EU) No 206/2012 of 6 March 2012 implementing Directive 2009/125/EC with regard to ecodesign requirements for air conditioners and comfort fans. Official Journal of the European Union, L 72, 10.3.2012, p. 7–27. 2012. URL: https://eur-lex.europa.eu/eli/reg/2012/206/oj.
- [98] European Committee for Standardization (CEN). EN 15251:2007 Indoor environmental input parameters for design and assessment of energy performance of buildings addressing indoor air quality, thermal environment, lighting and acoustics. https://standards.cen.eu. 2007.
- [99] American Society of Heating, Refrigerating and Air-Conditioning Engineers (ASHRAE). Thermal Environmental Conditions for Human Occupancy. Atlanta, GA, USA, 2020. URL: https://www.ashrae.org/technical-resources/standards-and-guidelines/standards-addenda/ashrae-standard-55-2020.
- [100] European Committee for Standardization (CEN). EN 14511:2018 Test methods and standards for air conditioners, liquid chilling packages and heat pumps. Accessed via International Energy Agency (IEA). 2018. URL: https://www.iea.org/policies/7031-en-14511-22018-test-methods-and-standards-for-air-conditioners-liquid-chilling-packages-and-heat-pumps.
- [101] Theis Bo Harild Rasmussen, Qiuwei Wu, and Menglin Zhang. "Primary frequency support from local control of large-scale heat pumps". In: International Journal of Electrical Power Energy Systems 133 (2021), p. 107270. ISSN: 0142-0615. DOI: https://doi.org/10.1016/j.ijepes.2021.107270. URL: https://www.sciencedirect.com/science/article/pii/S0142061521005093.





- [102] European Heat Pump Association. Market data European Heat Pump Association. 2025.

 URL: https://www.ehpa.org/market-data/#:~:text=Overall%2C%2Oheat%2Opump%
 20sales%20slowed,t%20of%20our%2Oenergy%2Ofuture.
- [103] ENTSO-E. Infrastructure Gaps Report. Accessed: 2025-09-01. 2024. URL: https://eepublicdownloads.blob.core.windows.net/public-cdn-container/tyndp-documents/TYNDP2024/forconsultation/Infrastructure_Gaps_Report.pdf.
- [104] Jonathan Volt et al. *Heat Pump Market: Country Fiches*. Tech. rep. JRC137131. European Commission, Joint Research Centre (JRC), May 2024. url: https://publications.jrc.ec.europa.eu/repository/bitstream/JRC137131/JRC137131_015.pdf.



